T.R.
BOLU ABANT İZZET BAYSAL UNIVERSITY
INSTITUTE OF GRADUATE STUDIES
Department of Chemical Engineering

PRODUCTION OF ACTIVATED CARBON FIBERS FROM DATE PALM FOR INDUSTRIAL WASTEWATER TREATMENT

MASTER OF SCIENCE

HUDA ASSI DAHAM AL-BAYATI

ACADEMIC SUPERVISOR
Assist. Prof. Dr. Cem GÖL
ACADEMIC CO-SUPERVIZOR
Prof. Dr. Waleed M. SH. ALABDRABA

BOLU, OCAK - 2024

APPROVAL OF THE THESIS

PRODUCTION OF ACTIVATED CARBON FIBERS FROM DATE PALM FOR INDUSTRIAL WASTEWATER TREATMENT submitted by **HUDA ASSI DAHAM AL-BAYATI** and defended before the Examining Committe Members listed below in partial fulfillment of the requirements for the degree of **Master of Science** in **Department of Chemical Engineering, Institute of Graduate Studies of Bolu Abant Izzet Baysal University in 5.01.2024** by

Examining Committee Members	**Signature**
Supervisor Assist. Prof. Dr. Cem GÖL Bolu Abant Izzet Baysal University	.....
Member Assist. Prof. Dr. Gamze DOĞDU YÜCETÜRK Bolu Abant Izzet Baysal University	.....
Member Prof. Dr. Murat DOĞRU Gebze Technical University	.....

Prof. Dr. İbrahim KÜRTÜL

Director of Instıtute of Graduate Studies

ETHICAL DECLARATION

In this thesis dissertation that was properly prepared according to the Thesis Writing Rules of Bolu Abant İzzet Baysal University of the Institute of Graduates Studies, I hereby declare that;

- All data, information, and documents presented in the thesis were obtained in accordance with the academic and ethical rules,
- All data, documents, assessments, and results were presented in accordance with the scientific ethical and moral rules,
- All works that were benefitted in the thesis were appropriately cited,
- No alteration was made in the data used,
- Study presented in this thesis is original,

Otherwise, I declare that I accept the loss of all my rights in case any contradiction that may arise against me.

The similarity rate obtained by using the Turnitin program, a plagiarism detection software, is within the limits approved by the University Senate.

_____

HUDA ASSI DAHAM AL-BAYATI

ABSTRACT

PRODUCTION OF ACTIVATED CARBON FIBERS FROM DATE PALM FOR INDUSTRIAL WASTEWATER TREATMENT
MSC THESIS
HUDA ASSI DAHAM AL-BAYATI
BOLU ABANT IZZET BAYSAL UNIVERSITY
INSTITUTE OF GRADUATE STUDIES
DEPARTMENT OF CHEMICAL ENGINEERING
(SUPERVISOR: Assist. Prof. Dr. Cem GÖL)
(CO-SUPERVISOR: Prof. Dr. Waleed M. SH. ALABDRABA)
BOLU, JANUARY 2024
(XIV + 118)

This study aims to produce activated carbon fibers (ACFs) due to the implementation of the experiment in the State of Iraq and the fact that Iraq ranks first in the world in the production of dates and the large amount of agricultural waste that results from it. Date palm fibers were identified as the raw material for the production of activated carbon fibers. The activated carbon fibers were chemically treated to increase their durability and practical efficiency through two basic processes. Practical experiments were carried out with the obtained activated carbon samples on contaminated oily water samples from the Baiji refinery in Salah al-Din Governorate. Different values of variables affecting the adsorption efficiency were determined (pH, stirring speed, carbon dose, contact time and temperature). Adsorption equilibrium was reached after 120 min at pH 6.0 with a stirring rate of 400 rpm at 70 °C. The results obtained showed that the chemical oxygen demand (COD) removal efficiency of ACF-NC-LDH reached 99.32% and the removal efficiency of all pollutants reached 99.26% at 1g/300ml carbon dosage. The COD removal efficiency of PAC-NC-LDH was about 89.31%, and the total removal efficiency of all pollutants was 90.3% at 1g/300ml carbon dosage. The experimental results show agreement with linear, Langmuir, and Freundlich isotherm models. The data were successfully fitted to a pseudo-second-order kinetics model, suggesting pore diffusion control. Thermodynamic parameters (ΔH^0, ΔG^0, and ΔS^0) were calculated, and showed spontaneous and endothermic adsorption. The process resulted in increased disorder at the activated carbon/industrial wastewater interface. In particular, the adsorption effectively reduced the concentrations of several contaminants to minimal levels. To ensure the acceptability of the optimisation process, response surface methodology was applied to activated carbon fibers (ACF-NC-LDH) and powdered activated carbon (PAC-NC-LDH). According to the results obtained, it was demonstrated that the produced activated carbon fibers and powdered activated carbon could be safely used in adsorption processes for the treatment of industrial wastewater.

KEYWORDS: Activated Carbon Fibers, Chemical Oxygen Demands, Adsorption, Date Palm Fibers, Response Surface Methodology.

ÖZET

ENDÜSTRİYEL ATIK SU ARITIMI İÇİN HURMA AĞAÇLARINDAN AKTİF KARBON FİBER ÜRETİMİ
YÜKSEK LİSANS TEZİ
HUDA ASSI DAHAM AL-BAYATI
BOLU ABANT İZZET BAYSAL ÜNİVERSİTESİ
LİSANSÜSTÜ EĞİTİM ENSTİTÜSÜ
KİMYA MÜHENDİSLİĞİ BİLİM DALI
(TEZ DANIŞMANI: Dr. Öğr. Üyesi Cem GÖL)
(İKİNCİ DANIŞMAN: Prof. Dr. Waleed M. SH. ALABDRABA)
BOLU, OCAK - 2024
(XIV + 118)

Irak, hurma üretiminde dünyada ilk sırada yer almaktadır ve bu sebeple büyük miktarda tarımsal atık meydana gelmektedir. Bu tez kapsamında aktif karbon lifi üretimi için hammadde olarak hurma lifleri kullanılarak aktif karbon lifi (ACF'ler) üretmek amaçlanmaktadır. Bu kapsamda elde edilen aktif karbon liflerine kimyasal iyileştirme iki temel basamakta, dayanıklılıklarını ve pratik verimliliklerini artırma amacıyla yapılmıştır. Elde edilen aktif karbon lifleri ile Salah al-Din Valiliği'ndeki bulunan Baiji rafinerisinden alınan petrol atığı ihtiva eden su örnekleri üzerine deneyler gerçekleştirilmiştir. Bu kapsamda, adsorpsiyon verimini etkileyen değişkenlerin farklı değerleri (pH, karıştırma hızı, karbon miktarı, temas süresi ve sıcaklık) belirlenmiştir. Adsorpsiyon dengesi, 70 °C'de, 6.0 pH'da ve 400 devir/dakika karıştırma hızında 120 dakika değerlerini ihtiva eden parametreler ile sağlandı. Elde edilen sonuçlar, ACF-NC-LDH'nin kimyasal oksijen ihtiyacı (KOİ) giderim verimliliğinin %99,32'ye ulaştığını ve tüm kirleticilerin giderim verimliliğinin %99,26 olduğunu gösterdiği 1g/300ml karbon miktarında. PAC-NC-LDH'nin (KOİ) giderim verimliliği yaklaşık olarak %89,31 idi ve tüm kirleticilerin toplam giderim verimliliği 1g/300ml karbon miktarında %90,3 olarak belirlendi. Deneysel sonuçlar, doğrusal, Langmuir ve Freundlich izoterm modelleri ile uyumlu olduğunu göstermektedir. Veriler, gözenek difüzyonu tarafından kontrol edilen bir yarı-ikinci derece kinetik modeline başarıyla uyarlanmıştır. ΔH^0, ΔG^0 ve ΔS^0 termodinamik parametre değerleri hesaplanmıştır, bu da adsorpsiyonun kendiliğinden ve endotermik özellikte olduğu belirlendi. Bu süreçte, aktivasyonlu karbon/endüstriyel atıksu arayüzündeki düzensizlik ve rastlantısallığın arttığını gösteren veriler elde edilmiştir. Önemli bir şekilde, çeşitli kirleticilerin konsantrasyonları, incelenen adsorpsiyon süreci tarafından çok düşük değerlere indirilmiştir. Optimizasyon sürecinin kabul edilebilirliğini belirlemek için aktif karbon liflerine (ACF-NC-LDH) ve toz aktif karbona (PAC-NC-LDH) Yanıt Yüzeyi Yöntemi (RSM) uygulanmıştır. Sonuç olarak üretilen aktif karbon liflerinin ve toz aktif karbonun endüstriyel atık suların arıtılması için adsorpsiyon işlemlerinde güvenle kullanılabileceğini gösterilmiştir.

ANAHTAR KELİMELER: Aktif Karbon Fiber, Kimyasal Oksijen İhtiyacı, Adsorpsiyon, Hurma Lifleri, Yanıt Yüzey Yöntemi

TABLE OF CONTENTS

LIST OF FIGURES

Page

LIST OF TABLES

Page

LIST OF ABBREVIATIONS AND SYMBOLS

AC : Activated Carbon
ACF : Activated Carbon Fiber
CF : Carbon Fiber
COD : Chemical Oxygen Demand
PAN : Polyacrylonitrile
TGA : Thermogravimelric Analysis
MCPA : 4-chloro-2-methylphenoxyacetic acid
EDTA : Ethylene diaminetetra-acetic acid
BET : Brunauer-Emmett-Teller
SEM : Scanning Electron Microscopy
XPS : X-Ray Photoelctron Spectroscopy
TEM : Transmissiom Elctron Microscopy
BET : Brunauer-Emmett-Teller
MB : Methylene Blue
XRD : X-Ray Diffraction
RSM : Response Surface Method
GAC : Granular Activated carbon
PAC : Powdered Activated Carbon
EAC : Extruded Activated Carbon
NRC : North Refineries Company
NC : N-doped Carbon layer
LDH : Layered Double Hydroxide
DI : Deionized
APS : Ammonium Persulfate
H : Enthalpy
G : Gibbs Energy
S : Entropy
T : Temperature
$\mathbf{C}_e$: Final Concentrations At Equilibrium
$\mathbf{C}_t$: Concentrations At Time
$\mathbf{C}_0$: İnitial Concentrations
$\mathbf{q}_e$: Uptake of Adsorbate Equilibrium
$\mathbf{q}_t$: Uptake of Adsorbate at Time
$\mathbf{q}_0$: Uptake of Adsorbate at Initial
$\mathbf{K}_c$: Equilibrium Constant
$\mathbf{R}_L$: Separation Factor
R : Universal Gas Constant

ACKNOWLEDGEMENTS

Praise be to God for His blessings, and He, the Exalted, the Highest, says (If you are grateful, I will certainly give you more).

I extend my thanks and gratitude to my supervisor, **Assist. Prof. Dr. Cem GÖL**. He was a professor, teacher, and brother. He did not skimp on providing information, even for a single moment. My Co-Supervisor: **Prof. Dr. Waleed M. SH. ALABDRABA** had a great role in overcoming problems and obstacles. For him, many thanks and gratitude.

Thanks to **Prof. Dr. Turgay PEKDEMIR** head of the Department of Chemical Engineering, Bolu Abant İzzet Baysal University.

I would also like to thank the **Assist. Prof. Dr Gamze DOĞDU YÜCETÜRK** and **Prof. Dr Murat DOĞRU** for their invaluable comments on my thesis.

Finally, thanks to **my parents, sisters, and brothers** had the biggest role in getting me to where I am now.

1. INTRODUCTION

Water and land resources will be contaminated if petroleum products leak into the environment (1,2). Several researchers (3,4) have reported on the detrimental effects on birds, marine life, and other species. Oil spills have been cleaned up using a variety of techniques, including in-situ burning, the use of sorbents, chemical techniques like the use of dispersants, mechanical techniques like skimming and solidification, and biological techniques like the use of bacteria or enzymes(5–10). Many of these techniques, according to some researchers, are expensive and don't eliminate the components from the spills (11). Planning for environmental cleanup should take into account a solution that won't cause further environmental issues. Natural adsorbents are numerous, affordable, and extremely effective in cleaning up oil spills, making them a highly promising option for environmental treatment. Numerous researchers have discussed the efficiency and environmental friendliness of using natural adsorbents to clean up oil spills (12). Peat moss, rice straws, raw cotton, kapok, milkweed, sugarcane bagasse, maize cobs, rice hulls, and various adsorbents have all been examined (13–17).

Petroleum refineries (18,19), industrial facilities (20), mines, and metal-processing enterprises (21) all regularly discharge oily effluent. These fluids are poisonous and break down oil slowly, endangering both land and marine environments (22,23). These wastewaters may be categorized into three primary groups according to the size of the oil droplet (DP): emulsions (dp 20 m), dispersed oil (150 m > dp > 20 m), and free-floating oil (dp > 150 m). Free-floating and distributed oil may be extracted extremely readily using common methods such as gravity separation, skimming, air flotation, centrifugation, coagulation, and flocculation (24,25). However, stable emulsions are difficult to properly remove using these techniques (26,27).

Emulsions are often removed from wastewater using an adsorption technique (22,28). For the removal of emulsified oil, several adsorbent materials have been investigated, such as biomaterials (29), coal (30), silica aerogel (25), barley straw (31), bentonite (32), meshed corncobs, and carbon (33). Commercially available activated carbon is frequently employed as an adsorbent to remove a variety of contaminants, including oil (34). It is available in granular or powder form. Adsorption, in its broadest sense, is the process of removing a component

from the fluid phase by attracting the component to the surface of a solid adsorbent and adhering to it thereby physical or chemical bonding (35). More specifically, adsorption processes typically take place in interfacial layers, which may be divided into two areas: the adsorbent surface and the adsorption space, where the enrichment of the adsorptive may take place. Depending on the type of forces involved, it may be categorized as either physical or chemical (31). Many physicochemical factors, such as the properties of the adsorbed material (molecular size, boiling point, molecular weight, and polarity), the properties of the adsorbent surface (polarity, pore size, and spacing), the impact of other ions, the particle size, pH of the solution, temperature, and contact time, can affect the effectiveness of the liquid phase adsorption process (36).

A primitive kind of graphite with an amorphous or random structure is known as activated carbon. It has a large range of pore diameters and is very porous, showing cracks, fissures, and slits of different molecular widths that are apparent (37). Activated carbon has a wide range of uses due to its high adsorption capacity, high level of surface reactivity, chemical, and mechanical durability (38). These distinctive properties are often the consequence of the inner pore structure, surface features, pore volume, porosity, chemical composition of the source materials, the presence of functional groups on the pore surface, and the activation process (39).

Adsorption onto activated carbon is a better method for treating wastewater because other physical and chemical techniques such as flocculation, coagulation, precipitation, and ozonation have been found to have limitations such as their high cost, formation of hazardous by-products, and intensive energy requirements (40). Activated carbons that are sold commercially are still regarded as pricey (41). This is because pollution control applications do not require the use of start-up resources such as coal, which are non-renewable and relatively expensive. (42). As a result, in recent years, there has been an increase in research interest in the production of activated carbons from renewable and less expensive precursors, mostly industrial and agricultural waste products, such as date pits (43), silk cotton hull and maize (44), jute fiber (45), groundnut shell (46), corncob (47), bamboo (48), rattan sawdust (49), and oil palm fiber (50).

Due to its many adtantages over other commercial storage materials, activated carbon fiber (ACF) is considered to be one of the best absorbents for adsorption applications. If it is made properly, it is a great microporous material

with the lowest microporosity. The relevance and use of ACF for adsorption applications are demonstrated by its high packing density and great volumetric capacity (51). Several applications, including as removal of heavy metals (52), medical devices (53), capacitors (54–56), refrigeration (57–59), catalysis (60–62), electrochemical applications, and natural gas, and biogas storage, and vapor sensing (63), benefit greatly from these ACF (64–67). Carbon fiber (CF) is commonly used to make ACF, and the processes are very similar to those used to make AC. A straightforward explanation of the activation procedure is an extra thermal treatment of the CF in an oxidizing environment at temperatures between 700 °C and 1000 °C (68). The common AC and ACF reveal variances in the pore structure. Adsorbate gas molecules must first travel via macropores and then mesopores for a second path before entering micropores in common AC, which has a ladder-like structure. Adsorbate gas that is directly exposed to the surface of the fibers in ACF can reach micropores in high quantities, aiding the adsorption process (68). ACF are manufactured for use in the industry by first pyrolyzing carbonaceous synthetic polymer materials such as rayon (51), pitch, saran, polyacrylonitrile (PAN), and phenolic resin. This is then followed by a further activation procedure. The cost of processing is a significant factor when using ACF in commercial applications. Recent studies have concentrated on producing cost-effective ACF from agricultural wastes in the form of biomass to reduce processing expenses (69,70). These raw materials have previously been processed to become natural fibers. By using biomass as ACF material, it is possible to solve the problem of waste disposal and turn waste into money.

A byproduct of many industrial and small-scale commercial operations is oily wastewater. Refineries produce a lot of wastewater due to their high water consumption. They frequently require high-quality water to fulfill environmental and design regulations. Furthermore, they could have to repurpose the cleaned wastewater in areas where water is limited. This implies that they must effectively remove dangerous contaminants from the wastewater. Typically, indicators like Total Organic Carbon (TOC) and Chemical Oxygen Demand (COD) are used to quantify the organic matter in wastewater (71).

A critical metric for evaluating wastewater's organic pollution content and water quality is chemical oxygen demand (COD) which is a substantial contaminant present in the wastewater from industrial and petroleum refineries. To lower COD,

a range of treatment methods have been used, including flocculation, filtration, ion exchange, reverse osmosis, and electro-dialysis. The environment and industrial processes may suffer from high COD levels. Wastewater treatment thus becomes necessary to reduce COD levels before discharge or reuse. Adsorption, one of the many techniques for reducing COD, is a promising strategy in which organic pollutants are adsorped onto the surface of an adsorbent, a solid substance (72).

1.1 Literature Review

Numerous studies investigated the viability of producing and manufacturing activated carbon using a variety of organic wastes. The first way in which this field helps to reduce environmental pollution is through the waste used in the active carbon production, and the second way is through the active carbon used in the pollutant's adsorption like heavy metals, petroleum oils, and other organic materials. A process known as adsorption involves one or more adsorbates that are attached to an adsorbent through chemical or physical connections. Due to its simplicity, effectiveness, economic viability, and social acceptability, adsorption is a common method used in wastewater treatment to remove contaminants from water.

Because of their high porous surface area, adjustable pore structure, thermostability, intriguing acid/base characteristics, and inexpensive cost if the preparation is made from byproducts, activated carbons are the most common adsorbents employed. According to Li and Wang (73), activated carbons are particularly effective in removing a variety of organic and inorganic pollutants that are dissolved in gaseous or aqueous systems.

Since people have been using activated carbon for such a long period, its origin is unknown with certainty. Before being utilized as an adsorbent, what is today known as activated carbon which has a highly developed porous structure was either wood char, coal char, or just a carbonaceous material that had partially been devolatilized. The first example dates to 3750 BCE when the Sumerians and Egyptians both used wood char as a smokeless fuel and to reduce copper, zinc, and tin ores for the creation of bronze (74). A papyrus text from Thebes (Greece) that dates to 1550 BCE contains the first evidence of the therapeutic use of carbon. Later, Hippocrates (about 400 BCE) advocated filtering water with wood char before ingestion to remove unpleasant flavors and odors and to ward off numerous ailments, such as epilepsy, chlorosis, and anthrax (75). It wasn't until Dr. D.M. Kehl

employed wood char to reduce gangrene's smells in 1793 that activated carbons were first reportedly used as a gas phase adsorbent. In England in 1794, activated carbon was utilized as a decolorizing agent in the sugar-producing business, which was the first industrial usage of the material. In the middle of the 19th century, activated carbon was used for the first time on a wide scale in the gas phase. To eliminate offensive odors, the Mayor of London authorized the installation of wood char filters in all sewage ventilation systems in 1854. Gas masks with carbon filters were first employed in chemical plants in 1872 to avoid mercury vapor inhalation (75). Due to stricter environmental regulations regarding water resources, the use of clean gas, the regulation of air quality, energy storage, and conversion, and the economic recovery of valuable chemicals, the rapid development of modern society during the 20th century encouraged a fast-growing production and use of activated carbon. This was especially true throughout the second half of the century. The use of these lignocellulosic products and other sources of waste biomass for the synthesis of activated carbons has also been recommended, along with the advice to replace goods manufactured from petroleum (76).

Fan et al. (74) examined the synthesis of activated carbon by Thermal Gravimetric Analysis (TGA) using corn stover and oat hulls. Without any pre-treatment, fast pyrolysis was carried out in a nitrogen-fluidized bed reactor at a typical biomass input rate of 7kg/h. At 500 °C in a fluidized bed reactor, Zhang et al. (77) looked at the carbonization of used oak wood, corn stover, and maize hulls. TGA was used to pyrolyze and subsequently gasify chars generated from sunflower shell, pinecone, rapeseed, cotton, and olive wastes in the work by Haykiri-Acma et al. (78). The acquired chars were heated to produce gasification while being surrounded by equal parts steam and nitrogen. Under isothermal conditions, the atmospheric reactivity of Pinus radiata, Eucalyptus maculate, and sugar cane bagasse was evaluated using a thermogravimetric analyzer (79). The heat-up's nominal heating rate was 40°C/min. The sugar cane bagasse, which is hulls of rice, straw from rice, and pecan shells was also studied in an inert environment furnace with a reaction at 750°C in a nitrogen gas atmosphere. The chars were started up to a 30% burn-off. (80).

The most important factor is the pyrolysis temperature, followed by the rate of decomposition heating, the flow rate of nitrogen, and lastly the length of the pyrolysis residence time. Higher pyrolysis temperatures frequently result in lower

yields of chars and ACs. According to Rehrah et al. (81), as temperature increases, more liquids and gases are produced while less solid material is produced. As the temperature rises, the amount of ash and fixed carbon increases while the fraction of volatile elements decreases. Therefore, charcoal produced at higher temperatures is of higher quality. The production of some non-condensable gaseous chemicals by the following breakdown of the char at higher temperatures also contributes to the rise in gas output. When primary degradation temperatures increase or primary vapor residence times inside the fragmented particle must be shortened, the char yields decrease (82). Tsai et al. also looked at the temperature for the chemical activation ($ZnCl_2$) method of producing ACs.(83). It was established that the temperature has a negative link with char yield, however soaking duration did not affect char yield.

Macias-Garcia et al. (84) utilized 1.5 mm Merck carbon and subjected it to different treatments: successive SO_2 and H_2S treatments at room temperature, SO_2 treatment at 900°C, and SO_2 treatment at room temperature. Additional testing was done on these samples to see how well they functioned as Cd^{+2} adsorbents for aqueous solutions. The scientists discovered that sulfur was introduced in significant amounts when heated in SO_2 to 900°C and in negligible levels when sulphurized in SO_2 at ambient temperature. It was determined that there was a connection between the sulfur supply's level and the drop in surface area and microporosity. The samples' elevated sulfur content had no discernible impact on the Cd^{+2} adsorption kinetics. It was found that the solution's treatment, temperatures, and pH all had an impact on the adsorption capacity. The best remedy was heated to 900°C and had an adsorption rate that was 70.3%. The adsorption increased at 45°C but decreased at pH 2.0 compared to the adsorption at 25°C and pH 6.2.

On activated carbon with various surface chemical properties, Krzysztof et al. (85) adsorbed phenoxy herbicides such as 2-(4-chloro-2-methyl phenoxy) acetic acid (MCPA), 2-(4-chloro-2-methyl phenoxy) propanoic acid (MCPP), and 4-(4-chloro-2-methylphenoxy)butanoic acid (MCPB). Nitric acid oxidation was used to demineralize activated carbon (AC-NM) and create an oxidizing adsorbent (AC-OX) with an acidic surface. A thermal treatment in ammonia at 900 °C was used to create basic activated carbon (AC-AM). Strong pH dependence was seen in the adsorption of herbicides; ionic strength had no influence. Przepiorski (86)

investigated how gaseous ammonia treatment at temperatures ranging from 400°C to 800°C affected the adsorption of phenol from an aqueous solution. It was discovered that at the ideal treatment temperature (700°C), the adsorption capacity toward phenol was increased by as much as 29%. The capacity of the activated carbons to adsorb phenol was higher in those with more micropores.

Mahdieh Raji et al. (72) used a heterogeneous Fenton catalyst for the treatment of melanoidin wastewater on an activated carbon fabric support covered with chitosan and loaded with zero-valent nanoiron. With chitosan coating on ACC, synthetic melanoidin effluent with 8000 mg/l COD could be treated with 88.4% and 76.2%, color and COD removal respectively.

Iqbal Erabee et al. (87) researched a down-flow fixed-bed activated carbon model water treatment method. The raw materials for the two forms of activated carbon powder and granular come from date kernels. The criteria that are assessed include pH, total suspended solids (TSS), total solute solids (TDS), chemical oxygen demand (COD), and biochemical oxygen demand (BOD). The volume of activated carbon was changed, while the column diameter and layer depths remained constant. Granular activated carbon removed 39.8% of BOD, 41.8% of COD, 81.8% of TSS, and 67.7% of TDS from the river water sample. The elimination efficiency of 34.7% of BOD, 17.6% of COD, 72.7% of TSS, and 50% of TDS are the specifications for activated carbon powder.

Research on the adsorption of chemical oxygen demand (COD) from wastewater treated with inexpensive activated carbon made from waste palm shells by chemical activation technique was reported by Abdelaziz A. Nayl et al. (88). Additionally, they studied several variables that affect the adsorption process, including temperature, stirring rate, contact time, pH and carbon dosage. According to the data, 95.4% of the COD was removed.

Research by F.M. Ferraz et al. (89) aims to recover oat hulls as activated carbon by using the adsorbent that is created when organic elements are removed from landfill leachate. Chemical oxygen demand (COD) and color measurements were used to evaluate the leachate's organic matter composition. Furthermore, it was established what the adsorbents' maximal adsorption capabilities were. In the beginning, adsorption batch experiments were conducted using the synthetic leachate, and factors including pH, temperature, contact time, and activated carbon dosage were assessed. It was also confirmed that the adsorbents worked well with

actual landfill leachate. It was discovered that utilizing a 20 g dosage of activated carbon in adsorption experiments conducted at 20°C and pH 4 was preferable for the removal of organic materials from the synthetic leachate. The activated carbon sample that was 100% phosphoric acid loaded and pyrolyzed at 500 °C under these experimental circumstances decolored the leachate and removed up to 90% of the COD.

In Tehran, Iran, Erfan Nabavi et al. (90) conducted a series of laboratory tests to assess the effectiveness of ozonation either alone or in conjunction with granular activated carbon (GAC) adsorption of leek field leachate. Oxidizing the GAC surface with ozone before treatment increased the removal of resistant pollutants from the leachate. TDS, COD, and BOD removal were investigated for ozone alone and in conjunction with GAC (ozone-GAC integrated adsorption) based on ozone concentration and GAC intensity. Subsequently, the outcomes were contrasted with those of additional chemical and physical therapies that had been noted in a few earlier investigations. The ideal operating conditions were obtained by evaluating the interaction and correlation between operating factors (i.e., ozone concentration, GAC density, and reaction time) through the creation of a central composite design using response surface methodology (RSM). Due to the low probability values (0.0001) of the three responses (COD, TDS, and BOD), statistical analysis and experience indicated that quadratic models were adequate and effective. The ideal parameters were 33.77min of reaction time, 1.00g/cm^3 GAC density, and 100 mg/l of ozone concentration. The model yielded clearance rates for dissolved solids, COD, and BOD of 46, 44.81, and 44.13%, respectively. When compared to the ozone-alone approach COD (25.1%) and TDS (25.7%) % and BOD (43.6%), combined ozone-GAC absorption employing ozone-modified GAC (COD (55.2%), TDS (54.4%), and BOD (56.5%) shown satisfactory performance among the purification methods evaluated. The treated effluent did not exceed discharge limits, thus additional biological treatments such as active nitrification or sludge are still required to finish the leachate decomposition process and adhere to environmental rules.

Activated carbon fiber (ACF) was made using acrylic textile fibers by Carrott et al. (91). With the active fibers at 900 °C. It was discovered that, with one fiber in particular, the number of micropores tripled, the average pore width abruptly rose, the average stack height, L, abruptly fell, and the reactivity decreased by more than

half throughout a relatively constrained burn range between 40% and 50%. The observed variations point to a shift in the c-activation process from one that largely involves single crystal attack and rearrangement at greater combustion to one that primarily involves gasification of amorphous or more reactive carbon at lower combustion.

Using textile polyacrylonitrile fibers, Junior et al. (92) produced and characterized carbon fiber felts and activated carbon fibers. Textile polyacrylonitrile fiber was used to create carbon fiber felt and activated carbon fiber feel. The oxidized material was then turned into felt and then transformed into carbon fiber felt and activated carbon felt. By using X-Ray photoelectron spectroscopy, carbon fiber hair, and activated carbon fiber hair were separated. The primary outcome was the dynamic transformation of textile polyacrylonitrile fibers into felt-like carbon fibers and activated carbon fibers into felts with large surface areas and high micropore contents.

Through a process of carbonization and chemical activation, Kumar et al.'s (93) research produced activated carbon fibers from plastic solid waste. The obtained activated carbon materials' shape, composition, thermal stability, and pore structure were all described.

Chitosan-loaded activated carbon fibers (CS/ACF) were effectively created by Yue Teng et al. (94) for the adsorption of Pb(II)-EDTA from electrical effluent. The CS was effectively loaded onto the surface of the ACF, many oxygen/nitrogen functional groups were observed according to the results of the characterization. The adsorption capabilities of ACF and CS/ACF of Pb(II)-EDTA were investigated using batch adsorption experiments. PH_0 had a mildly negative influence on Pb(II)-EDTA uptake by CS/ACF throughout a large range (2.00-12.00), whereas PH_0 had a considerably beneficial impact on Pb(II)-EDTA uptake by ACF. Adsorption equilibrium on CS/ACF could be obtained in 30min after 99.40% of Pb(II)-EDTA (0.1988mmol • g) was removed. ACF, on the other hand, could only remove 52.75% of the Pb(II)-EDTA (0.1055mmol • g).

By using amine-modified cellulose-based activated carbon fiber (KF1500LDA), Matsuzawa et al. (95) created activated carbon fiber (ACF) with improved phosphate ion adsorption capability. Raw material for the KF1500LDA has undergone hydrogen oxidation. To increase the quantity of phosphate ion adsorption, diethylenetriamine (N-(2-aminoethyl)-1,2-ethylenediamine) was

combined with peroxide solution for two hours before reacting with it at 10°C for six hours. The highest rate of absorption occurred at an equilibrium pH of 3.0, which was 0.13mmol/g.

To collect carbon dioxide and store CH_4 and H_2, Raeesh Muhammad et al. (96) produced activated carbon nanofibers made from spider silk fibers. The methane storage capacity for the produced sample was 8.6mmol/g at 0°C, 25 pressure, while the H_2 storage capacity was 4.1 wt% at 196°C, 25 bar. Additionally, as demonstrated by the adsorption and desorption cycles, the produced carbon material demonstrated simple regeneration and minimal adsorption capacity loss.

A variety of porous carbons made from bamboo bark were created by Wenjun Wu et al. (97) using a two-step process that involved carbonization and activation of potassium carbonate (K_2CO_3). Rhodamine B (RhB) was eliminated from the wastewater and carbon dioxide from the flue gas using porous carbonaceous char made from biomass. The structure of surface evolution of K_2CO_3 activated carbon porous was studied using surface topography studies using Brunauer-Emmett-Teller (BET), scanning electron microscopy (SEM), and electron microscope (TEM). The activated biochar has a significant carbon dioxide (CO_2) adsorption capacity at 800°C, reaching 6 and 3.44mmol/g at 0.0°C and 25.0°C at 1.0bar, respectively. The sample's specific surface area rose after activation from 80.35 m^2 /g to 1439 m^2 /g. The adsorbent, on the other hand, demonstrated exceptional cycle stability and selectivity for carbon dioxide and nitrogen oxide. The porous carbon adsorption properties of the dyes in aqueous solution at room temperature were also examined in addition to CO_2 adsorption from flue gas. The results show that RhB can be successfully removed from wastewater by employing carbon that is porous and made of bamboo veneer.

An N-doped AC was created by Li et al. (98) using urea as the nitrogen supply and corncob as the carbon precursor. This AC demonstrated good electrochemical performance. To increase the ammonia removal capacity, Soo-Jin et al. (99) fluoro-oxidized activated carbon fibers (ACFs). By using XPS analysis, it was established that polar groups, such as C-F, C-O, and COOH, had been introduced into the ACFs. BET and t-plot techniques were used to examine the N_2/77K adsorption isotherms' specific surface area, aggregate volumes, and tiny holes. The use of the gas detection tube approach demonstrated the effectiveness of ammonia removal. As a result, when the surface treatment duration rose, the ACFs' unique surface area

and micropore size were partially damaged. However, the oxygen-fluorinated ACF enhanced the polar functional groups on the surfaces of the ACF that contained fluorine and oxygen, which boosted the effectiveness of the ACFs generated by removing ammonia.

Activated carbon fibers (ACFs) were effectively created from palm oil stems by Jian Lin et al. (100). The raw fibers' thermal resilience was increased by an efficient chemical procedure using diluted sulfuric acid in preparation for additional heat treatment. An activator, CO_2 was employed to create a porous structure with various pore sizes. With increasing activation temperature and time, the pore volume total (V_{total}) and surface area of specific (SBET) of the resulting ACFs both exhibited an upward trend. The ACFs produced at 900°C for 90 min had higher SBET and V_{total} values of more than $1800\,m^2/g$ and 0.7ml/g respectively. The synthesis of functional groups containing oxygen occurred throughout the activation process with CO_2 as a result of more graphical carbon being degraded on the ACF surface as the activation duration was extended. ACFs have demonstrated good chromium adsorption ability due to the number of pores and surface functional groups and will be a substitute material for industrial adsorption usage.

Activated carbon fiber (ACF) was created by Ka-Lok Chiu et al. (101) by annealing and activating cotton with $ZnCl_2$ in argon. It was discovered that the cotton preserved its original fiber structure and transformed it into microporous ACF. Its $2060 m^2/g$ BET surface area. The adsorption of methylene blue (MB) in water at various pH levels was used to assess the adsorption capability of this ACF product. It is discovered that the Langmuir isothermal model and the pseudo-2nd-order kinetic model both did an excellent job of explaining the adsorption procedure. The ACF sample could successfully adsorb the methyl bromide in both neutral and alkaline conditions.

The ACF generated from Oil Palm Empty Fruit Bunch fibers by the one-step direct activation technique (ACF-D) was compared to the ACF produced by the traditional two-step carbonization and activation (ACF-ND) by Chee-Heong Ooi et al. (102). The various characteristics of the created ACFs were looked at. EDS, SEM, FTIR, and XRD were used to characterize raw EFB and ACFs. According to the findings, EFB has an oxygen content of 36.67wt% and a carbon content of 63.33wt%. ACF-D was discovered to have a lot of carbon (93.63wt%), but little oxygen (5.19wt%). ACF-ND produced a sample with a lower oxygen content (3.85

wt%) and a greater carbon content (95.68 wt%). For both ACF samples, there is no obvious distinctive peak in the XRD findings.

Wan-Cheng Tan et al. (103) created ACF using the natural fibers of oil palm fruit bunches that were empty. To study the pyrolysis and combustion behaviors of the various gases, thermogravimetric analysis was carried out utilizing two distinct gases, namely nitrogen gas and oxygen gas. The results of derivational thermometry were then used to calculate the carbon temperatures of the peaks. To examine the impact of the carbonization temperatures on the features of the nanopores, namely surface area, pore size distribution, and pore size of the generated ACF, different carbonization temperatures ranged from 85 °C to 200 °C were used to carbonize the EFB fibers. The as-prepared ACF showed good nanoscale characteristics, including a surface area of 2740m^2/g.

Wee-Keat Cheah et al.'s method (104) of produced ACF from empty oil palm fiber (EFB). The ACF produced following the carbonization and activation operations had uniformly wide pores with thick channel walls, according to the FESEM results. The optimum ACF preparation was determined to be at a 1.5:1 ratio of acid fiber to EFB, where the ACF's 1.2nm-diameter pores were examined with a mostly tiny pore size of 0.39cm^3/g and a (BET) area of surface of 869m^2/g.

Based on two precursors, namely viscose rayon and phenolic resin, Vivekanand Gaur et al. (105) created activated carbon fibers (ACFs) by carbonization followed by physical activation with steam or carbon dioxide. They tested the manufactured ACF samples in a fixed bed tube reactor for their suitability for the non-equilibrium adsorption of SO_2, benzene, toluene, and m-xylene (BTX), which are major gaseous pollutants in the environment. The adsorption capacity of ACF for BTX and SO_2 was linked to the compositional and surface characteristics of the ACF samples. They found that BTX absorption increased as the BET area or micropore size increased. On the other hand, they discovered that BTX adsorption was negatively impacted by surface groups that contained electronegative oxygen atoms.

To create activated carbon fiber (ACF)/carbon composite films, Yonghong Wu et al. (106) compressed and carbonized a powdered mixture of phenolic resin and activated carbon fibers. They investigated how the separation performance of an emulsified water-oil solution composite membrane was affected by ACF dosage, transmembrane pressure, and feed flow. The findings demonstrate that ACF

addition is advantageous in improving the separation performance of films made from oily wastewater.

Ling Zhang et al. (107) generated activated carbon fibers using coconut fiber as the raw material by carbonization and KOH activation procedures. They methodically detailed the activated carbon fibers' form, content, surface area, pore structure, and thermal stability. It has been discovered that the activation procedure significantly improves the specific surface area of carbon fibers by creating plenty of micropores (0.7-1.8nm) and a few medium-slit holes (2-9nm). The activated carbon fibers have a specific area of surface and volume of pore of 1556cm^2/g and 0.72 cm^3 /g respectively. By pyrolyzing the tar deposits left behind after the carbonization process, the activation process can help smooth up the surface of the activated carbon fiber. Methylene blue, Congolese red and neutral red were among the organic dyes whose adsorption capabilities and kinetics were examined to analyze the adsorption characteristics of the generated activated carbon fibers. The adsorption capabilities of the dyes varied greatly with the pH value of the solution and increased with increasing starting dye concentrations.

Table 1.1. summarises the literature on adsorption of pollutants by activated carbon with the respective removal efficiencies.

Table 1. 1 Literature on adsorption of pollutants by activated carbon with their respective removal efficiencies.

Ref.	Type	Year	Pollutants	Raw materials	Removal efficiency %
(72)	AC	2021	COD	-	76.2
			Colors		88.4
(87)	AC	2018	COD	Date pits	41.8
			BOD		39.8
			TDS		67.7
			TSS		81.8
(88)	AC	2017	COD	Date palm	95.4
			BOD		92.8
(89)	AC	2020	COD	Oat hulls	90.0
(90)	AC	2022	COD	Commercial	44.8
			BOD		44.1
			TDS		46.0
(108)	ACF	2021	COD	Commercial	94.0
			Cr(VI)		97.0
(109)	ACF	2021	COD	Commercial	72.0
			Colors		91.0
(110)	ACF	2017	COD	Commercial	82.3
			TOC		79.5
(111)	ACF	2023	COD	Commercial	71.2
			TOC		67.4
			NH4+-N		69.3
(112)	ACF	2021	COD	Commercial	96.0

			BOD		95.6
			TDS		91.0
			TSS		76.6

1.2 Aim and Scope of the Study

If petroleum products seep into the environment, water and land resources would suffer. Several researchers have discussed the negative effects on other species, including birds and marine life. Researchers have used a variety of techniques to eliminate contaminants, such as in situ burning, mechanical methods such as "skimming" and hardening, chemical techniques such as the use of dispersants, and biological techniques such as treatment with bacteria or enzymes. Activated carbon is one of the most effective modern methods for adsorbing environmental pollutants from water.

This study aims to produce activated carbon fibers using natural palm fibers, which are considered one of the most abundant agricultural pollutants in Iraq, in three methods to determine which method is better and to obtain the best production in terms of adsorption effectiveness. Activated carbon fibers could be produced to absorp organic pollutants from the wastewater. Chemical oxygen demand (COD) was determined as a way to determine the amount of organic matter causing water pollution. Iraq is considered to be one of the places with the most water contaminated with oil pollutants (113), and the Baiji refinery will be selected as a site for receiving water contaminated with oil and organic waste. In addition, to increase the efficiency of activated carbon fibers and increase absorbency, the fibers will be chemically treated. In addition to the tests, calculations, and results to be carried out, the Response Surface Theory (RSM) will be used, which aims to conclude whether or not the study is useful according to the variables used in the experiment.

2. THEORETICAL FUNDAMENTALS

2.1 Activated Carbon

Activated carbon (AC) is increasingly employed in a range of industrial processes, including air and gas cleaning using typical reusable material recovery procedures (114). Furthermore, activated charcoal is being used more frequently to treat water, including water for drinking, water in the ground, industrial water, and wastewater. In this application, its primary role is to absorb dissolved organic impurities and filter out compounds that change the flavor, color, and odor of hydrocarbon halogens and other organic pollutants. (115). The pharmaceutical, food, beverage, and other sectors, as well as others, rely on liquid treatment, purification, and decolorization. This is yet another important application for activated carbon. Activated carbon (as shown in Figure 2. 1) must be employed in the best feasible form based on the physical and chemical qualities of the chemicals to be absorbed (116).

A variety of raw materials, including coal, peat, lignite, bitumen coal, fruit stones (like olive seeds), coconut shells, and more, are used to create activated carbon. These materials can be activated in two different ways (117). During the gas activation process, carbonized material is exposed to the oxidation properties of a gas stream, such as moisture, carbon dioxide, air or a mixture of these materials. Activation temperatures typically range from 700 °C to 1100 °C. A water-gas reaction develops as a result (118).

$$C + H_2O \rightarrow CO + H_2$$

$$C + 2H_2O \rightarrow CO_2 + 2H_2$$

After the carbon is partially gasified, a porous, highly active carbon skeleton is created. In the chemical activation phase, non-incinerated carbonaceous matter is initially mixed with dehydration or oxidized chemicals and heated to temperatures between 400 °C and 800 °C. The activation agent, which could include zinc chlorine, acid phosphoric, sulfur dioxide, or another material, can be removed and recovered by leaching (119).

The actual activation procedure is carried out in fluid bed reactors, multiple-hearth, shaft, or rotary kilns. Activated carbon may be found in a variety of forms, including:

- Extruded (often as cylindrical pellets) (120)
- Broken (activated carbon that is broken or granular) (120)
- Powder with a range of particle sizes (121)
- Spherical activated carbon pellets, activated carbon fibers, carpets, and honeycombs are some of the specially-made varieties. (122).

The adsorptive capacity of the end products created with activated carbon is significantly influenced by the manufacture, activation, and basic raw materials used. (123). The choice of activation method has a significant impact on the size of the inner surface area and the pore structure (124).

Figure 2. 1 Types of activated carbon (125)

2.1.1 Activated Carbon Application Area

Activated carbon has several applications (Figure 2.2). Depending on the application, a unique kind of activated carbon is employed (126). Therefore, it's crucial to select the appropriate grade and size while considering the pollutant you want to eliminate or the amount of purity you want to take into consideration(127).

- **Gas and Air**

To filter gases, many types of activated carbon can be used. Cloth, pelletized, and granular activated carbon are examples of the specific forms that can be used depending on the desired results (128). Applications for activated carbon in gas purification include filtering breathing air in air conditioners and eliminating hydrogen sulfide from natural gas. In this second use, activated carbon aids in purging the recirculated air of radon and smells (129).

- **Mining**

Activated carbon is also used in the mining process to extract gold and other precious metals. Due to its adsorption capabilities, activated carbon is employed in the latter stages of mining to extract carbon from cyanide (129,130).

- **Food and Drinks**

In the food and beverage industry, activated carbon is used to improve the flavor, smell, and purity of a variety of foods and beverages, including concentrated juice. Activated carbon can be used to decolorize sweeteners and remove undesirable by-products from them (131).

- **Water Treatment**

Both primary and tertiary treatments for water treatment include adsorption by using activated carbon. Granular and powdered activated carbon are both used to purify water (132). The primary goal of the first treatment is to eliminate and retain big particles. Activated carbon is used to reduce taste and odor in the last stages of water purification (133).

Figure 2. 2 Activated carbon application area (134)

2.1.2 Types of Activated Carbon

Depending on the source material and the processing methods used to generate it, the final product's physical and chemical properties may differ significantly. As a result, there are many variations of commercially produced carbons that may be produced (135). Because of this, industrially produced activated carbons are highly customized to provide the best outcomes for a given application (136). Activated carbon is generated in three primary categories, notwithstanding this variation: Powdered Carbon Activated (PAC), Granular

Carbon Activated (GAC) and Extruded Carbon Activated (EAC) shown in Figure 2.3.

Figure 2. 3 Main types of activated carbon, (A) granular activated carbon, (B) extruded activated carbon, (C) powdered activated carbon (137).

2.1.2.1 Powdered Activated Carbon (PAC)

As its name suggests, PAC is in the shape of particles, often measuring between 10μm and 100μm in diameter. One benefit of PAC is that it may be used for brief durations when issues emerge and then stopped when it is no longer necessary (138). This can be a huge economic advantage for issues like algal toxins or tastes and odors that may only seldom occur. The fact that PAC is currently disposed of in garbage together with treatment sludge or backwash water is a drawback (139). Figure 2.4 shows the powdered activated carbon.

Figure 2. 4 Powdered Activated Carbon (137).

2.1.2.2 Granular Activated Carbon (GAC)

Granular activated carbon (Figure 2.5), commonly referred to as GAC, is a high-purity type of carbon distinguished by its enormous surface area and employed in several liquid and gas phase purification applications in Figure 2.5. The granules' usual particle sizes range from around 0.2mm to 5mm, with the selection of "mesh

size" dependent on the intended application for the material. Powder-activated carbon (or PAC) is often defined as particles less than 0.2mm. The extruded pellet, which provides a consistent cylinder of carbon with a standard 3mm or 4mm diameter, is the other primary physical form of activated carbon. The most common materials used to make granular activated carbon are bituminous coal, coconut shells, and some types of wood (140). The decision is also influenced by the end user the client has in mind. Each raw material produces granular activated carbon with somewhat varied physical qualities, in terms of purifying performance (141).

Granular activated carbon has minuscule holes and channels, or pores, on its surface that can only be seen with a strong enough microscope. A teaspoon of granular activated carbon has the same surface area as a football pitch thanks to these pores, according to an often-cited figure (142).

The pollutants are held inside these holes in a procedure known as adsorption when a polluted fluid passes through a filtering device made of granular activated carbon (143). This allows the cleaned fluid to flow through. Granular activated carbon is frequently used to remove taste, odor, and color from water as well as residues of other dissolved pollutants including pesticides and herbicides (144).

Granular activated carbon (GAC) may be recovered for reuse through a process known as thermal reactivation, which is one of the main benefits of employing GAC for fluid purification rather than powder-activated carbon. Spent carbon can be put through a high-temperature kiln until the pores are filled with impurities and the treatment goal is no longer met. Granular activated carbon is reactivated and ready to be utilized repeatedly in the customer's process once the contaminant molecules are driven out of the pores and destroyed (145).

This method of recycling granular activated carbon not only saves money but also has significant environmental advantages, since it reduces CO_2 emissions by over 90% when compared to using new, "virgin," material (146).

Figure 2. 5 Granular Activated Carbon (137).

2.1.2.3 Extruded Activated Carbon (EAC)

Extruded activated carbon (Figure 2.6) is a cylindrical block with a diameter ranging from 0.8mm to 130mm that is constructed of a binder and powdered activated carbon. They are typically used for gas phase applications due to their good mechanical strength, low dust content, and low-pressure loss. CTO (Chlorine, Taste, and Odor) filters are furthermore offered. (147–149).

Figure 2. 6 Extruded Activated Carbon (150)

2.1.3 History of Activated Carbon

Activated charcoal was initially employed by the Egyptians to process ore into bronze about 3750 B.C., which is the first known application of the substance. By 1500 B.C., the Egyptians were also employing it to write on papyrus, treat digestive disorders, and absorb offensive smells (151). The antibacterial qualities

of activated charcoal were discovered by the Ancient Hindus and Phoenicians about 400 B.C., and they started utilizing them to cleanse their water (152). It was common practice to keep water in burned barrels throughout any lengthy sea cruise. Hippocrates and Pliny were pioneers in the use of activated charcoal in medicine around the year 50 A.D. They used it to treat a wide range of conditions, including vertigo, chlorosis, and epilepsy, among others. Following the prohibition of science during the Dark Ages, charcoal made a comeback in the 1700s and 1800s as a component of medicinal treatments because of its ability to absorb fluids and gases as well as its disinfecting capabilities (153). This historical period saw the use of charcoal powders to treat stomach acidity, fetid ulcers, and even nosebleeds when subsulphate of iron had failed, as well as charcoal poultices prepared from charcoal and bread crumbs or yeast (a favorite of army and naval physicians). Even lozenges, crackers, and tooth powders were starting to be advertised as charcoal by the 1900s (154,155).

Today, activated carbon is employed in real-world settings including homes, hospitals, and care facilities for both people and animals. Charcoal is utilized in medical institutions all around the world for a variety of purposes, including filtering lab technician masks, devices for liver and kidney dialysis, and even as markers in breast cancer surgery (156,157). Veterinarians use charcoal to help eliminate toxins from pets who may have swallowed anything that might be detrimental to them (like when dogs eat chocolate!), much as charcoal has been used to help remove toxins from people (158). Additionally, activated charcoal has established itself in daily life, appearing in items like our Black Bamboo Activated Charcoal and Forest Path soaps as well as in air filters and water filtration systems (159).

2.2 Activated Carbon Fibers ACFs

Because of its numerous benefits over other commercial storage materials, activated carbon fiber (ACF) ranks as one of the best absorbent materials in adsorption applications. It is an excellent microporous material with minimal mesoporosity and, most likely, no macroporosity, highlighting its value and applicability for adsorption applications. If it possesses outstanding porosity and volumetric capacity (160). Depending on the source material and how it is formed and processed, ACF (Figure 2.7) can be produced in a wide range of compositions, structures, and methods. It is difficult to make unambiguous generalizations

regarding ACF and the materials based on ACF (161). ACF has lately piqued the curiosity of many scientists worldwide due to its high adsorption capacities and speedy adsorption rates when compared to other carbons. Numerous instruments and methods, such as small angle scattering and scanning electron microscopy (162).

ACFs, or activated carbon fibers, are porous carbons that are shaped like fibers and have an aspect ratio greater than 10. They have a well-defined porous structure and a high adsorption capacity. To meet the requirements of particular applications, ACFs are often prepared from general-purpose carbon fibers using a heat treatment that results in high porosity (163). ACF has been the most recent improvement in the family of porous carbon for adsorption thanks to its large surface area. Potential applications for adsorption have expanded thanks to this enormous benefit for the past 50 years, the primary study areas on the development of ACFs have been the knowledge of ACF processing, from the synthesis of initial precursors to the derivation of end products, and the characterization of ACF in specific applications (164).

Figure 2. 7 Activated Carbon Fibers (165).

2.2.1 Activated Carbon Fiber Production

Carbon from carbonaceous resources including bamboo, and husks of coconuts, willow peat, trees, coir, lignite, coal, and oil pitch is used to make activated carbon fiber. By using one of the techniques listed below, it can be created (166): Carbonization Process, Physical Activation, and Chemical Activation.

2.2.1.1 Carbonization Process

When preparing AC, the carbonization procedure is crucial since it determines how the finished product will be imprinted. To generate the appropriate quality of the finished AC, it is crucial to carefully choose the carbonization settings (167). The carbonization temperature is one of several variables that might alter the structure during the carbonization process. Typically, materials are carbonized by researchers between 500°C and 900°C. When carbonized at high temperatures, the samples will release more volatiles, which will eventually affect the product yield and porosity (117,168). However, the ability to react to the wide range of carbonization temperatures still depends on the characteristics of the initial raw material. Carbonization consists of two main steps: oxidative and nonoxidative pyrolysis (141,163,169).

2.2.1.2 Physical Activation

Using heated gases, the raw material is transformed into activated carbon fiber. The gases are subsequently ignited by air, producing a graded, segregated, and dustless type of activated carbon. Typically, a sequential process method is used for this (170):

- **Carbonization:** Carbon-containing materials are pyrolyzed between 600 and 900 °C, often in an inert environment with gases like argon or nitrogen (162,171).
- **Activation/oxidation:** At temperatures exceeding 250°C, often in the range of 600-1200 °C, Oxidizing atmospheres (oxygen or steam) are exposed to raw materials or carbonized materials. (172).

2.2.1.3 Chemical Activation

The carbon material is injected with certain compounds. The chemical is often one of the following kinds: calcium chloride 25%, zinc chloride 25%, hydroxide of potassium 5%, hydroxide of sodium 5%, carbonate of potassium 5%, phosphoric acid 25%. Extremely high temperatures (250°C to 600°C) are then applied to the carbon. (173). It is thought that the warmth at this point activates the carbon by causing the substance to open up and develop additional tiny holes. Due to lower temperatures, higher quality consistency, and quicker activation times (174).

2.2.2 Aquatic Environment Pollutants

A stream, river, lake, ocean, aquifer, or other body of water can get contaminated by hazardous substances often chemicals or microorganisms—and lose quality, becoming poisonous to both humans and the environment. Water contamination is a widespread problem that puts our health in peril (175). Unsafe water kills more people annually than war and all other forms of violence combined. Our actual access to freshwater, which accounts for less than 1% of the global supply, is constrained. If nothing is done, the issues will only become worse by 2050, when it is predicted that the global demand for fresh water will be a third more than it is now. Water is extremely vulnerable to pollution (176). Water is known as the "universal solvent" because it can dissolve more chemicals than any other liquid on Earth. Because of it, Kool-Aid and vivid blue waterfalls exist. Additionally, it explains why water is so easily polluted. It readily dissolves and mixes with harmful substances from businesses, communities, and farms, contaminating the water.

2.2.2.1 Agricultural

The agriculture waste (Figure 2.8) is not only the largest user of freshwater but also a substantial water polluter, using over 70% of the world's surface water resources. Water contamination is mostly caused by agriculture globally. (177). Nutrient contamination, which is caused by excessive nitrogen and phosphorus in the air or water, is the largest danger to the quality of the world's water supplies. Blue-green soups of toxic algae known as "algal blooms" may be hazardous to both people and wildlife (178).

Figure 2. 8 Agricultural Wastes (179).

2.2.2.2 Sewage and Wastewater

Water is used for waste disposal coming from our toilets, sinks, and showers as sewage. When you consider metals, solvents, and toxic sludge, it furthermore originates from industrial, commercial, and agricultural operations (180). Stormwater runoff, which occurs when rain causes impermeable surfaces to leak chemicals, oil, grease, and debris into our rivers, is another term for this phenomenon. (181). More than 80% of wastewater generated worldwide, according to the UN, is released back into the environment untreated or without being recycled; in some of the least developed countries, the figure even exceeds 95%. In the United States, wastewater treatment facilities process around 34 billion gallons of wastewater each day (182). These facilities filter out pollutants such as bacteria, phosphorus, and nitrogen from sewage as well as heavy metals and toxic chemicals from industrial waste before releasing the cleansed waters back into rivers (183).

2.2.2.3 Oil Pollution

Even though large spills frequently make the news, most oil pollution is caused by consumers, including gasoline and oil that leak from millions of automobiles and trucks each day. Additionally, rather than coming from tanker accidents, approximately half of the estimated 1 million tons of oil that enters river ecosystems each year originates from land-based sources including factories, farms, and urban areas (11). Around 10% of the oil in rivers comes from tanker spills, whereas just a third comes from maritime activities regularly, including both legal and illicit discharges. Seeps, which are fissures in the ocean floor, are another natural way that oil is discharged (9).

2.2.3 Air Pollutants

Air pollution refers to any physical, chemical, or biological change in the air. Noxious gases, dust, and smoke are the main contributors to air pollution's negative effects on plants, animals, and people. A certain percentage of gases are present in the atmosphere. If the make-up of these gases changes, it is risky to survive. (184). The increase in the earth's temperature brought on by this imbalance in the gaseous composition is referred to as global warming (Figure 2.9).

The following are some ways that air pollution harms the ecology: Diseases, Global Warming, Acid Rain, Ozone Layer Depletion, and Effect on Animals.

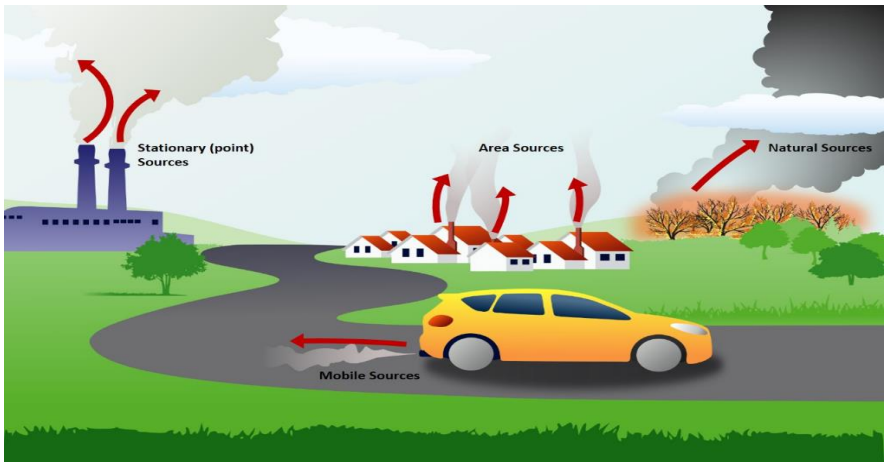

Figure 2. 9 Sources of air pollution (185).

2.3 Adsorption

The adsorption process occurs on a surface and moves a molecule from a fluid bulk to a solid surface. This might be caused by physical forces or chemical bonds. It is usually reversible, in which case it is responsible for both the release and removal of chemicals (186). This process is frequently shown as being in equilibrium by using specific equations that quantify the amount of material adhered to the surface given the concentration in the fluid. These equations are known as isotherms, and the most popular ones are the Langmuir and Freundlich equations (187) because temperature is one of the most important environmental factors that affect adsorption and because their properties are temperature-dependent. Adsorption is essential to ecology because it regulates the movement of materials throughout ecosystems, between the geosphere, hydrosphere, and atmosphere, and initiates other vital processes including ionic exchange and enzyme reactions (188).

Adsorption is a mass transfer mechanism that occurs when gases or solutes stick to solid or liquid surfaces. The molecules or atoms on the solid surface have excess surface energy as a result of the unbalanced forces, which leads them to adsorb. (189). These unbalanced forces cause some substances that collide with solid surfaces to be pulled to the surface and stay there. Based on the different adsorption forces, the adsorption process may be divided into two groups: chemical adsorption and physical adsorption (Table 2.1). Physical adsorption occurs when van der Waals forces between molecules interact, like when using activated carbon to absorb gas (190). Physical adsorption frequently occurs without selection at low temperatures with a rapid adsorption rate, and little heat being created during the

process. The structure of the molecules that make up the adsorbed material hardly changes as a result of the weak intermolecular contact, which also results in low adsorption energy and readily removable adsorbed materials. Adsorption that results from chemical bonding is referred to as chemical adsorption. Chemical adsorption involves the formation and destruction of chemical bonds (191). Both the quantity of heat absorbed or emitted during adsorption and the activation energy required are higher. Physical and chemical adsorption processes commonly co-occur. The results of many adsorption procedures account for the bulk of adsorption in wastewater treatment technology. Due to the interplay of adsorbents, adsorbates, and other factors, some forms of adsorption may have a considerable effect (192).

Table 2. 1 Comparison of physical adsorption with chemical adsorption (193,194).

	Adsorption categories	
	Physical adsorption	**Chemical adsorption**
Adsorption force	Van der Waals force	Chemical bond force
Selectivity	Nonselective adsorption	Selective adsorption
Adsorption layer	Single or multiple layers	Single layer
Adsorption heat	Low	High
Adsorption rate	Fast	Slow
Stability	Instable	Stable

2.3.1 Adsorption isotherm

The adsorption isotherm depicts the relationship between the adsorbate in the surrounding phase and the adsorbate adsorbed on the surface of the adsorbent at equilibrium and constant temperature. Adsorption isotherm is significantly required to precisely describe how solutes interact with adsorbents and to make the most of adsorbents (195). The best-fitting isotherm model is then used to examine adsorption behavior after several isotherm models are frequently used to correlate isotherm data. Each pair's adsorption isotherm is unique. Freundlich and Langmuir isotherms are the two primary methods for predicting the adsorption tendency of a material. (196).

2.3.2 Adsorption Equilibrium

2.3.2.1 Effect of pH

In addition to its various physicochemical effects, it is determined to be the pH, which is important in the ion exchange-governed adsorption processes that

permit the modification or changing of surface charges. Deng and Ting, (2005) affect the surfaces of the adsorbents in terms of functional group dissociation and surface charge, in addition to affecting the metal species in solution (197). It follows that more H^+ ions are adsorbed when the environment is more acidic. As a result, metal ions are more likely to be sorbed at lower pH values, which might be interpreted as an increase in q_e values. Inglezakis et al. The functional groups connected to the metal surfaces and the rivalry between protons and other important groups attached to the adsorption sites are two factors that affect how pH levels decline. The charge of the functional groups that are connected, which guarantees the efficacy of the electromechanical sorption of cations, also influences the pH rise (198).

2.3.2.2 Effect of dosage

In the field of adsorption technology, particularly concerning nanomaterials, the mass of the adsorbent plays a pivotal role in defining its adsorptive capacity. The adsorbent's optimal value, which is indicative of the maximal amount of adsorbate it can adsorb, is closely associated with its functional groups. Another critical factor influencing adsorption efficiency is the dosage of the nanomaterial employed (199). Prior studies, including Arshadi et al. (200), have underscored the importance of identifying an appropriate adsorbent dosage that achieves desired removal efficiencies in a cost-effective manner. It has been observed that with an increase in adsorbent dosage, the availability of active sites augments, leading to enhanced removal percentages of a given adsorbate concentration. This trend continues until a saturation point is reached, beyond which any further increase in dosage does not contribute to higher removal efficiency. Identifying this threshold dosage is crucial for scaling up the adsorption process. Moreover, as elucidated by Sheth et al. (201), the optimal dosage varies with different adsorbents due to the diversity in their functional groups and active sites, necessitating tailored approaches for each adsorbent type.

2.3.2.3 Effect of Temperature

Materials' equilibrium adsorption capacities are susceptible to temperature variations. In addition, shorter distances between particles and faster redox reactions are both possible at higher temperatures (202). These contracting values could be influenced by the biosorbent's species, quantity, and environmental

factors, among other things. However, the system's temperature may provide the adsorbed species with enough energy to enable faster desorption than the rate of adsorption (203).

The impact of temperature on the adsorption of heavy metals has been studied extensively. The most common observation is that for heavy metals, sorption capacity increases with temperature. The most frequent discovery is that warmth increases sorption capacity. This could be a result of the solution's viscosity being less stiff at high temperatures, which speeds up the diffusion of metal ions (204). Temperature is known to have a substantial influence on the adsorption process by changing how adsorbent molecules interact and are soluble.

2.3.2.4 Effect of Contact Time

As the adsorbate takes longer to bind to the active site of the adsorbent, the adsorption capacity will increase with increased contact time. To permeate the surface of such an adsorbent, the presence of active sites is crucial. The equilibrium point is attained when the metal ions have fully occupied all of the active sites (205).

How thoroughly heavy metals are removed from aqueous solutions depends on how long the adsorbent is in contact with the metal ions (206). Metal ion removal was shown to increase increasing contact time (207). The elimination of heavy metals frequently increases up until equilibrium is reached. However, the initial concentration of metal ions has a big impact on the equilibrium. There are many places now as a result of the rapid initial acceptance rate. As the adsorption rate reduces as the sites are occupied, the time it takes for equilibrium to arrive is determined by the transfer rate from the unpackaged fluid phase to the adsorbent-metal interface (208)

2.3.2.5 Effect of Stirring Speed

To more effectively remove dyes from the solution, mixing speed enhances turbulence and reduces the thickness of the boundary layer surrounding the adsorbent (209). The effects of mixing speed on adsorption capacity and removal efficiency shown in Figure 2.10.

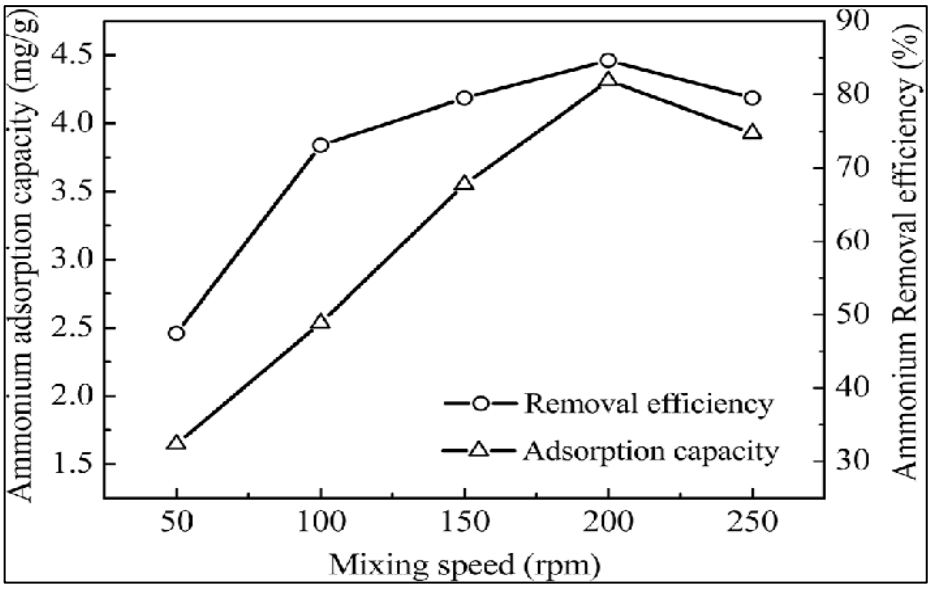

Figure 2. 10 The effects of mixing speed on adsorption capacity and removal efficiency of ammonium (210).

3. MATERIALS AND METHODS

3.1 Materials

3.1.1 Experimental Setup and Equipment Details

Experiments and experimental calculations were carried out in the water treatment laboratory of the College of Engineering at Tikrit University in Iraq. Contaminated water samples were collected from the Baiji refinery under the supervision of the North Refineries Company (NRC). The raw material for the production of activated carbon fiber is the date palm fiber, which was obtained from local palm farms. The work system consists of laboratory equipment used to carry out burning, activation, treatment, measurement, and calibration operations. In the beginning, the raw material is prepared, then it is thoroughly cleaned of dirt and dust. A muffle furnace was used to complete the carbonization process. After the activation process, the sample is washed, and a pH meter is used to ensure that the pH has reached an equilibrium state. Samples are then prepared for carbonization, activation, and treatment processes, each of which will be explained in detail (Figure 3.1).

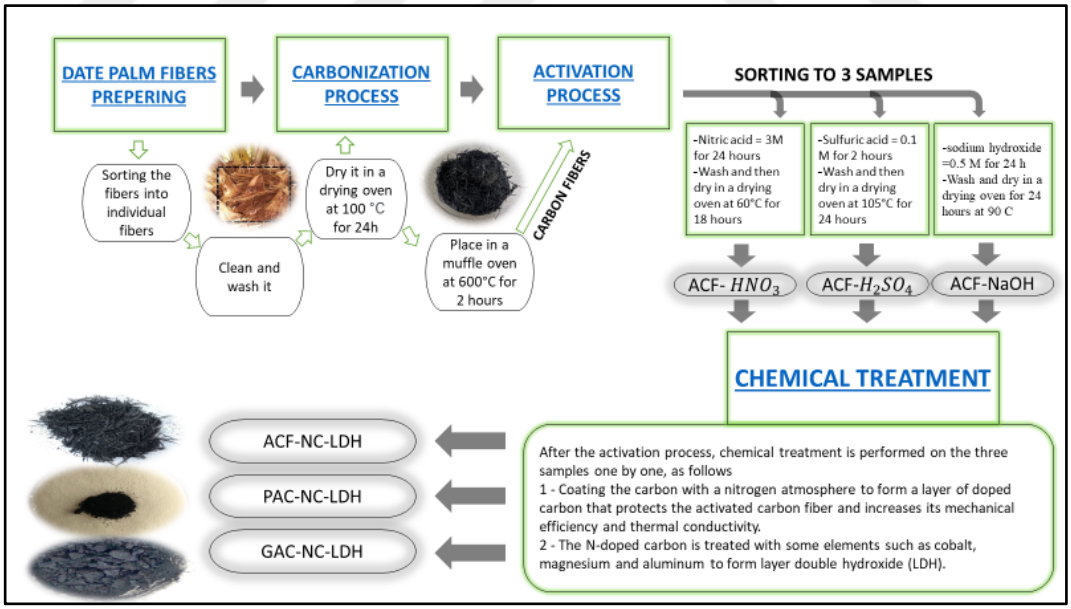

Figure 3. 1 Experimental Setup for different types of Activated Carbon (AC) Production.

3.1.2 Date Palm Fibers

This specific fiber has certain unique qualities, such as being 100% biodegradable and compostable, having a structural tensile strength that is 5 times

more than steel and comparable to flax and sisal, and having greater thermal insulation qualities than carbon fiber (2). Natural fiber composites' quality as well as their suitability for diverse industrial applications depend greatly on the physical qualities of the fibers. Natural fibers' mechanical characteristics are strongly influenced and governed by several crucial factors, including their structure, microfibrillar angle, chemical composition, cell size, and flaws. The Middle East and North Africa are home to around 140 million date palm trees. Date production is now dominated by Egypt, Iran, Saudi Arabia, Iraq, the United Arab Emirates, Pakistan, and Sudan. Date palms are pruned for agriculture every year, producing more than 48.8 million tons of waste. Therefore, date palm fiber production is now quite successful. All of these nations use date palm byproducts such as fronds, leaves, leaflets, rachis, and fruit branches to produce sustainable textile fibers. The chemical Composition of Date Palm Fibers detailed in Table 3.1.

Table 3. 1 Chemical Composition (%) of Date Palm Fibers (211).

Constituents	Cellulose	Hemicelluloses	Lignin	Ash	Extractive
Leaflet	40.21	12.80	32.2	10.54	4.25
Leaf	54.75	20.00	15.30	1.75	8.20
Rachis	38.26	28.17	22.53	5.96	5.08

The primary cell wall and additional secondary walls of date palm fibers are made up of several helically wrapped cellular micro-fibrils made of long-chain cellulose molecules, which might affect the fiber's mechanical characteristics (211). The three primary components of every cell wall are cellulose, hemicelluloses, and lignin. The most important structural elements in most natural fibers are cellulose and lignin. Despite being resistant to hydrolysis, strong alkali, and oxidizing agents, cellulose is also somewhat degradable when subjected to chemical treatments. On the other hand, lignin, a complex hydrocarbon polymer, often provides plants with their stiffness and aids in the movement of water. Figure 3.2 shows the part that the fibers taken from it.

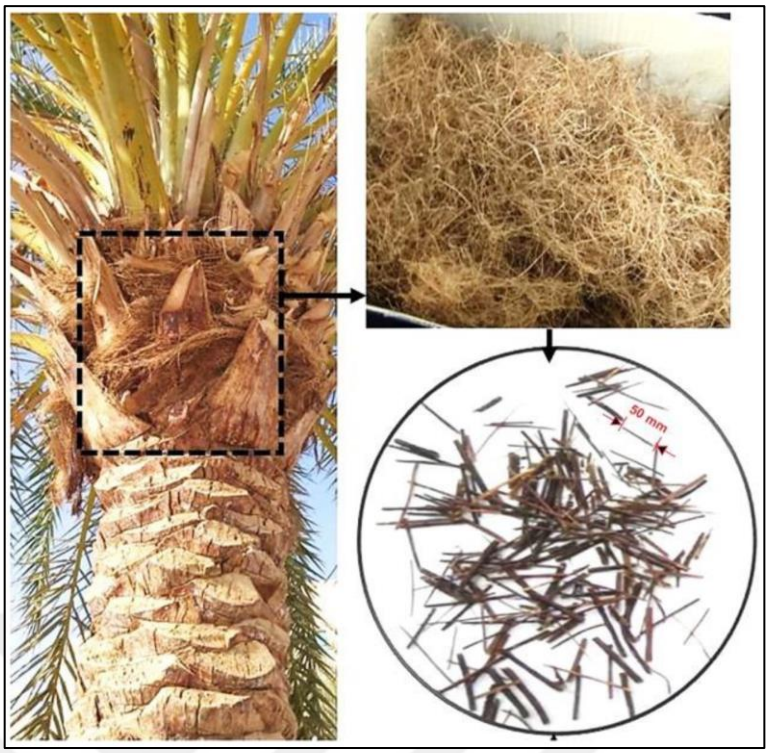

Figure 3. 2 Date Palm Tree (212).

3.1.3 Technical Specification of Test Equipment

Several carefully selected devices have been used to obtain typical controls determined by the parameters of the study, in Table 3.2, they are preferably summarized together with their specifications.

Table 3. 2 The devices and tools used in study.

Equipment	Picture	Technical Properties
Drying oven		**Brand:** p-selector **Accuracy:** ± 5 ℃ **Operating Range:** 20℃ - 200℃
Magnetic Digital Stirrer and Hot Plate		**Brand:** labnet international **Speed Range:** 60 –1150 rpm **Temp. Range:** 5 ℃ – 550 ℃

Hach COD Reactors		digests up to 15 samples simultaneously. **temperature** between 37 to 165°C, **time** between 1-minute to 8 hours[2]
Hach DR/870 Colorimeter		**Photometric range:** 0-2 A **Operating temperature:** 0-50°C **Dimensions (W x H x D):** 33/8" x 93/8" x 17/8"
Electrical Balance		**Brand:** OHAUS **Maximum range:** 410 g **Item number:** 80103854 **Pan size:** 120 mm
Muffle Furnace	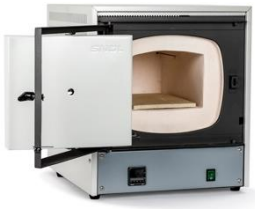	**Brand:** Snol 6.7/1300 LSM01 **Maximum temp.:** 1100 °C **Type:** Peripheral
pH Meter		**Brand: Fisherbrand** **Type:** FE 150 **Parameter:** pH/mV/ Temperature **Accuracy:** ± 0.2
Jar Test		Programmable jar test PB – 900 SERIE

3.2 Methodology

3.2.1 Preperation of the Raw Materials

Date palm fibers were identified as a raw material for the production of activated carbon fibers and powder activated carbon. The fallen date palm fibers (as seen in Figure 3.1) were collected from the trees located, considering the selection of the good ones. The fibers are broken up in the form of separate strands, then cleaned and washed well with distilled water to get rid of pollutants that may harm the production process. In addition, it was washed again with deionized (DI) water to remove any impurities or ions that could cause undesirable reactions. After the washing process, the fibers are dried in a drying oven at 100℃ for 24h to remove moisture, and then the material is ready for the carbonization process.

Figure 3. 3 Date palm fibers after sorting process.

3.2.2 Carbonization Process

The dried palm fibers were previously placed in special packages, taking into account that they are closed tightly to ensure that no air enters them, then they are inserted into the muffling oven (Figure 3.4) at a temperature of 600℃ for 2h (213). The packages are removed from the muffle furnace, and thus we have obtained carbon fibers (inactive) (214).

Figure 3. 4 Muffle furnace and carbon fiber produced.

3.2.3 Activation Process

After completing the carbonization process, unactivated carbon fibers were obtained. The chemical activation process was carried out on carbon fibers using nitric acid HNO_3 at a concentration of 3M, the sample was placed in nitric acid for 24h, after which the sample was washed with deionized water repeatedly to obtain a neutral pH value. Then the sample is dried at 60°C for 18h. To activate the second sample, dilute sulfuric acid H_2SO_4 at a concentration of 0.1M was used. The second sample was soaked in the acid for 2h (215). Then the sample is washed in de-ionized water repeatedly, then the sample is dried in a drying oven at 105°C for 24h. In addition, a third sample of carbon fibers was prepared and activated using sodium hydroxide at a concentration of 0.5M for 24h, washed with non-ionic water several times, and then dried in a drying oven for 24h at 90°C (216). Figure 3.5 shows the three samples under activation process.

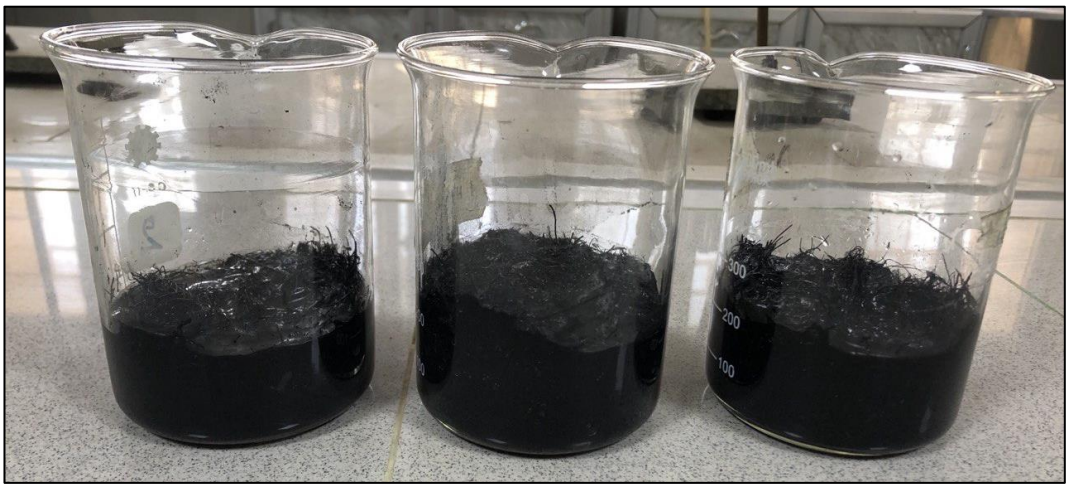

Figure 3. 5 The three samples under activation process.

3.2.4 Chemical Treatment

The rapid development in the production of active carbon has led researchers to move toward increasing the removal efficiency and reducing the cost of the raw material produced from it. Therefore, the need has emerged to improve cheap raw materials and improve production methods. Chemical treatment by carbon coating with a nitrogen atmosphere leads to the creation of a layer of doped carbon that protects the activated carbon fibers and increases their mechanical efficiency and thermal conductivity. In addition, some elements such as cobalt, magnesium, and aluminum are treated to form double-layer hydroxide (LDH). Because they have many uses in medicine administration, carbon dioxide sequestration, energy conversion and storage, catalysis, and environmental remediation, layered double hydroxides (LDHs) are an extremely flexible class of materials. In addition, a lot of LDH exists in nature in the form of minerals. Their potential uses can be further expanded by modifying their chemical composition and creating 3D or nano-hybrid materials through processes such as lamination. The activated carbon fibers are laminated with a hydroxide network after creating the doped carbon layer (217). This network stimulates the activated carbon to absorb the largest possible number of pollutants, which greatly increases the removal efficiency.

For the sample that is activated by nitric acid HNO_3, the encapsulation process is carried out by preparing two solutions of hydrochloric acid HCl (1 M, 50 ml), then 2.3 ml of aniline is added to one of the solutions, and 5.8 g of ammonium persulfate is added to the second solution. The first solution containing aniline is added to the activated carbon fibers. Then the second solution containing ammonium persulfate is gradually added to the mixture for 25 min using a burette. Finally, the resulting mixture is placed in an ice atmosphere (a container covered with ice) and placed in a magnetic mixer for 6 h stirring speed of 800 rpm as shown in Figure 3.6. Then the sample is placed in a muffle furnace at a temperature starting from 5 °C and up to 400 °C gradually for 3 h. Thus, we have obtained ACFs coated with an N-doped carbon layer (ACF-NC).

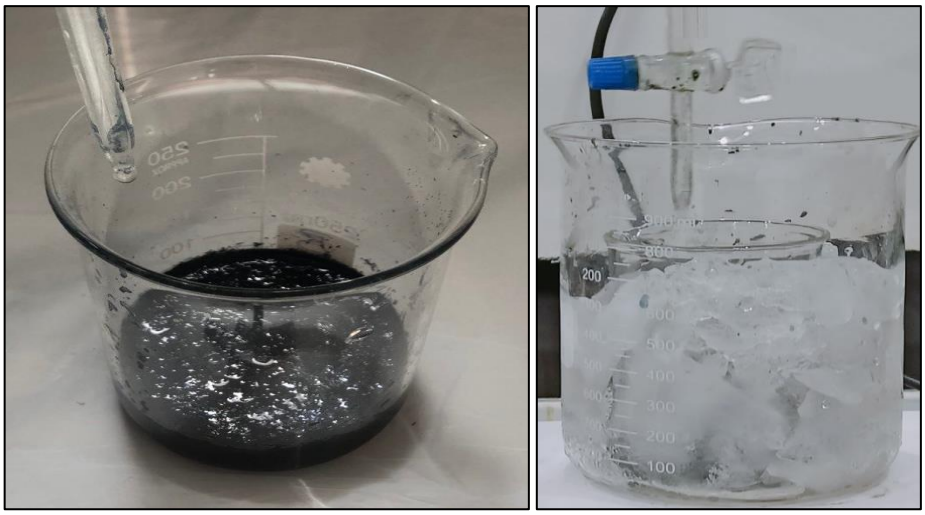

Figure 3. 6 Chemical treatment process for the N-doping.

Then 1 g of urea, 1 g of $CoSO_4 \bullet 7H_2O$, 1 g of $MgSO_4 \bullet 7H_2O$, and 1 g of $Al_2(SO_4)_3 \bullet 18H_2O$ are added to 100ml of deionized water (DI), then the mixture is placed in a stainless steel container and placed in a drying oven at 100 °C for 12 hours. Then it is rinsed with non-ionic water and placed in a drying oven at 60 °C for 6 hours. Figure 3.7 shows the three solution prepared for treatment processes.

Figure 3. 7 The three solutions preparing for treatment processes.

The nanosheets have grown on the surface of ACF-NC in the form of a lattice structure, whereby we have obtained (ACF-NC-LDH) as shown in (Figure 3.8a). The same treatment steps were carried out on the second sample activated by dilute

sulfuric acid, after completing the treatment steps, an activated carbon coated with a layer of N-doped carbon with a lattice structure (PAC-NC-LDH) was produced as shown in (Figure 3.8b). That is, the product may change from fiber form to powder form. More specifically, the turning point was immediately after using the ice bath. As for the third sample activated with sodium hydroxide, after performing the same chemical treatment stages, the sample appeared in the form of granular agglomerates coated with a layer of N-doped carbon with a network structure (GAC-NC-LDH) as shown in (Figure 3.8c).

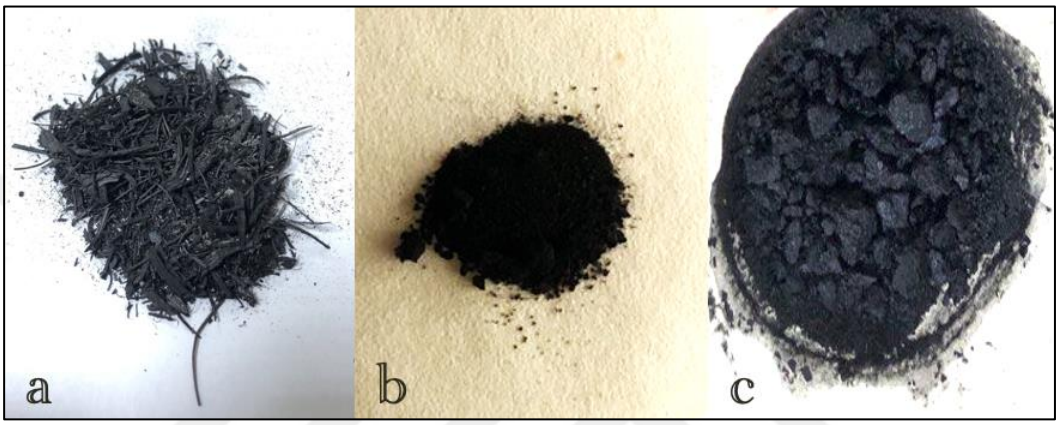

Figure 3. 8 The Produced three samples after chemical treatment, (a) ACF-NC-LDH (b) PAC-NC-LDH (c) GAC-NC-LDH

3.2.5 Adsorption Models of Equilibrium

3.2.5.1 Concentration of COD

The chemical oxygen demand (COD), a useful indicator of how much oxygen may be used by processes in a measured solution, is used in environmental chemistry. It is frequently stated as the mass of oxygen used over the volume of the solution, or milligrams per litre (mg/l), in SI units. It is simple to determine the concentration of organics in water using a COD test. Quantifying the quantity of oxidizable contaminants present in surface water (such as lakes and rivers) or wastewater is the most typical application of COD. In terms of water quality, COD is useful since it provides a measure of how an effluent would affect the receiving water.

The concentrations of COD in a range of samples were analyzed in a laboratory environment by the guidelines provided in the Guidance Handbook for Water and Industry Sewage Analysis (218). The COD adsorbed by AC at equilibrium at periods t, q_t, and q_e (mg/g) were calculated using the following equations (219,220).

$$R\% = \frac{C_o - C_t}{C_o} \times 100\% \quad (1)$$

$$q_t = \frac{(C_o - C_t)V}{m} \quad (2)$$

$$q_e = \frac{(C_o - C_e)V}{m} \quad (3)$$

Where q_t is the quantity of COD that activated carbon has absorbed at time (t). At the beginning, time (t), and equilibrium, respectively, COD concentrations in the solution are represented by the letters C_o, C_t, and C_e. V stands for "volume of solution" and "m" for "mass of activated carbon."

3.2.5.2 Thermodynamics methods

An essential stage in assessing thermodynamic viability, process spontaneity, and adsorption processes is the examination of thermodynamic parameters. The following equations (4) and (5) were supposed to be reliant on thermodynamic variables such as the change in Gibbs free energy (ΔG^0), enthalpy (ΔH^0), and entropy change (ΔS^0) (221).

$$\Delta G^0 = -RT \ln K_c \quad (4)$$

$$\Delta G^0 = \Delta H^0 - T\,\Delta S^0 \quad (5)$$

Where K_c stands for the adsorption distribution coefficient defined by the following formula:

$$K_c = q_e/C_e \quad (6)$$

Where qe is the amount of COD present on the surface of the adsorbent (in mg/l) and Ce is the concentration at equilibrium in solution (in mg/l). The global gas constant is R (8.314 J/mol.K), while G^0, H^0 , and S^0 are the standard changes in free energy, enthalpy, and entropy, respectively (222). K_c is the equilibrium constant (q_e/C_e), and T is the temperature. As a result, the intercept and slope of the plot of ln K_c vs 1/T were used to calculate the values in the adsorption process.

3.2.5.3 Adsorption Isotherms

The overall equilibrium distribution between the stationary and mobile phases controls how much of the solute is retained. The distribution constant being constant reflects the linear isotherm. It is possible to get it across a small concentration range without any selective interactions between the adsorbent and the adsorbate (223). The solute in the column eluate has a Gaussian distribution as a result. The sorption isotherm becomes curved and produces an asymmetric, expanded peak form in the

presence of such interactions or at greater concentrations. Adsorption isotherms may be determined using a variety of techniques (224). They have been developed taking into account sorption effects, pressure gradients, gas defects, and other considerations for both the case of ideal GC (elution at infinite dilution) and nonlinear nonideal GC (finite concentration). The challenge is to quantify the quantity of adsorbed solute and its related equilibrium concentration (pressure) in the mobile phase for each point of the isotherm, regardless of the chromatographic method employed to determine it (225). The needed information may be acquired using either the peak maxima technique, which involves injecting a series of adsorbate samples of changing sizes into the column, or the elution by characteristic point and frontal analysis by characteristic point methods, which involve using a single chromatogram (226).

The technique was made simpler by studying the adsorption capacity of adsorbents using adsorption isotherms. Adsorption isotherm is the relationship between the amount of adsorbate on the adsorbents and the ideal adsorbate values at constant temperatures (227). The adsorption isotherm equation described the relationship between the amount of solute immobilized and the concentration of the solute in the aqueous medium. The adsorption isotherms are evaluated to explain the process (228). These isotherms also specify the forces in nature that bind the adsorbate and adsorbent together, such as chemical or physical forces (229). According to Chowdhury et al. (230), the concentration will negatively affect the adsorption frequency because of the quantity of accessible sites. Since the adsorbed quantity closely reflects the solids' concentration in the fluid in the linear isotherm (passing through into the origin), it is advantageous to create large solid loads at low solid concentrations in the fluid, as illustrated in Figure 3.3 (231).

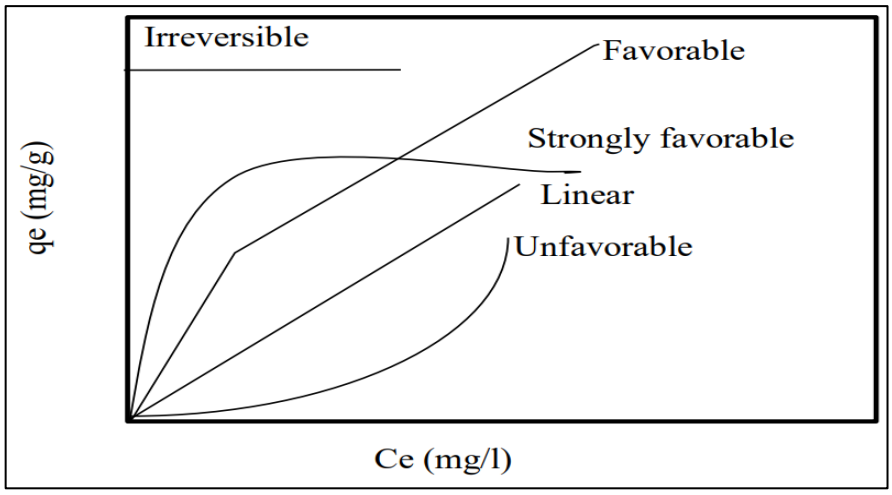

Figure 3. 9 Isotherm adsorption curves.

3.2.5.3.1 Langmuir isotherm equation

The Langmuir equation is based on the assumption that the unimodal, evenly distributed, saturated monolayer of adsorbed species onto an adsorbent represents maximal adsorption (232). According to the Langmuir model, once the adsorbate has occupied a position, additional adsorption will not take place there. Adsorption happens consistently on the binding sites of the adsorbents (233). The Langmuir isotherm model's nonlinear equation may be expressed as follows:

$$q_e = \frac{q_0 k C_e}{1+kC_e} \quad (7)$$

The Langmuir isotherm can be linearized into the form (234):

$$\left(\frac{C_e}{q_e}\right) = \frac{C_e}{q_0} + \frac{1}{q_0 k} \quad (8)$$

q_0 : maximum adsorption capacity (mg/g).

q_e : uptake of adsorbate equilibrium (mg/g).

K : energy of adsorption (l/mg);

Ce : final concentrations at equilibrium (mg/l);

The essential characteristics of the Langmuir isotherm can be expressed in terms of a dimensionless constant separation factor RL that is given by the following equation [108]:

$$RL = \frac{1}{1+kC_o} \quad (9)$$

3.2.5.3.2 Freundlich isotherm equation

The Freundlich adsorption isotherm, one of the most extensively used mathematical models, offers an equation that accounts for surface heterogeneity as well as the probability function of catalyst surfaces and their energies (235). The

first binding sites to be occupied, according to this theory, are those with a greater affinity for adsorbing molecules. In addition, increasing surface handling tends to reduce binding power (236). The Freundlich model is used to:

$$q_e = kC_e^{\frac{1}{n}} \quad (10)$$

The Freundlich can be linearized in the logarithmic form and the Freundlich constants can be determined (237):

$$\log(q_e) = \log k + \left(\frac{1}{n}\right)\log C_e \quad (11)$$

q_e: the value of sorbate uptake in equilibrium (mg/g).

k: Freundlich isotherm constant (mg1-(1/n) L1/ng-1).

Ce: final concentrations of the adsorbate in equilibrium(mg/l).

1/n: adsorption intensity

The present driving forces for adsorption as well as the degree of surface heterogeneity are shown by the Freundlich parameter, n. The n parameter is a number for the boundary conditions between 0 and 10. If n is more than 10 it results in an irreversible isotherm. The n value less than unity indicates strong adsorption, while n value higher than unity imply preferred adsorption.

3.2.5.3.3 Tempkin isotherm

Adsorbing species-adsorbate interactions are explicitly taken into account by a component in the Temkin isotherm model (238). This model assumes that, due to adsorbate-adsorbate interactions, (i) the heat of adsorption of each molecule in the layer decreases linearly with coverage and (ii) adsorption is characterised by a uniform distribution of binding energies up to a maximum binding energy. The Freundlich equation implies that the decline in the heat of sorption is logarithmic, whereas the Tempkin isotherm assumes that it is linear. The following equation (Eq. (12)) is a typical way to apply the Tempkin isotherm (239):

$$q_e = \frac{RT}{b_T}\ln A_T + \frac{RT}{b_T}\ln C_e \quad (12)$$

The Temkin constants A_T (L/mg) and b_T (J/mol) are used. R is the universal gas constant, 8.314 $Jmol^{-1}\ K^{-1}$, and T is the absolute temperature in Kelvin. The slope and intercept of the plots produced by graphing q_e vs time ln C_e are used to get the A_T and b_T constants.

3.2.6 Kinetic Study

Kinetic tests are performed on the adsorption process rates and possible rate-limiting stages. Give really important details on how long it takes for balance to develop. To be employed at a suitable industrial scale in wastewater treatment facilities, an adsorbent must not only have a high capacity for adsorption and removal but also a high adsorption rate (240). Predicting adsorption kinetics is essential in a wastewater treatment process since it gives important information about the technology being utilized and is a rate-limiting phase. Intraparticle diffusion, pseudo-first-order, and pseudo-second-order are common kinetic models. The third model is based on a rate of diffusion restricting analysis. Kinetics determination is crucial for the design of the sorption process and the reaction kinetics regulating step as the chemical reaction occurs (241). Adsorption kinetics (t) describes the connection between the amount of adsorbate adsorbed on the adsorbents (q_t) and the contact time (242).

3.2.6.1 Pseudo-first-order kinetic model

The pseudo-first-order model addresses the adsorption of liquid-solid phase systems based on adsorption capacity. The following is a typical representation of it. utilizing the fictitious first-order Lagrange model (243):

$$\frac{dqt}{dt} = K\,(q_e - q_t) \tag{13}$$

The essential formula of this equation is given by (244):

$$\mathrm{Log}(q_e - q_t) = \mathrm{Log}\, q_e - \frac{k1}{2.303}t \tag{14}$$

Where q_e is the amount of adsorbate that the adsorbent can hold in equilibrium (in mg/g), q_t is the amount that can be held in contact time (in mg/g), t is the time and k_1 is the fictitious first order rate constant.

3.2.6.2 Pseudo- second-order kinetic model

In systems where chemisorption acts as the rate-regulating step, it is acknowledged that the kinetic model of pseudo-second-order is well employed. The pseudo-second-order model's expression is as follows (245):

$$\frac{dqt}{dt} = k_2\,(q_e - q_t)^2 \tag{15}$$

The essential formula of this equation is given by (246):

$$\frac{1}{q_t} = \frac{1}{k_2 q_e^2} + \frac{1}{q_e}t \tag{16}$$

Where q_e is the amount of adsorbate that the adsorbent can hold in equilibrium (in mg/g), q_t is the amount that can be held in contact time (in mg/g), and k_2 is the fictitious second-order rate constant.

3.2.6.3 Intra-particular diffusion model

Before connecting the pores of the adsorbent, adsorbate molecules must transfer the adsorbate process from the bulk phase to the solid surface. The computation is based on an internonlinear model, regardless of whether diffusion within the pores is the rate-limiting phase: The following is an expression for the intra-particle diffusion model (247):

$$q_t = k_d\, t^{\frac{1}{2}} + C \qquad (17)$$

Where C (mg/g) is the intercept, which reflects the thickness of the boundary layer, and qt (mg/g) is the adsorption capacity at time t (min), k_d (mg/g $min^{-0.5}$) is the intra particle diffusion rate constant. The intra-particle diffusion model can be used in a particular adsorption process to adsorbate molecule movement in microspores or surface dispersion from the bulk, which leads to external surface adsorption. However, the model's close-fitting line shows a rather smooth development over time, pointing to a steady increase in adsorbate uptake (248).

3.2.7 Characterization and Testing of Catalysts

3.2.7.1 X-Ray Diffraction (XRD)

X'Pert^3 MRD Materials Research X-ray Diffraction System from Malvern Panalytical (as shown in Figure 3.10). A CuK radiation Nickel filter with a wavelength of (λ= 1.5406 Å) is used to conduct an X-Ray diffraction examination to determine the crystallinity of the powder leftover from the calcination procedure used to create the composite catalysts. The results are gathered for the 2 range from 20 to 80 degrees with a scanning speed of 5 degrees per minute. At Iran's Sharif University of Technology, the tests are carried out.

Figure 3. 10 X-Ray Diffraction device

3.2.7.2 Surface Area and Pore Volume Measurements

The prepared samples are measured using the Brunauer, Emmett, and Teller (BET) method by Thermo Analyzer (USA) as seen Figure 3.5, which degasses the samples with nitrogen while maintaining a vacuum of 25 bar. The tests are conducted at the Petroleum Research and Development Center (PRDC) lab of the Iraqi Ministry of Oil.

Figure 3. 11 Surface Area and Pore Volume Measurements device

3.2.7.3 Scanning Electron Microscope SEM Analysis

The scanning electron microscope (SEM) uses a focused beam of high-energy electrons to generate a variety of signals at the surface of solid specimens. The samples were examined microscopically using a VEGA3 Electron Microscope (Figure 3.12) in Iran.

Figure 3. 12 VEGA3 Electron Microscope

3.2.8 Response surface method

Researchers frequently employ the RSM approach while preparing for and enhancing their studies. The RSM methodology is a computational and numerical approach for designing and enhancing the experiment, enabling the identification of optimal parameters with the least number of tests. RSM was initially employed in empirical research, but more recently, it has also been applied to numerical studies. thanks to its benefits, which include decreasing processing costs while increasing experimental RSM and forecasting nonlinear optimization processes. is a technique that scientists regularly employ when organizing and improving studies (249).

When a first-order model exhibits a lack of fit as a result of the interaction between variables and surface curvature, a second-order model can considerably enhance the optimization process. An example of a second-order model is:

$$Y = a_0 + \sum_{i=1}^{n} a_i x_i + \sum_{i=1}^{n} a_{ii} x_i^2 + \sum_{i=1}^{n} \sum_{i=1}^{n} a_{ij} x_i x_j \quad (18)$$

4. RESULTS

4.1 Adsorbent Characterization Results

4.1.1 BET Analysis

BET analyses were carried out to assess the porosity and ultrastructural characteristics of the as-prepared ACF-NC-LDH and PAC-NC-LDH. The Brunauer Emmett-Teller (BET) technique determines the surface area of any adsorbent. BET examination of the carbon fibers (CF) before activation and treatment showed that their surface area was 46.2 m^2/g, the pore volume was 0.0611cm^3/g, and the pore diameter was 1.09 nm. The outcome revealed that the ACF-NC-LDH that had been produced had a surface area of 275.62 m^2/g. The average pore width was 2.7812nm, and the pore size was 0.1957 cm^3/g. The produced PAC-NC-LDH has a surface area of 147.75 m^2/g, a pore volume of 0.0942 cm^3/g, and an average pore diameter of 2.466 nm. The values indicate that the surface area and pore size of ACF-NC-LDH are much larger than that of PAC-NC-LDH and this explains the resulting difference in adsorption efficiency between them. Pore diameters are classified by IUPAC (250) as belonging to one of three categories: micropores (diameters less than 2 nm), mesopores (diameters between 2nm and 50nm), or macropores (diameters more than 50nm). As for GAC-NC-LDH, the surface area was very small, about 10 m^2/g, the pore volume was 0.016 cm^3/g, and the average pore diameter was 0.62 nm. Based on the BET examination of carbon fiber, the surface area was about 46.2 m^2/g, and after examining on the three samples shown in the previous figure for the BET examination, it was found that the surface area of GAC-NC-LDH had become 10 m^2/g, so this sample will be neglected and not included in the adsorption experiments due to their small surface area and low efficiency. The reason for this is likely the chemical reactions that occurred during the formation of N-DOPED and the LDH process, as the sample was activated with NaOH, which is a strong base, and then it was treated with sulfates and acids, which caused the breakdown of its crystalline structure (251).

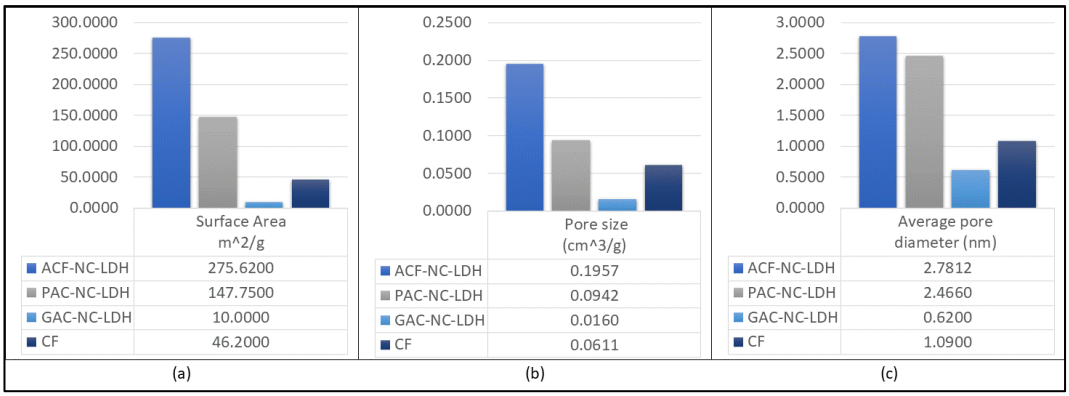

Figure 4. 1 BET analysis for ACF-NC-LDH, PAC-NC-LDH, GAC-NC-LDH and CF, (a) surface area, (b) pore size, (c) average por diameter.

4.1.2 SEM Analysis

Figure 4.2a shows the transformation of the ACFs from twisted and interlaced to rougher after being coated with an N-doped carbon layer, which may provide sufficient active sites for the in-situ creation of MgCoAl-LDH. Some used a network topology to give a bimodal pore size distribution (pore size was mostly distributed between 40 µm and 50 µm). The virgin fibers' surface was quite smooth and had a diameter of about 4 µm (Figure 4.2c), (252).

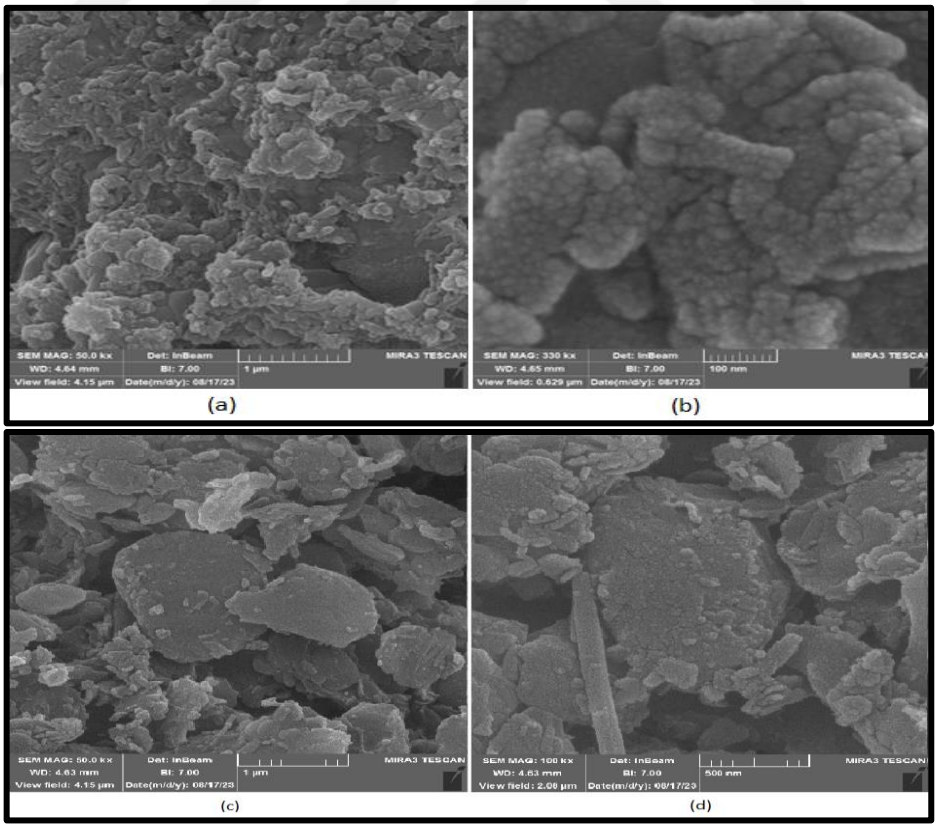

Figure 4. 2 SEM images of ACFs (a,b) Activated carbon fiber ACF after treatment process (ACF-NC-LDH) (b,c) carbon fiber (CFs)

After a normal hydrothermal reaction, a substantial number of evenly distributed, vertically oriented LDH sheets with a width of about 2μm were adhered to the carbon fiber surface. However, due to the inclusion of the N-doped carbon layer and the constrained growth of LDH on the fiber surface, which covered several naturally existing microscopic holes (2nm) on the surface of the fiber as shown in Figure 4.2b. On the surface of pristine ACFs, a buildup of irregular and microscopic LDH sheets known as ACF-NC-LDH develops randomly and is spread, in contrast to pure fibers with smooth surfaces (Figure 4.2d).

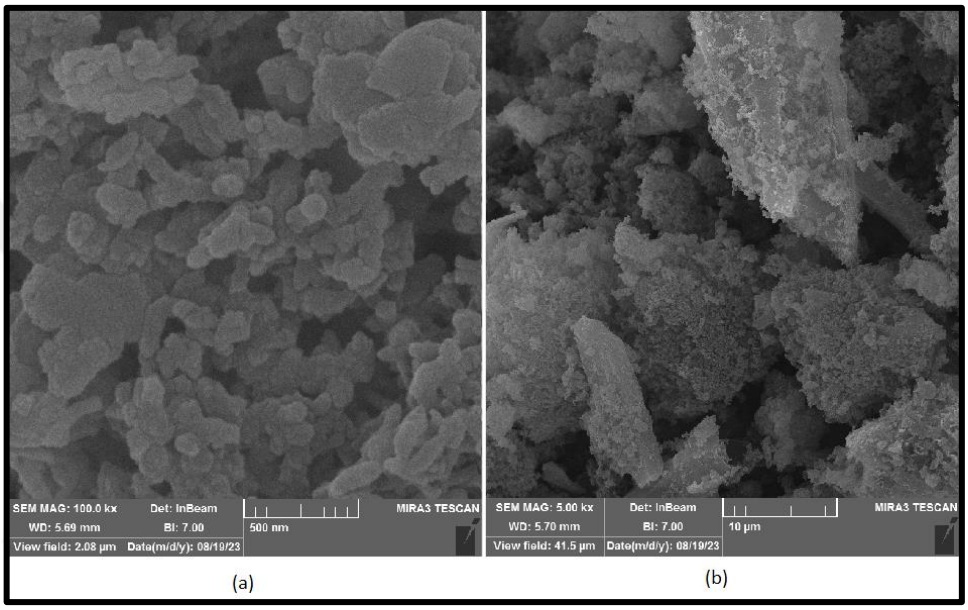

Figure 4. 3 SEM images of Powdered activated carbon PAC after treatment process (PAC-NC-LDH)

Figure 4.3b clearly shows the granular layer randomly spread on the surface of the activated carbon powder. This is called PAC-LDH. Activation of the N-doped layer led to the bonding of some carbon molecules to each other, making them appear in the form of individual PAC-NC-LDH blocks, as in Figure 4.3a. The diameter of the grains ranged between 30-50nm.

4.1.3 X-ray diffraction analysis (XRD)

The prepared ACF-NC-LDH's XRD data is displayed in Figure 4.4. Sample peaks may be found in (2θ = 24.62341, 43.9242). The crystallization sizes, according to these statistics, are 1.676 and 1.569, respectively. The crystal size L was calculated using Scherer's equation as follows.

$$B(2\theta) = \frac{K\gamma}{L\cos\theta} \quad (19)$$

Where:

B: is the Full Width at Half Maximum (FWHM) of the peak at 2θ.

K: is the Scherrer's constant, which, depending on the crystal shape, can range from 0.6 to 2.08; in this case, we focus on it.

The average crystal size obtained by applying Scherrer's equation to X-ray diffraction data is 1.6230 nm. It has been observed that the closest value was achieved by Ali Hashem et al. (253) and that it has the same peak at 2θ equal to 24.62 by comparing the sharp peak acquired at that value. This indicates that a good level of crystallinity was attained. On the other hand, for PAC-NC-LDH, a peak appeared at 2θ equal to 23.42 (Figure 4.4), and its crystallization volume was equal to 1.2763 nm. The same result was found by Li-an Xing et al. (254) when 2θ equals 21 demonstrating that the contaminants produced by KOH during the activation process were eliminated by washing with a solution of hydrochloric acid and deionized water. The resultant activated carbon is an amorphous substance. The large peak at about 23 indicates that the material had just a small amount of graphitization throughout the activation phase.

For CF before the chemical treatment process, two peaks appeared at 2, equal to 24.26 and 43.9 (Figure 4.4), and the average size of the crystals was equal to 1.0418nm. This shows, as noted, that ACF-NC-LDH has the highest crystalline size and highest crystallization peaks. A higher crystallinity level indicates a higher adsorption capacity.

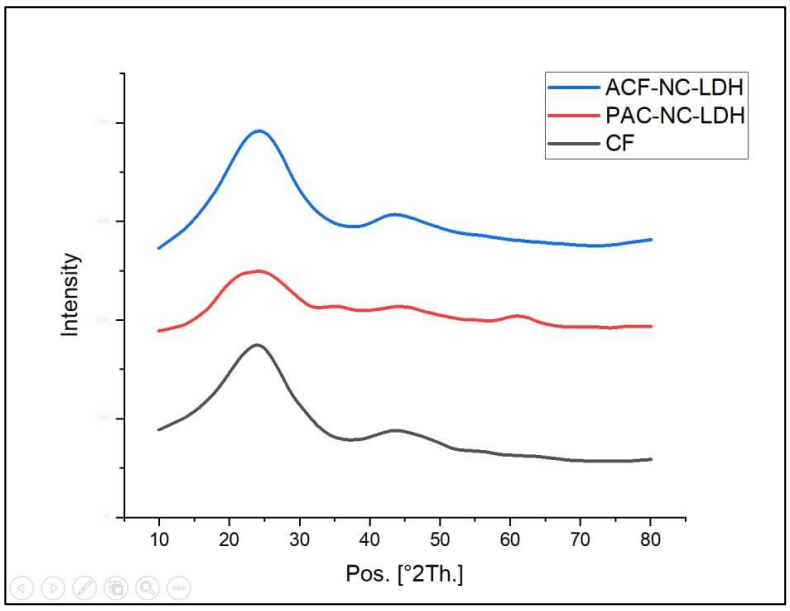

Figure 4. 4 X-Ray analysis for the activated carbon samples.

4.2 Effects of Experimental Parameters

4.2.1 Effect of pH

To measure the effect of changing the pH of the adsorbent on the adsorption efficiency, the pH values were determined starting from 2 by 2 in increments up to 12, considering the concentration of activated carbon in water as 1 g/300 ml for 120 min. as shown in Figure 4.5 and Figure 4.6. The results showed that the highest removal percentage was at pH 6 for the two samples (activated carbon fibers and activated carbon powder). By observing Figure 4.5, it is evident that the removal rate increased when changing the pH values from 2 to 4, as it was 50.6% and became 60.7%. The highest removal percentage was at pH 6, where it was 89.2%, then the removal percentages decreased again at values greater than 6 for PAC-NC-LDH. As for activated carbon fibers, as noted in Figure 4.6, the removal rates were (63.7% and 73.7%) at pH values (2 and 4), respectively. Aside from that, the maximum removal percentage, which reached 95.9% at pH 6, also fell at pH values above 6. It is most likely the reason for the higher value of the adsorption percentage (R%) observed at pH 6 because, at low pH values, positive charge sites are created on the activated carbon surface, resulting in a significantly higher attraction to electrostatic charges between the electrically charged activated carbon surface and organic compounds (COD). The decrease in the value of (R%) when pH > 6 may be due to an increase in resistance to the diffusion of molecules of organic matter brought on by an excess of OH- ions.

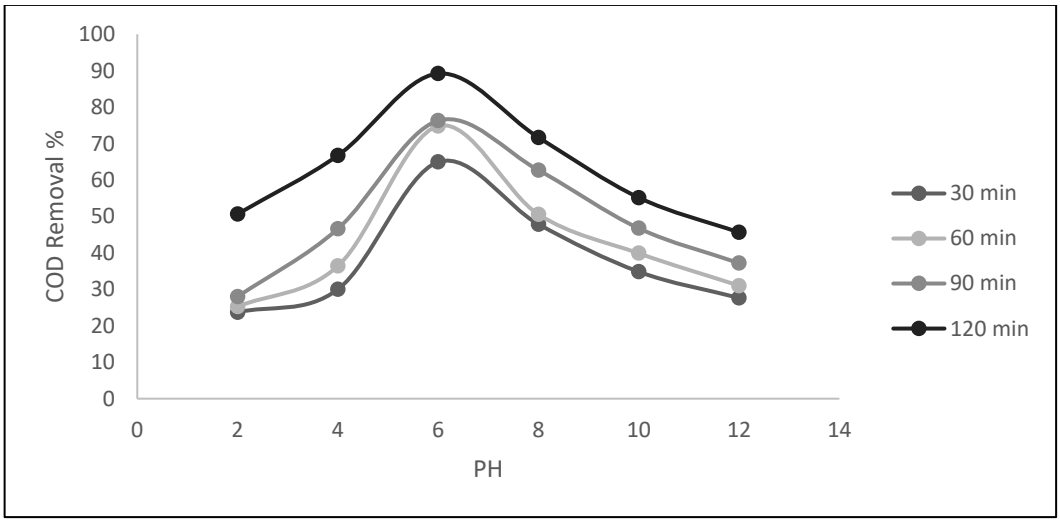

Figure 4. 5 The effect of pH on removal for PAC-NC-LDH

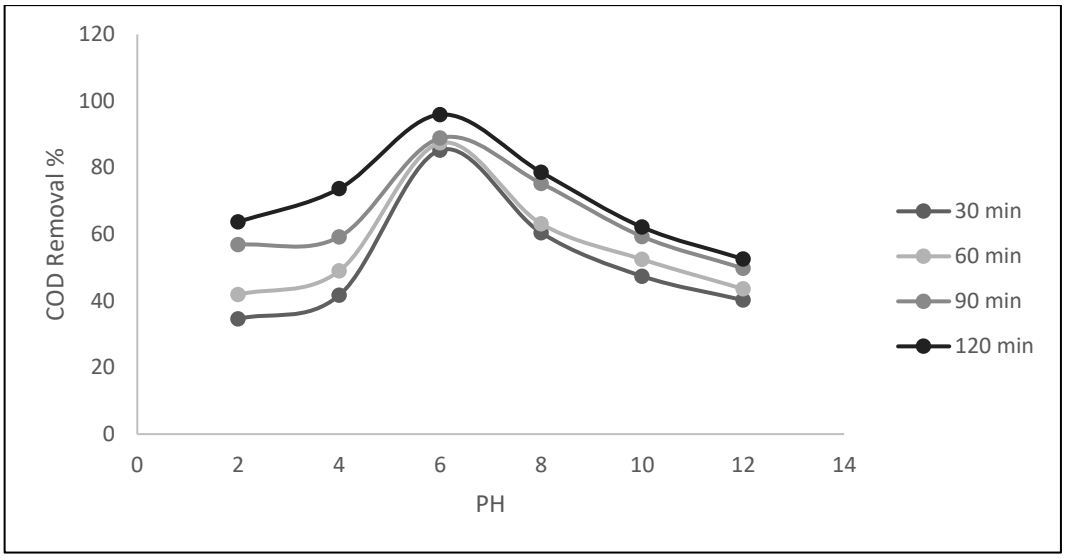

Figure 4. 6 The effect of pH on removal for ACF-NC-LDH

From the observation of Figure 4.7, it is clear that the removal results for activated carbon fibers are higher than the removal results for activated carbon powder, as the highest removal rate for activated carbon fibers under the influence of pH was 95.9%, while for activated carbon powder, the highest removal rate was 89.9%. This increase is due to the increase in the pores in the activated carbon fibers, which allow the adsorption of the largest possible percentage of COD organic pollutants inside.

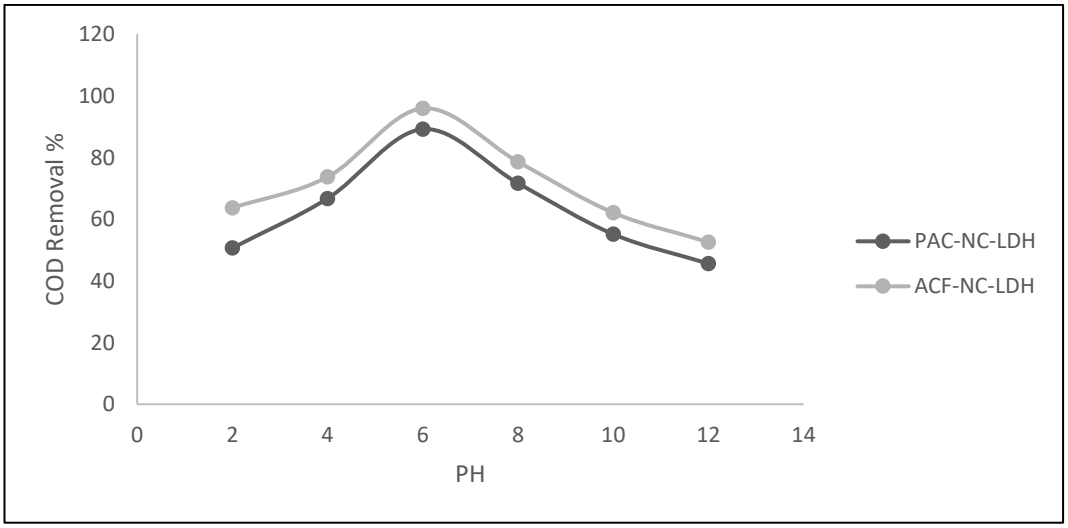

Figure 4. 7 Comparation between ACF-NC-LDH and PAC-NC-LDH under pH effects.

4.2.2 Effect of Stirring Speed

As indicated in Figure 4.8 for PAC-NC-LDH, the obvious effect of stirring speed is observed. Various speeds were taken starting from 100 rpm up to 600 rpm with the rest of the variables remaining constant. The pH value was 6, the carbon

concentration was 1 g/300 ml, and the temperature was 25 °C for 120 min. The results showed that the removal rate increased continuously with the increase of the stirring speed up to 400 rpm, and then the removal rate was fixed after that, that is, there was no longer an effect of increasing the stirring speed, as the removal rate reached (36.99% and 89.25%) at the stirring speed 100 rpm and 400 rpm, respectively.

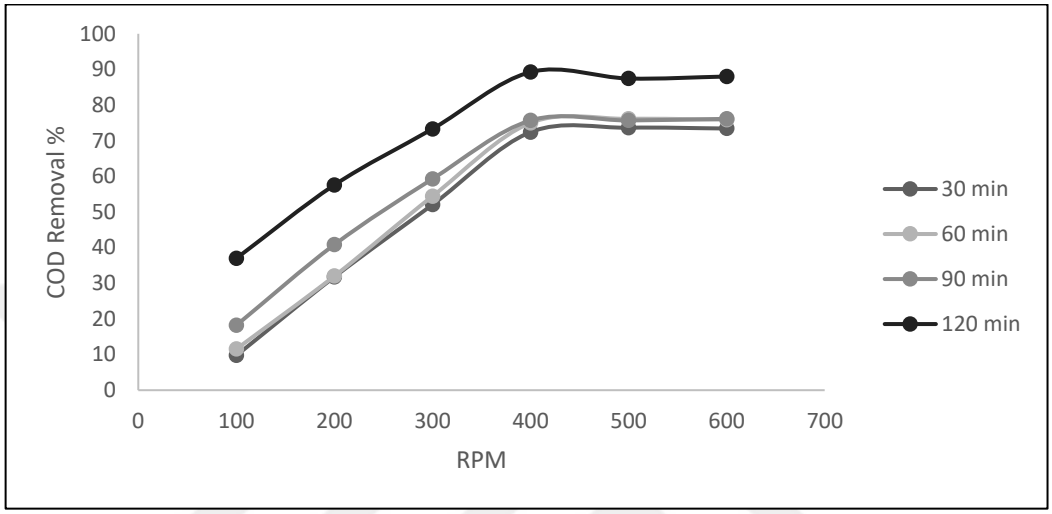

Figure 4. 8 The effect of stirring speed on removal% for (PAC)

On the other hand, considering Fig. 4.9 for ACF-NC-LDH, the removal percentage was (44.57% and 96.04%) at a movement speed of 100 rpm and 400 rpm respectively. The stirring process helps to increase the susceptibility of the pores to absorb the greatest amount of COD organic adsorbents, and as the stirring process increases, the pores reach a saturated state, so that increasing the stirring above the required level has no effect, and this is what happened at 400 rpm. Either the diffusion pore or the diffusion film regulates the rate of absorption. The liquid coating within the particulate is thicker at low speeds, and the diffusion of film seems to represent the rate-limiting step. Low transfer of mass from the adsorb to the particle inside affects the adsorption kinetics. When moving quickly, the diffusion film builds up to its maximum value, turning the diffusion pore into a rate.

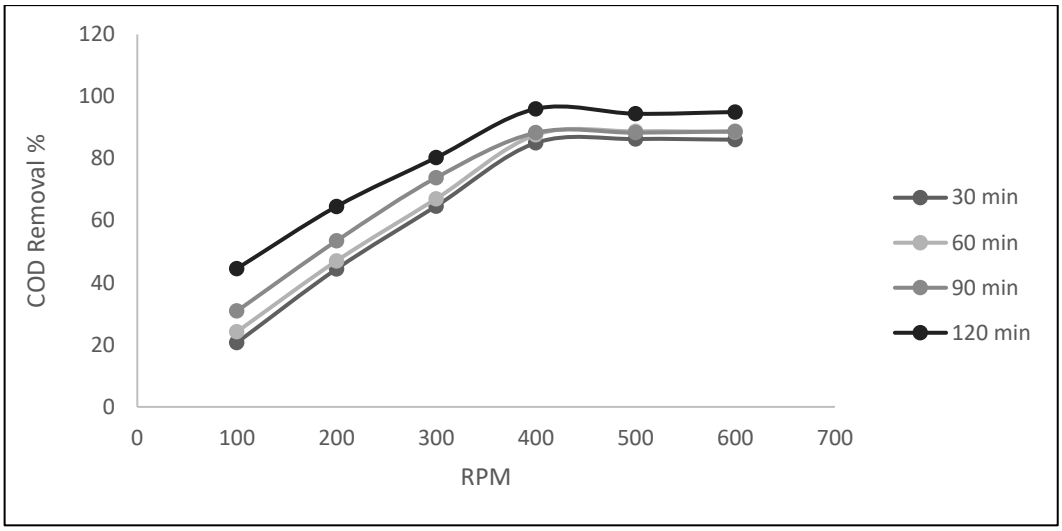

Figure 4. 9 The effect of stirring speed on removal% for (ACF)

In Figure 4.10, it appears that the removal rate of activated carbon fibers under the effect of changing the stirring speed is higher than that of activated carbon powder, where the highest removal rate of activated carbon fibers reached 96.04%, and the highest removal rate of activated carbon powder reached 89.25% at a stirring speed of 400 rpm. This is because the pores of the activated carbon fibers have a higher ability to attract pollutants than the activated carbon as a powder at high stirring speeds.

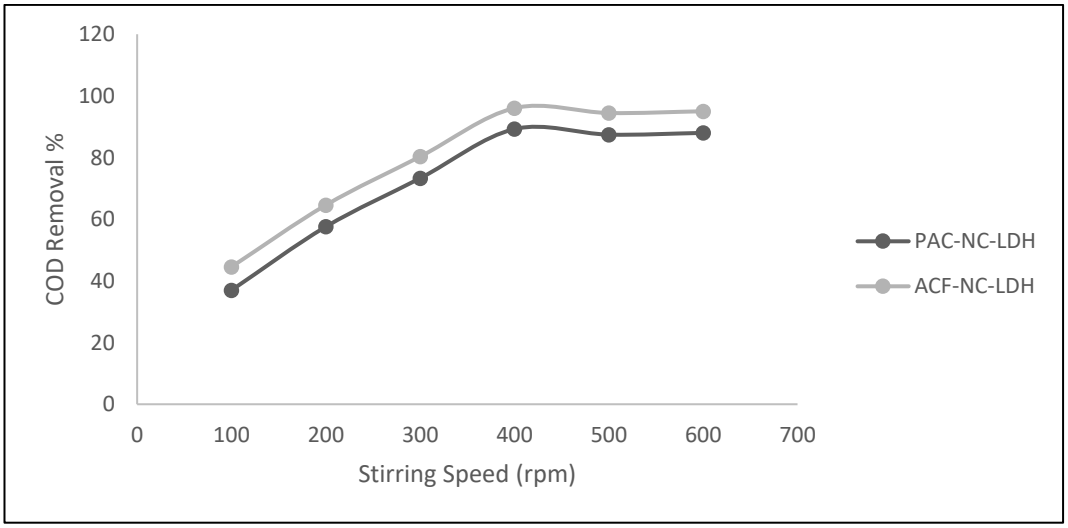

Figure 4. 10 Comparation between ACF-NC-LDH and PAC-NC-LDH under stirring speed effects.

4.2.3 Effect of Dosage

Different doses of the adsorbents were used between 0.1 g/300ml and 2 g/300ml at a stirring speed of 400 rpm, pH 6, and a temperature. of 25 °C for 120 min. Figure 4.11 shows the effect of changing the dose on the removal rate of PAC-

NC-LDH. The findings demonstrate that the clearance rate dramatically increased as the dosage of activated carbon increased. as the removal rate reached (45.02%, 75.31%, and 89.25%) at doses (0.1, 0.5, and 1g/300 ml), respectively.

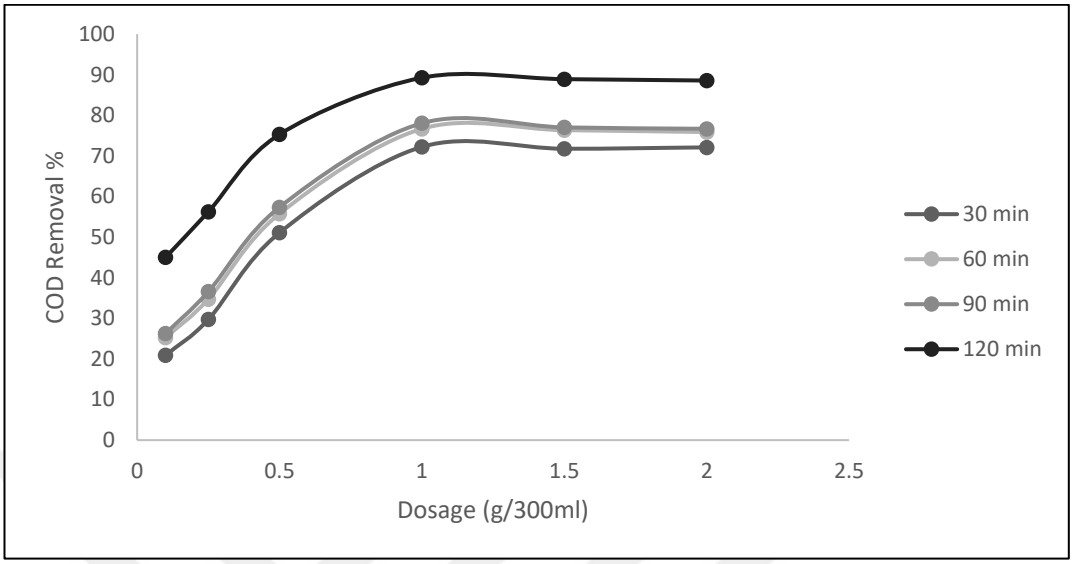

Figure 4. 11 The effect of dose on removal% for (PAC-NC-LDH)

Given in Figure 4.12 for ACF-NC-LDH, the removal rates were (52.11%, 82.4%, and 1.96%) at doses (0.1, 0.5, and1g/300 ml), respectively. It is noted that the elimination rate in both forms is fixed at a dose of 1g/300 ml. According to several research, the proportion of organic compounds removed rises when the adsorbent dose is increased. These characteristics were ascribed to an increased availability of adsorption sites due to the increase in adsorbent mass. On the other hand, it was observed that the rate of elimination was essentially constant after a particular dosage (1 g/300 ml). The steady removal efficiency explained the impact of active site overlap, which results in a decrease in both the total surface area of the adsorbent and the quantity of the accessible active site. As anticipated, increasing the sample dosage results in a bigger surface area and a greater number of adsorption sites, which improves the adsorption of organic pollutants at a constant starting concentration of the pollutant. The basic explanation for this feature is that when the dosage of adsorbent is increased, more and more adsorption sites become accessible, and the adsorption sites stay unsaturated throughout the adsorption reaction. In a batch sorption investigation, the solid/solution ratio plays a significant role in determining the adsorbent capacity.

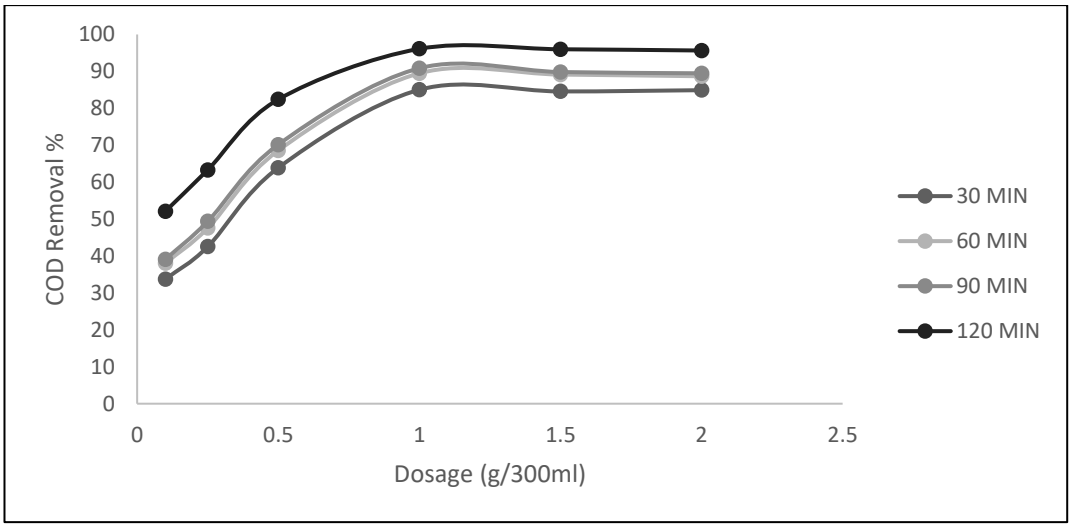

Figure 4. 12 The effect of dose on removal% for (ACF-NC-LDH)

Figure 4.13 shows the removal rates under the effect of changing the activated carbon fibers, the highest removal rates for the activated carbon powder, and this is evidence that the activated carbon fibers have higher adsorption sites than the activated carbon powder.

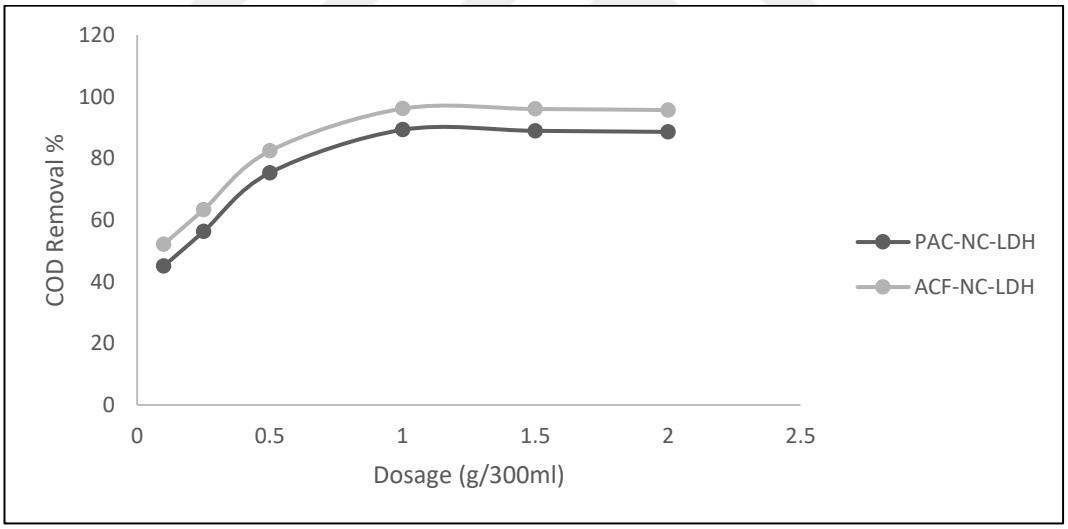

Figure 4. 13 Comparation between ACF-NC-LDH and PAC-NC-LDH under dose effects.

4.2.4 Effect of Contact Time

Contact time is one of the important factors affecting the efficiency of organic pollutants. For an adsorbent to be effective as an adsorbent, adsorption must be rapid and quantitative. The experiment was applied at times starting from 30 min up to 180 min at a temperature of 25 °C, a stirring speed of 400 rpm, a pH of 6, and a dose concentration of 1 g/300 ml. In all previous experiments, we notice that with the increase in contact time, the removal efficiency increases and reaches its peak

at the highest time applied in the experiments, which is 120 min. This experiment was conducted to show whether increasing the time increases the removal efficiency continuously. Figure 4.14 shows the effect of contact time on the removal efficiency for PAC-NC-LDH. The removal efficiencies were (55.8%, 71.3%, 78.1%, and 89.3%) at contact time (30, 60, 90, and 120min), respectively.

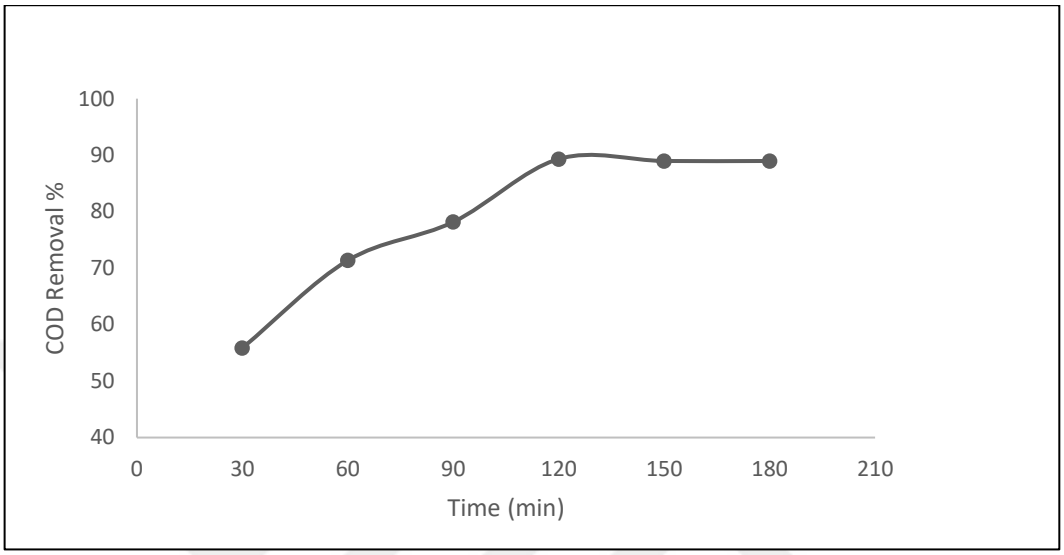

Figure 4. 14 Effect of contact time on removal % for (PAC-NC-LDH)

Figure 4.15 shows the effect of contact time on the removal efficiency for ACF-NC-LDH. The removal efficiencies were (69.95%, 85.68%, 92.25%, and 96.24%) at contact time (30, 60, 90, and 120 min), respectively. In both cases, it is noted that the removal efficiency increases with the increase in contact time until it reaches a certain limit and then becomes stable, as it was proven during the period from 120 min to 180 min, which may be explained by the enormous number of active sites that are available for COD adsorption during the first contact period. Because the adsorption process has a propensity to attain equilibrium fast and because different solid wastes have been combined to act as exchange agents for organic ions. There are a fixed number of active sorption sites in a system, so it is important to note that each active site can only adsorb one ion in a monolayer. As a result, the uptake of metal by the adsorbent surface will initially be rapid and then slow down due to the competition of ions for available active sites.

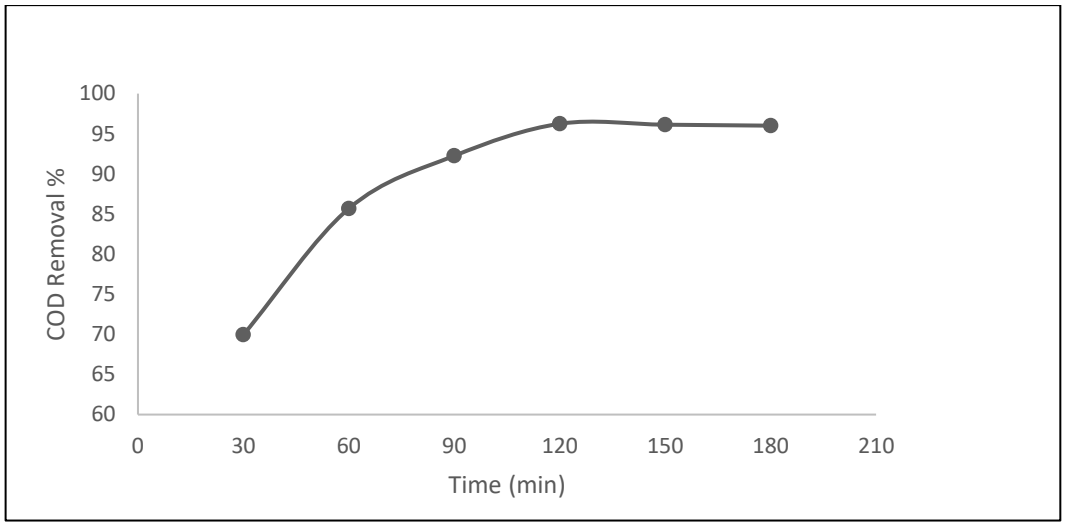

Figure 4. 15 Effect of contact time on removal % for (ACF-NC-LDH)

Figure 4.16 shows that the removal efficiency of activated carbon fibers is higher than the removal efficiency of activated carbon powder for all contact times. This explains that activated carbon fibers have more adsorption sites than their counterparts, which gives them preference in the adsorption of organic pollutants.

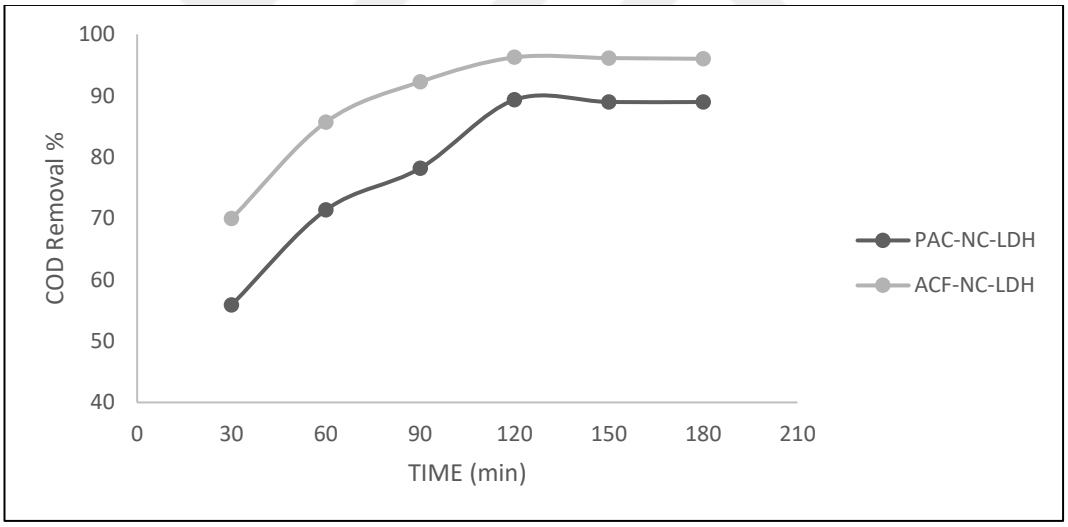

Figure 4. 16 Comparation between ACF-NC-LDH and PAC-NC-LDH under contact time effects.

4.2.5 The Effect of Temperature

Temperatures between (20-90 °C) were used to study how temperature affects removal effectiveness. The experiments were run for 120 min at a stirring speed of 400 rpm and a dosage of 1 g/300 ml at a pH of 6. The temperature was raised from 20 °C to 70 °C, which resulted in greater adsorption of COD. The removal effectiveness of the PAC-NC-LDH is shown in Figure 4.17 as a function of temperature, with the adsorption efficiency being (44.25% and 89.31%) at temperatures of (20 – 70 °C), respectively.

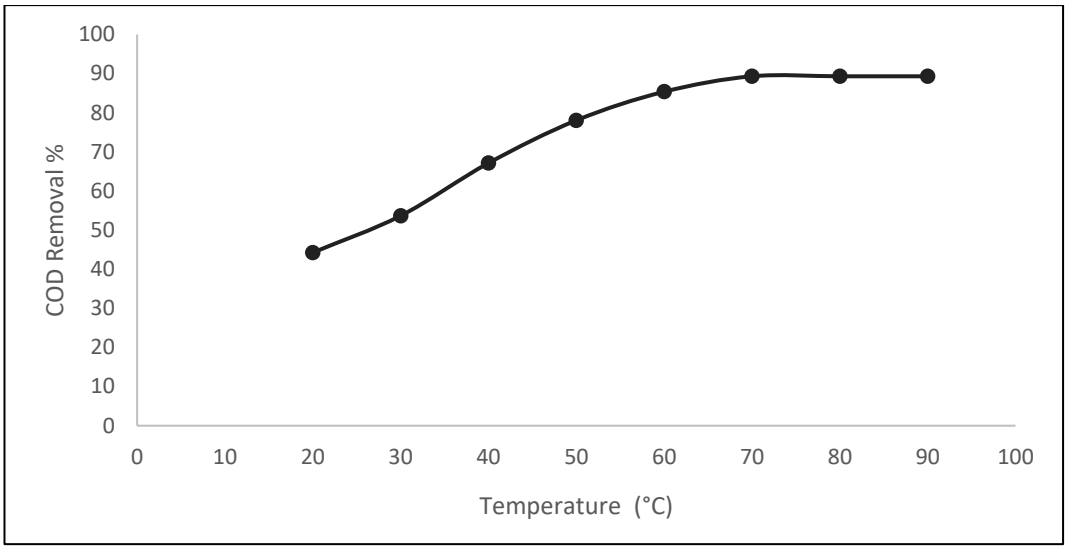

Figure 4. 17 Effect of temperature on removal% for (PAC-NC-LDH)

The impact of rising temperature on the ACF-NC-LDH's capacity for adsorption is seen in Figure 4.18. Absorption effectiveness at 20 ℃ and 70 ℃ was 53.42 and 96.16 %, revealing that for PAC and ACF, respectively, higher temperatures were more favorable for the adsorption of organic contaminants in general. When the temperature was increased to 80 ℃ and then 90 ℃, the adsorption efficiency remained constant as it was at 70 ℃. This explains that the adsorption sites were filled with adsorbed materials and there was no ability to absorb more pollutants. A kinetically regulated endothermic process is demonstrated by the fact that the temperature rise increased the pollutant adsorption rate because more diffusion increased the mass transfer of the pollutant particles.

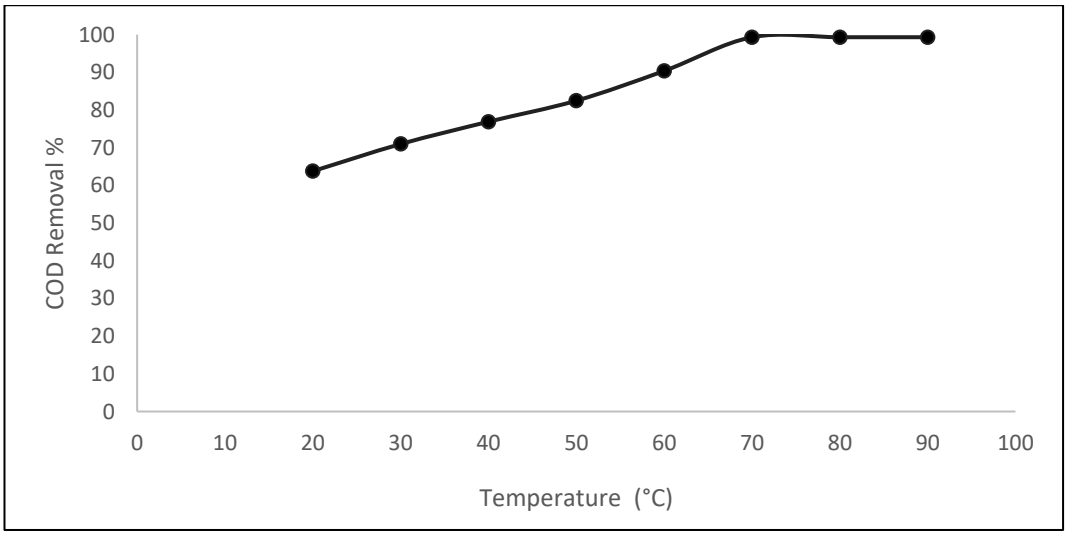

Figure 4. 18 Effect of temperature on removal% for (ACF-NC-LDH)

Figure 4.19 demonstrates that for all temperatures, activated carbon fibers have a better removal efficiency than activated carbon powder. This demonstrates

that compared to their competitors, activated carbon fibers contain more adsorption sites, giving them an edge in the adsorption of organic contaminants.

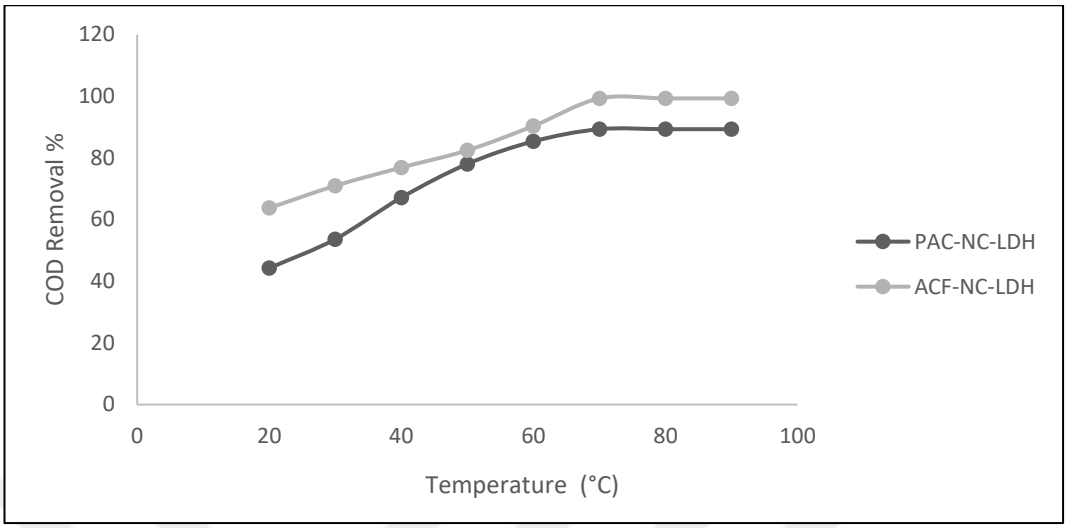

Figure 4. 19 Comparation between ACF-NC-LDH and PAC-NC-LDH under temperature effects.

Samples of polluted water were taken from the Baiji refinery for a full month, and the samples were examined before and after using the activated carbon fiber produced. After conducting experiments on pH, stirring speed, dose, temperature, and time determine the optimal conditions for conducting the final experiment. The experiment was conducted at a pH of 6, stirring speed of 400rpm, a dose of activated carbon of 1g/300 ml, and a temperature of 70℃ for 120min for ACF-NC-LDH and PAC-NC-LDH on a polluted water sample that was examined in the Baiji refinery. The results showed that the removal rate of all organic pollutants, including oil and other pollutants shown in Table 4.1 reached 99.26% for ACF-NC-LDH and 90.3% for PAC-NC-LDH as indicated in Figure 4.20. These results indicate the high efficiency of the chemical treatment process in increasing the percentage of removal of oily residues and other organic residues compared to previous studies in which active carbon was produced from palm fibers. According to Abd El Aziz Nayl et al. (88), the total removal rate reached about 91% after they produced active carbon from date palm fibers without any chemical treatment. As for Jinhui Wang et al. (252), the total removal rate reached about 95% after they used the treatment. Chemical coating and lamination to improve commercial activated carbon fibers. Hence, it can be said that the total removal rate that we obtained (99.26%) was excellent and exceeded most previous studies.

Table 4. 1 The removal rates of all organic pollutants, including oil.

The Pollutant	Total (Mg/L)	ACF-NC-LDH (remaining)	Removal efficiency	PAC-NC-LDH (remaining)	Removal efficiency
COD	890	6	99.32%	92	89.66%
OIL	871	4.2	99.51%	92	89.44%
Sulfate	380	2.9	99.23%	34	91.05%
Heavy metals	488	4.2	99.13%	36	92.62%
TDS	721	9	98.75%	91	87.38%
Na	466	1.7	99.63%	22	95.28%
Total amount	3816	28	**99.26%**	367	**90.38%**

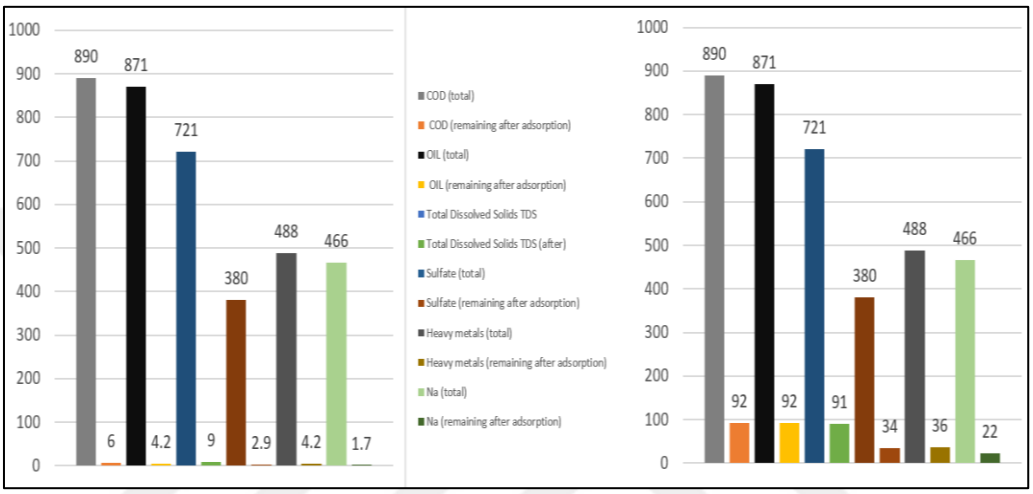

Figure 4. 20 The amount of wastewater before and after final adsorption process

4.3 Thermodynamic adsorption results

The thermodynamic parameters of COD adsorption on PAC-NC-LDH and ACF-NC-LDH, including Gibbs free energy ΔG° (kJ/mol), standard enthalpy ΔH°(kJ/mol), and standard entropy ΔS° (kJ/mol. k), were calculated using the equations previously reported in the section materials and methods. The slope and intercept of the plots of ln K_{eq} against 1/T were used to obtain the values of ΔH° and ΔS°. Figure 4.21 depicts the plot of 1/T vs ln Keq for COD for PAC-NC-LDH and ACF-NC-LDH, respectively. Table 4.2 displays the (ΔH°), (ΔS°), (ΔG°), and R^2 of several plots for adsorption on PAC-NC-LDH and ACF-NC-LDH.

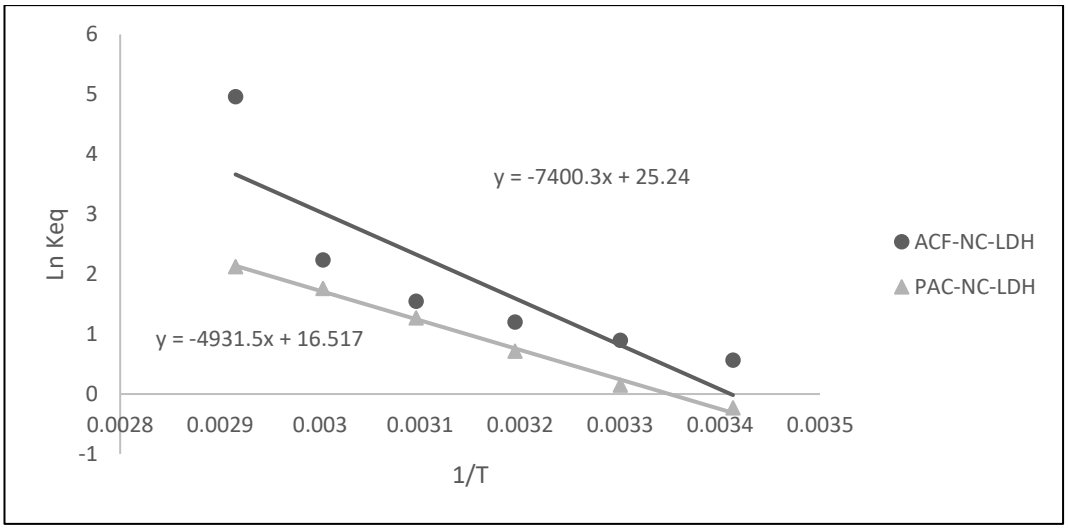

Figure 4. 21 Slopes of (1/T) and (Ln K_{eq}) for (PAC-NC-LDH) and (ACF-NC-LDH).

The two processes that make up the adsorption process in a solid-liquid system are (a) the desorption of previously adsorbed water molecules, and (b) the adsorption of adsorbate species. The adsorption process is endothermic because the material molecules must displace more than one water molecule to adhere. The endothermic nature of the activated carbon from the COD adsorption system is indicated by the computed positive values of ΔH°. The spontaneous behavior and viability of the adsorption process are both confirmed by the negative values of (ΔG°). The magnitude of (ΔG°) grew as the temperature climbed, which suggests that the system's level of spontaneity also increased. The interface of activated carbon/industrial waste treated in the adsorption process shows increased randomness and disorder, as indicated by the calculated positive values (ΔS°).

Table 4. 2 Thermodynamic results for PAC-NC-LDH and ACF-NC-LDH.

	PAC-NC-LDH			**ACF-NC-LDH**		
T (°C)	ΔG° (kJ/mol)	ΔS° (kJ/mol.K)	ΔH° (kJ/mol)	ΔG° (kJ/mol)	ΔS° (kJ/mol.K)	ΔH° (kJ/mol)
20	0.56	0.137	41	-1.38	0.209	61.52
30	-0.36			-2.25		
40	-1.85			-3.13		
50	-3.40			-4.16		
60	-4.88			-6.20		
70	-6.05			-14.14		
80	-6.05			-14.14		
90	-6.05			-14.14		

4.4 Kinetic adsorption results

The removal of heavy metals and other potentially dangerous substances from aqueous solutions, including dyes, has recently been the subject of much research. Kinetic processes have been the main focus of the majority of adsorption research. The adsorption process benefits from the kinetic data analysis since it provides information on the adsorbate uptake rate, which regulates the resident time in the adsorbent. Adsorption kinetics refers to the pace at which contaminants are drawn out of the water-based solution. The study of kinetics is crucial for evaluating the efficiency of adsorption, outlining the mechanism by which events occur, and providing dynamic evidence for the amount of time needed to achieve an equilibrium, the rate of adsorption, and the limiting step of adsorption. The values of k_1 and q_e were calculated using the slopes and intercepts of the straight lines generated in log (q_e - q_t) vs. t plots, as illustrated in Figure 4.22 for pseudo-first-order.

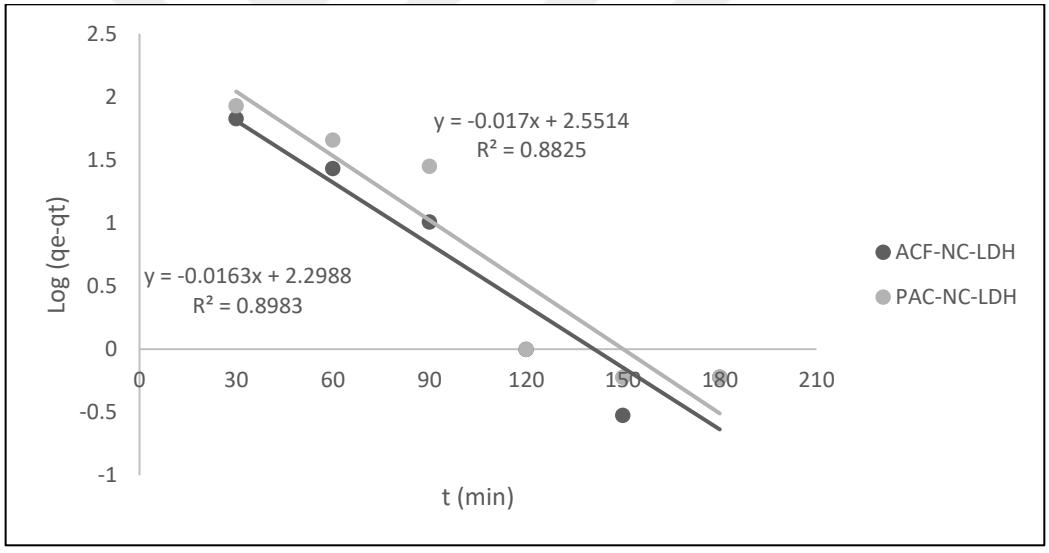

Figure 4. 22 Pseudo first order model for PAC-NC-LDH and ACF-NC-LDH.

By plotting t/q_t vs. time, as seen in Figure 4.23, the values of k_2 and qe were calculated and are reported in Table 4.3.

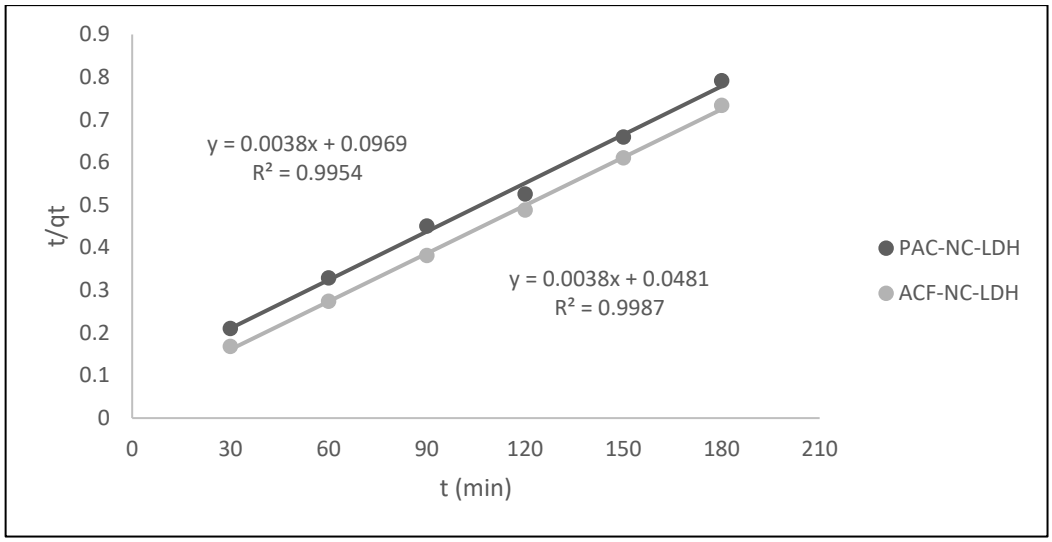

Figure 4. 23 Pseudo second order for PAC-NC-LDH and ACF-NC-LDH

A high adsorption rate is a necessary quality in addition to the adsorbent's adsorption capacity and removal effectiveness if it is intended for use in wastewater treatment plants. Using experimental data at various starting concentrations, the kinetics study onto adsorbents were studied using pseudo-first-order, pseudo-second-order, and intra-particle diffusion models. These models were used to get the computed parameter values in line with equations (14), (15), (17), and (18). The accuracy between the estimated and experimental q_e values, as well as R^2 for each applied model, are used to determine which model is the most beneficial.

Table 4. 3 Kinetic adsorption results for PAC-NC-LDH and ACF-NC-LDH

	Pseudo-first-order parameter				**Pseudo-second-order parameter**		
	k_1 (/min)	**q_e, calc.(mg/g)**	**R^2**	**q_e, exp (mg/g)**	**k_2 (/min)**	**q_e, calc.(mg/g)**	**R^2**
ACF-NC-LDH	0.0163	9.96	0.89	246	3.0 x 10^{-4}	263.1	0.99
PAC-NC-LDH	0.0170	12.82	0.88	228.3	1.4 x 10^{-4}	263.1	0.99

As can be seen, for (ACF-NC-LDH) and (PAC-NC-LDH), respectively, the correlation coefficient values for pseudo-first-order kinetics (R^2 = 0.8983) are lower than those for pseudo-second-order kinetics (R^2 = 0.9987) and for pseudo-first-order kinetics (R^2 = 0.8825) are lower than those for pseudo-second-order kinetics (R^2 = 0.9954). According to the coefficient of correlation values of the results with a pseudo-second-order kinetic model which most closely fits the

obtained experimental data, the primary adsorption mechanism for the investigated adsorption procedure for removing COD from industrial wastewater by preparing the activated carbon fiber is chemisorption reaction. Intraparticle diffusion (IPD)-governed kinetics data analysis. The dispersion mechanism and rate-limiting mechanisms that affect the adsorption kinetics are identified using this connection. The diffusion models frequently have as their basis the following mechanistic steps. Internal mass transfer inside the adsorbent particle's internal structure (intraparticle diffusion), external mass transfer across the boundary region surrounding the adsorbent particles, diffusional mass transfer through a pore or surface, or a combination of these processes, as well as adsorption/desorption at a surface site. The intraparticle dispersion model states that the speed at which the adsorbate diffuses in the direction of the adsorbent determines the rate of adsorption. By this idea, $t^{\frac{1}{2}}$ rather than t, the adsorbate uptake qt varies almost proportionately with the contact time. If the product of the graph between the adsorption amplitude and the square root of time is a straight line passing through the origin, then the intraparticle diffusion step is the only velocity-determining step. However, the deviation of the straight line from the point of origin (and this is noted by the cut-off value C when it is greater than zero) as a result of the change in mass transfer in the initial and final stages of the adsorption process indicates that the adsorption process consists of several steps, including adsorption on the outer surface and internal diffusion.

Figure 4.24 shows the diffusion curve diagram for both samples produced. Furthermore, in Table (4.4) the C values (147.37 and 91.52) for both ACF-NC-LDH and PAC-NC-LDH respectively were larger than zero, demonstrating that the adsorption process rate limiting, rather than intra-specific diffusion, contributes to the diffusion of the border layer.

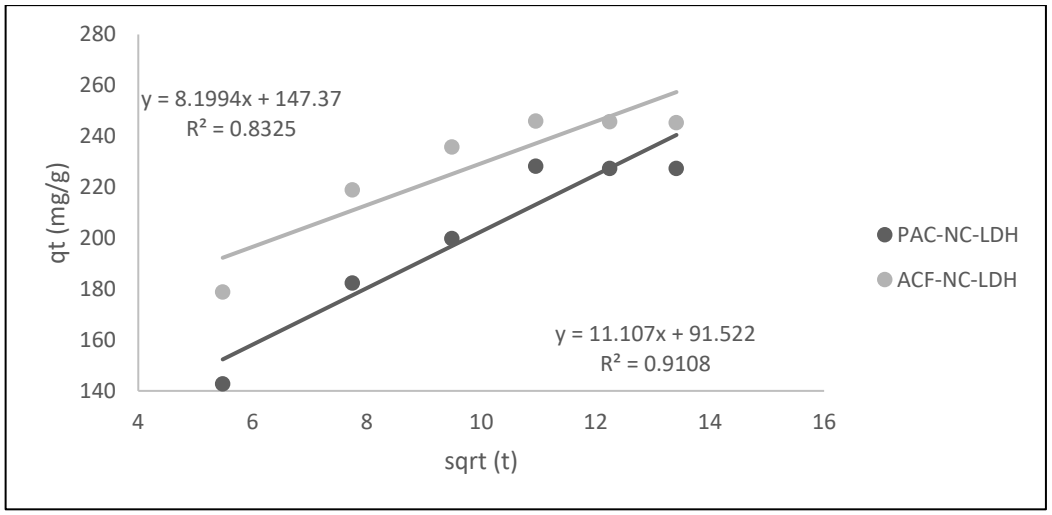

Figure 4. 24 The intraparticle diffusion model for (PAC-NC-ACF) and (ACF-NC-LDH).

Table 4. 4 The results of intra-particular diffusion model.

Model	**Intra-particular diffusion**		
Parameters	**C**	**K_d**	**R^2**
ACF-LC-LDH	147.37	8.1994	0.8325
PAC-NC-LDH	91.522	11.107	0.9108

4.5 Adsorption isotherm models

4.5.1 Langmuir adsorption isotherm

The monolayer adsorption of a solute from a fluid solution on an outer layer with a limited number of identical sites is consistent with the Langmuir adsorption isotherm. The model is based on several fundamental hypotheses, including The capacity of the adsorbent to hold the adsorbate is finite (at equilibrium); (i) sorption takes place at predetermined homogenous sites inside the adsorbent; (ii) once a dye molecule occupies a site; and (iii), (iii), (iv), and (v) all sites are identical and energetically equivalent. The Langmuir isotherm model states that during homogeneous energy of adsorption onto the surface, there is no adsorbate migration in the plane of the surface. The Langmuir isotherm model was chosen to determine the maximum adsorption capacity corresponding to complete monolayer coverage on the sorbent surface.

For the Langmuir isotherm, C_e/q_e is plotted versus C_e, as shown in Figures 4.25, and Figure 4.26. The Langmuir isotherm model is appropriate for COD adsorption from industrial wastewater treated by ACF-NC-LDH, according to straight lines ($R^2 > 0.99$) that were obtained and for PAC-NC-LDH was ($R^2 < 0.99$).

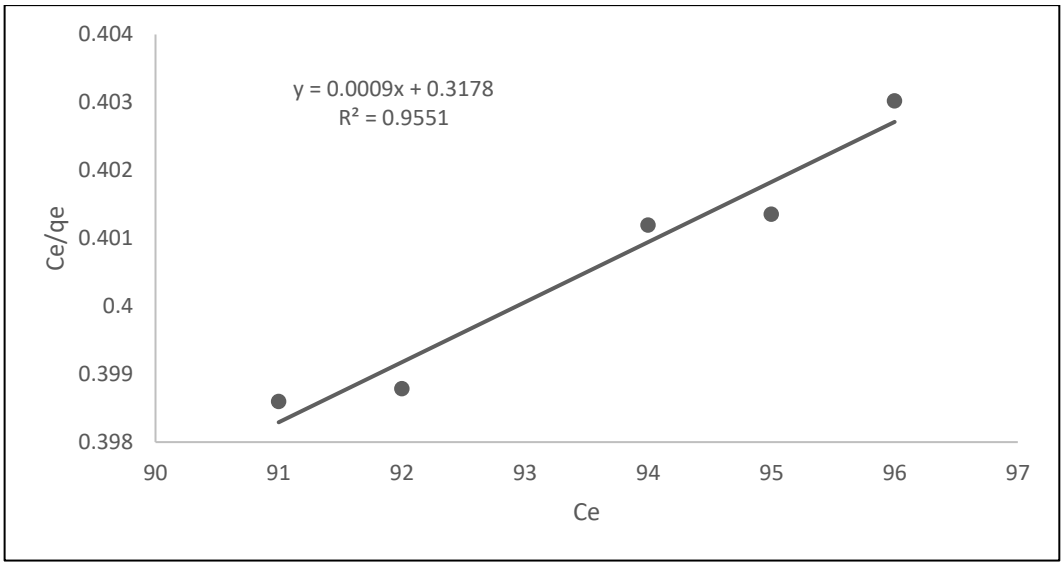

Figure 4. 25 Langmuir adsorption isotherm for PAC-NC-LDH.

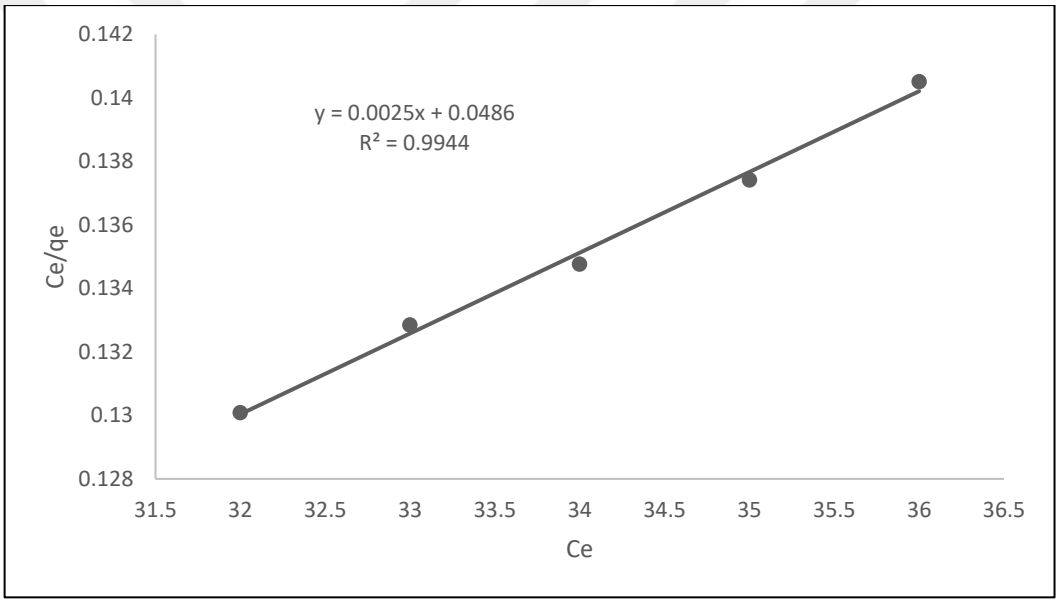

Figure 4. 26 Langmuir adsorption isotherm for ACF-NC-LDH

The RL value indicates that the isothermal form is either unfit (R_L), linear (R_L = 1), fit (0 < R_L < 1), or irreversible (R_L = 0) (255). As shown in Table 4.5, for the two adsorption systems, the RL values at different concentrations range between 0 and 1, which indicates a suitable adsorption. Low values of R_L indicate high and favorable adsorption for both samples.

Table 4. 5 Langmuir adsorption isotherm parameters.

Sample	**Langmuir adsorption isotherm**			
	R^2	**R_L**	**q_o (mg/g)**	**k (l/mg)**
PAC-NC-LDH	0.9551	0.284-0.293	111.11	0.00283
ACF-NC-LDH	0.9944	0.0219-0.0229	400	0.05

4.5.2 Freundlich adsorption isotherm

The first established model for the sorption process is the Freundlich isotherm model (255). The Freundlich equation is also used to propose that sorption energy rapidly reduces upon completion of the sorption centers of an adsorbent. The model applies to adsorption on heterogeneous surfaces with interaction between adsorbed molecules.

From plotting log (C_e) and Log (q_e) the 1/n value has been calculated as shown in Figures 4.27 and Figure 4.28. As shown in Table 4.6, the values of n are (1.2 and 2.7) for each of (PAC-NC-LDH and ACF-NC-LDH), respectively, where (n>1), which means that the adsorption is a favorable physical process. The heterogeneity factor is 1/n, and n is a measurement of the adsorption's departure from linearity. According to its value, the relationship between solution concentration and adsorption is not linear to the extent shown below: Adsorption is linear if n is equal to unity; chemical adsorption is implied if n is less than unity; and advantageous physical adsorption is implied if n is more than unity.

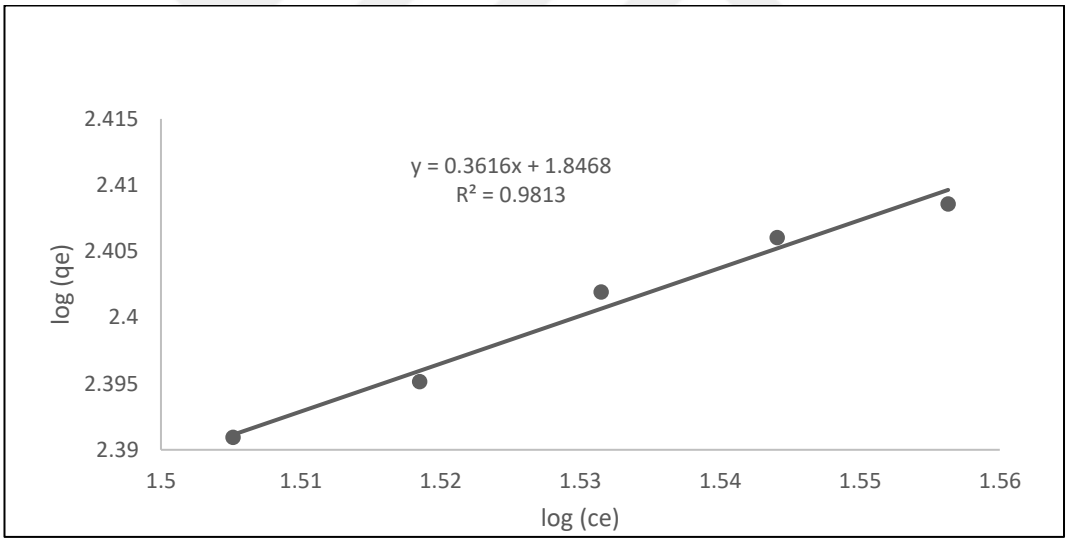

Figure 4. 27 The Freundlich adsorption isotherm model for ACF-NC-LDH.

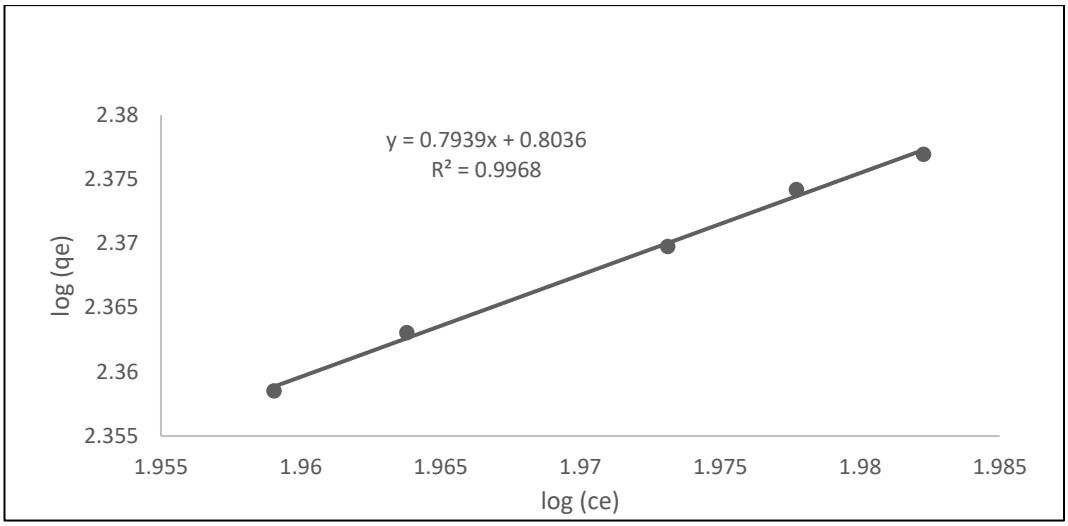

Figure 4. 28 The Freundlich adsorption isotherm model for PAC-NC-LDH.

Table 4. 6 Freundlich adsorption isotherm parameters.

Samples	Freundlich adsorption isotherm			
	R^2	**1/n**	**n**	**k**
PAC-NC-LDH	0.9968	0.7939	1.2	6.3
ACF-NC-LDH	0.9813	0.3616	2.7	70.2

In addition, the values of R^2 are (0.99 and 0.98) for each of (PAC-NC-LDH and ACF-NC-LDH), respectively, which means that the Freundlich adsorption isotherm applies to the powder sample more than its counterpart (ACF-NC-LDH).

4.5.3 Temkin Isotherm

Temkin makes the supposition that the quality of different binding sites makes them not all equal. Adsorption will only take place at specific locations, ideally the higher energy locations, yet there will be repulsion at empty locations when the nearby locations are filled, then low-energy locations. Adsorbent interactions between adsorbent species are explicitly taken into account by a factor in the Temkin isothermal model. This model makes two key assumptions: (i) adsorption is defined by a uniform distribution of binding energies, up to a maximum binding energy; and (ii) adsorption is characterized by a linear reduction in heat of adsorption for all molecules in the layer with coverage owing to adsorption-adsorption interactions. The Freundlich equation demonstrates that the reduction in the heat of absorption is linear rather than logarithmic, which is the assumption used in the derivation of the Tempkin isotherms. The Tempkin constants A_T (l/mg) and b_T (J/mol) are used in the following diagram to represent

how the Tempkin isotherms are often utilized. R is the universal gas constant, which has the value of 8.314 $J.mol^{-1}\ K^{-1}$, and T is the absolute temperature in Kelvin. The slope and intercepts of the plots produced by plotting q_e vs, $logC_e$ are used to calculate the A_T and b_T constants.

Plotted by plotting log C_e with q_e, Figures 4.29 and 4.30 show the Temkin model for PAC-NC-LDH and ACF-NC-LDH, respectively. It turns out that both samples apply to the Temkin model, as shown in Table 4.7. The R-value is (.9970 and 0.9821 for PAC-NC-LDH and ACF-NC-LDH, respectively.

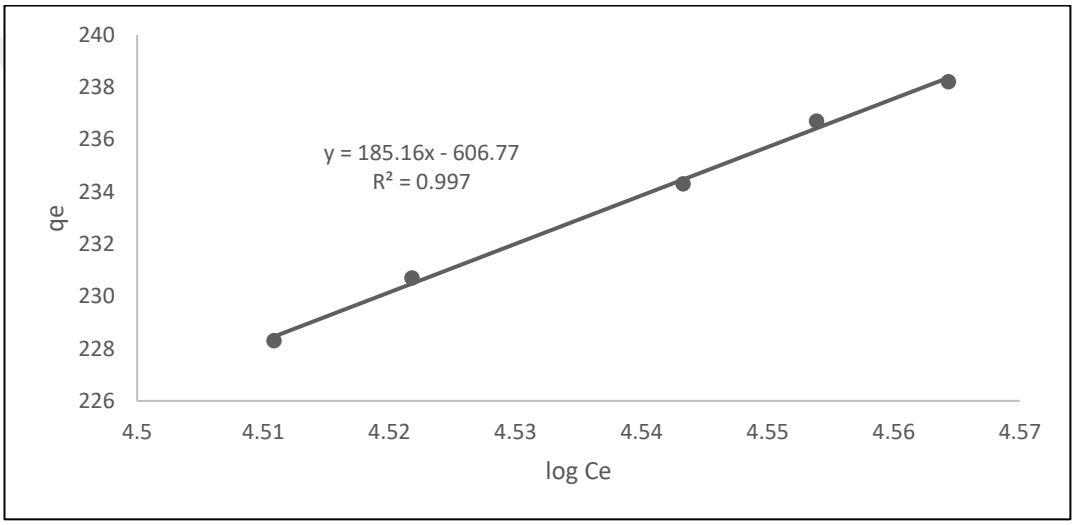

Figure 4. 29 The Temkin isotherm model for PAC-NC-LDH

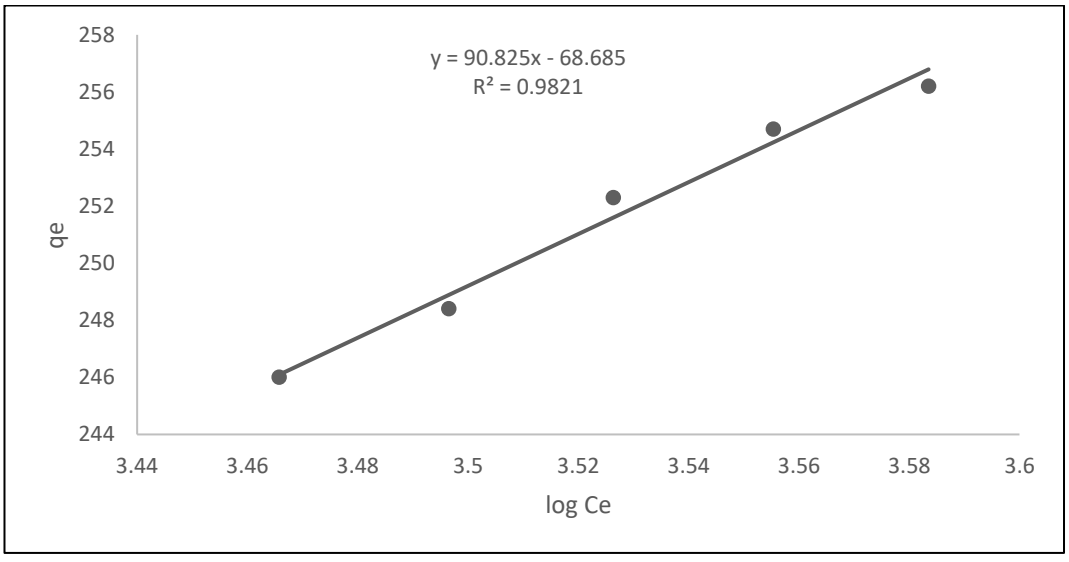

Figure 4. 30 The Temkin isotherm model for ACF-NC-LDH

Table 4. 7 Temkin isotherm results.

Parameters / Sample	Temkin isotherm model		
	R^2	A_T (l/mg)	b_T (J/mol)
ACF-NC-LDH	0.9821	0.469	27.278
PAC-NC-LDH	0.9970	0.037	13.380

An increase or decrease in the values of A_T and b_T affects this relationship.

- A_T is the adjustment factor representing the effect of surface reactions on adsorption. An increase enhances the chemical impact on the adsorption process.

- b_T is a coefficient controlling the structural effect on the surface. An increase suggests a lesser structural impact, possibly due to the formation of a chemical layer that reduces structural effects.

It is expected that A_T is larger for active carbon fibers, indicating a more significant chemical impact on the adsorption process. Meanwhile, b_T also signifies a structural influence, and it seems to have a higher b_T value for active carbon fibers. This higher b_T may suggest a lesser structural impact compared to activated carbon powder.

4.6 Response Surface Method (RSM)

The theoretical model that connects certain controllable variables (factors) to a response is frequently either unavailable or extremely complicated. Information on the relationship between the causes and the response in this situation should be gathered empirically. The Central Compsite Design of Response Surface Methodology (RSM) is a group of statistical and mathematical methods for studying situations like the one being presented using an empirical model.

ACF-NC-LDH was analyzed using the response surface method RSM and ANOVA tables by MINITAB software. Table 4.8 shows the P-value and F-value for the ANOVA analysis where both pH and time were chosen as variables versus COD which was selected as the response. In Table 4.8, the F-value for the PH, which was 0.71, indicates that the regression equation can account for the majority of the variance in response. To determine if the F distribution is statistically significant, the P-value is utilized. A P-value of less than 0.05 indicates that the model is statistically significant. It should be noted that the P-values for pH and time were (0.005, and 0.041), respectively, indicating that the variables indeed impact the process's outcomes and that the model is statistically significant.

The degree to which the points on a normal probability plot match a straight line is one technique to evaluate the normality of a distribution. As seen in Figure 4.31, Minitab often provides the normal probability plot directly. Which variables have the most influence on the experiment is determined through the Pareto chart (Figure 4.31a), which shows that the square vector of pH is the most influential, followed by time. The vertical line can be observed at 2.101, which indicates that the distribution is statistically significant when the line intersects more vectors. It appears that the model has a normal distribution when observing the figure (Figure 4.31b). This is known by observing the points that the closer they are to the reference line, the more normal the distribution is. Figure 4.31c shows that the model has a normal distribution, as a pyramid-shaped histogram with a peak appears. The more points on the versus order represent an irregular shape with pulses, the more it indicates that the distribution is normal and has an impact on the efficiency of the target, as in Figure 4.31d. The Response Optimizer tool shows that the best value for obtaining the lowest COD is at a pH of 6.4 and a time of 120 min, and shows the 3D surface plot of COD vs PH and time (Figure 4.32).

Table 4. 8 The ANOVA table of pH and time as variables and COD as response for ACF-NC-LDH.

Source	**DF**	**Adj SS**	**Adj MS**	**F-Value**	**P-Value**
Model	5	392844	78569	9.88	0.000
Linear	2	112864	56432	7.10	0.005
PH	1	5643	5643	0.71	0.041
TIME	1	107221	107221	13.48	0.002
Square	2	269638	134819	16.95	0.000
PH*PH	1	269337	269337	33.86	0.000
TIME*TIME	1	301	301	0.04	0.848
2-Way Interaction	1	10341	10341	1.30	0.269
PH*TIME	1	10341	10341	1.30	0.269
Error	18	143168	7954		
Total	23	536012			

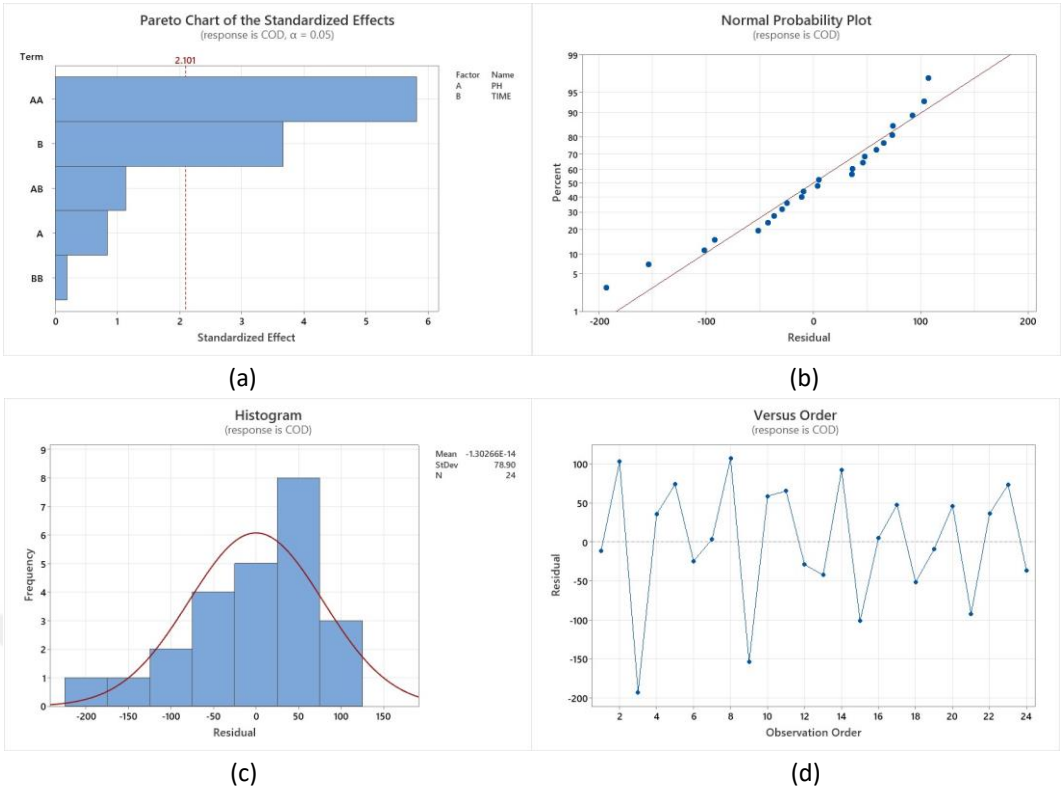

Figure 4. 31 Normal probability plots of pH and time as variables and COD as response for ACF-NC-LDH.

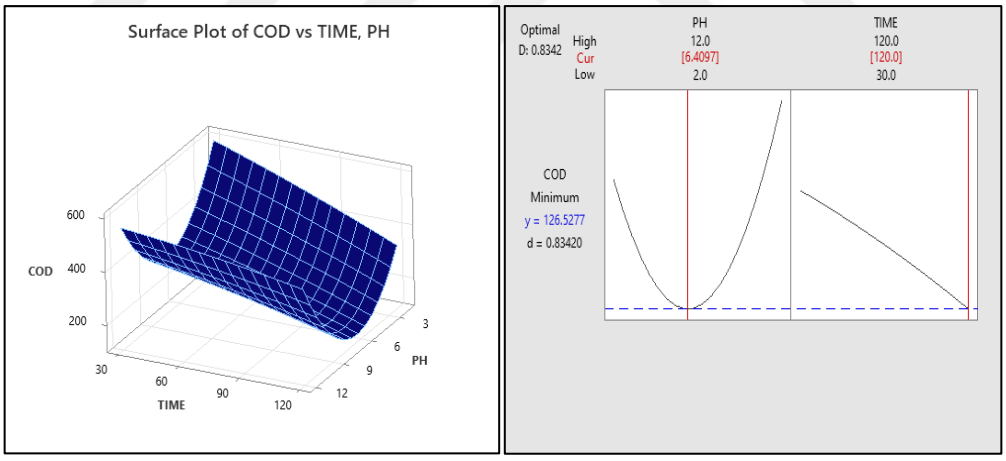

Figure 4. 32 The left: 3d surface plot for COD vs time and PH, The right: the optimum values of time and PH for lower COD for ACF-NC-LDH.

The P-value and F-value for the ANOVA analysis in which COD was chosen as the response and both stirring speed and time were chosen as variables are shown in Table 4.9. The F-value for the stirring speed, which was 1390.01, indicates that the regression equation can account for the majority of the variance in response Table 4.9. To determine if the F distribution is statistically significant, the P-value is utilized. A (P-value) of less than 0.05 indicates that the model is statistically

significant. It should be noted that the P-values for stirring speed and time were (0.000, 0.000), respectively, indicating that the variables indeed impact the process's outcomes and that the model is statistically significant. The degree to which the points on a normal probability plot match a straight line is one technique to evaluate the normality of a distribution. As seen in Figure 4.33, Minitab often provides the normal probability plot directly. Through the Pareto chart (Figure 4.33a), which demonstrates that the vector of stirring speed is the most significant variable, it is possible to identify which factors have the most impact on the experiment. The vertical line can be observed at 2.1, which indicates that the distribution is statistically significant when the line intersects more vectors. When looking at the Figure 4.33b, it looks like the model has a normal distribution. By examining the points, it can be determined that the distribution is more normally distributed the closer the points are to the reference line. Figure 4.33c displays a pyramid-shaped histogram with a peak, demonstrating the model's normal distribution. As shown in Figure 4.33d, the more points on the versus order that show an irregular shape with pulses, the more strongly it suggests that the distribution is normal and affects the effectiveness of the target. The response optimizer tool demonstrates that a speed of stirring of 509.09 rpm and a duration of 120 minutes result in the lowest COD, and displays a 3D surface plot of COD versus stirring speed and time (Figure 4.34).

Table 4. 9 The ANOVA table of stirring speed and time as variables and COD as response for ACF-NC-LDH.

Source	**DF**	**Adj SS**	**Adj MS**	**F-Value**	**P-Value**
Model	5	1007720	201544	344.62	0.000
Linear	2	865212	432606	739.71	0.000
Stirring speed	1	812920	812920	1390.01	0.000
Time	1	52292	52292	89.41	0.000
Square	2	133359	66679	114.02	0.000
Stirring speed*stirring speed	1	129329	129329	221.14	0.000
Time*time	1	4030	4030	6.89	0.017
2-way interaction	1	9149	9149	15.64	0.001
Stirring speed*time	1	9149	9149	15.64	0.001
Error	18	10527	585		
Total	23	1018247			

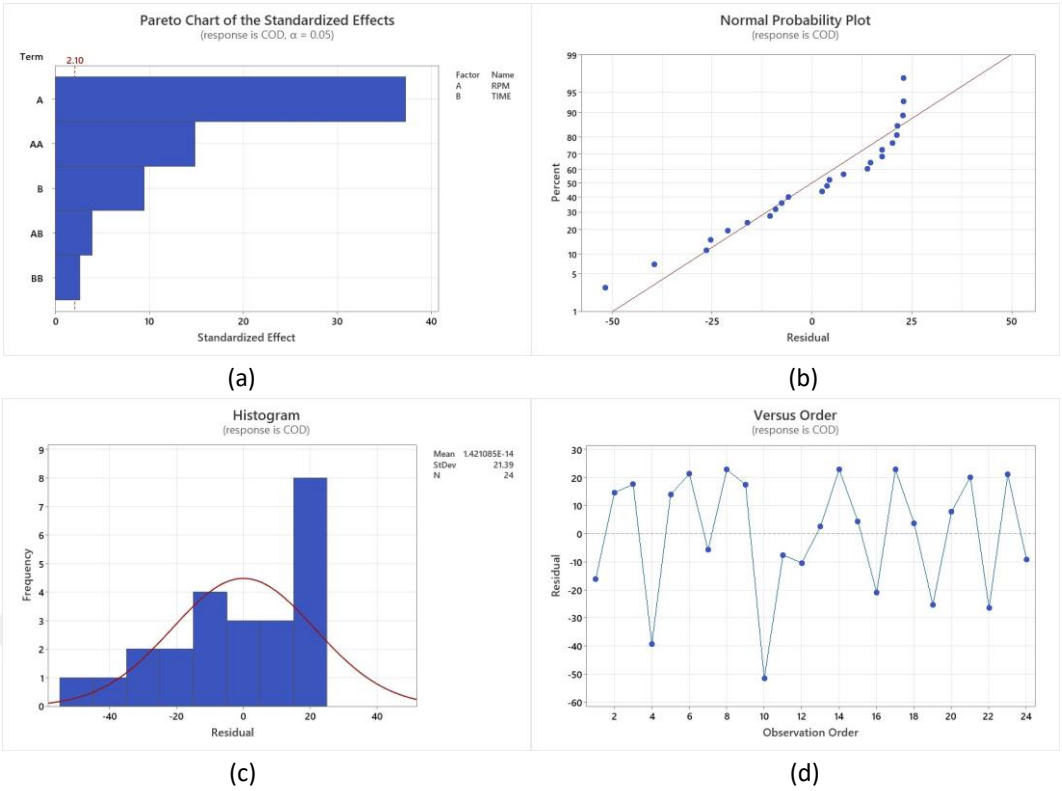

Figure 4. 33 Normal probability plots of stirring speed and time as variables and COD as response for ACF-NC-LDH.

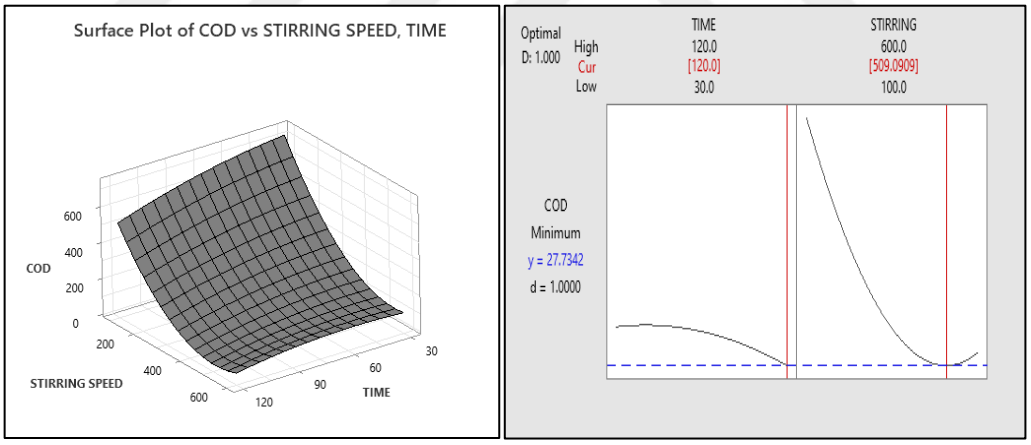

Figure 4. 34 The left: 3d surface plot for COD vs time and stirring speed, The right: the optimum values of time and stirring speed for lower COD for ACF-NC-LDH.

Table 4.10 displays the P-value and F-value for the ANOVA study in which dosage and time were chosen as factors and COD was selected as the response. The regression equation can explain the bulk of the variance in response, according to the F-value for the dose, which was 440.82 in Table 4.10. The P-value is used to assess the statistical significance of the F distribution. When the (P-value) is less than 0.05, the model is considered statistically significant. It should be noted that

the P-values for the dosage and time were (0.000, and 0.000), respectively, demonstrating that the variables do indeed affect the process' results and that the model is statistically significant. One method to assess a distribution's normality is to see how closely the points on a normal probability plot resemble a straight line. Figure 4.35 illustrates how Minitab frequently offers the normal probability plot directly. It is possible to determine which variables have the most effects on the experiment by using the Pareto chart (Figure 4.35a), which shows that the vector of dosage is the most important variable. The vertical line can be observed at 2.1, which indicates that the distribution is statistically significant when the line intersects more vectors. The model appears to have a normal distribution considering Figure 4.35b. The distribution is shown to be more regularly distributed the closer the points are to the reference line by looking at the points. The normal distribution of the model is illustrated by a pyramid-shaped histogram with a peak in Figure 4.35c. The efficacy of the target is impacted by the number of spots on the versus order that exhibit an irregular shape with pulses, as illustrated in Figure 4.35d. The more such points, the more firmly the distribution is thought to be normal. The response optimizer tool shows that dosage for 120 minutes at 1.4434 yields the lowest COD and shows a 3D surface plot of COD against dosage and time (Figure 4.36).

Table 4. 10 The ANOVA table of dosage and time as variables and COD as response for ACF-NC-LDH.

Source	**DF**	**Adj SS**	**Adj MS**	**F-Value**	**P-Value**
Model	5	776571	155314	136.97	0.000
Linear	2	542223	271111	239.08	0.000
Dose	1	499870	499870	440.82	0.000
Time	1	42353	42353	37.35	0.000
Square	2	169689	84844	74.82	0.000
Dose*dose	1	166829	166829	147.12	0.000
Time*time	1	2860	2860	2.52	0.130
2-way interaction	1	2951	2951	2.60	0.124
Dose*time	1	2951	2951	2.60	0.124
Error	18	20411	1134		
Total	23	796982			

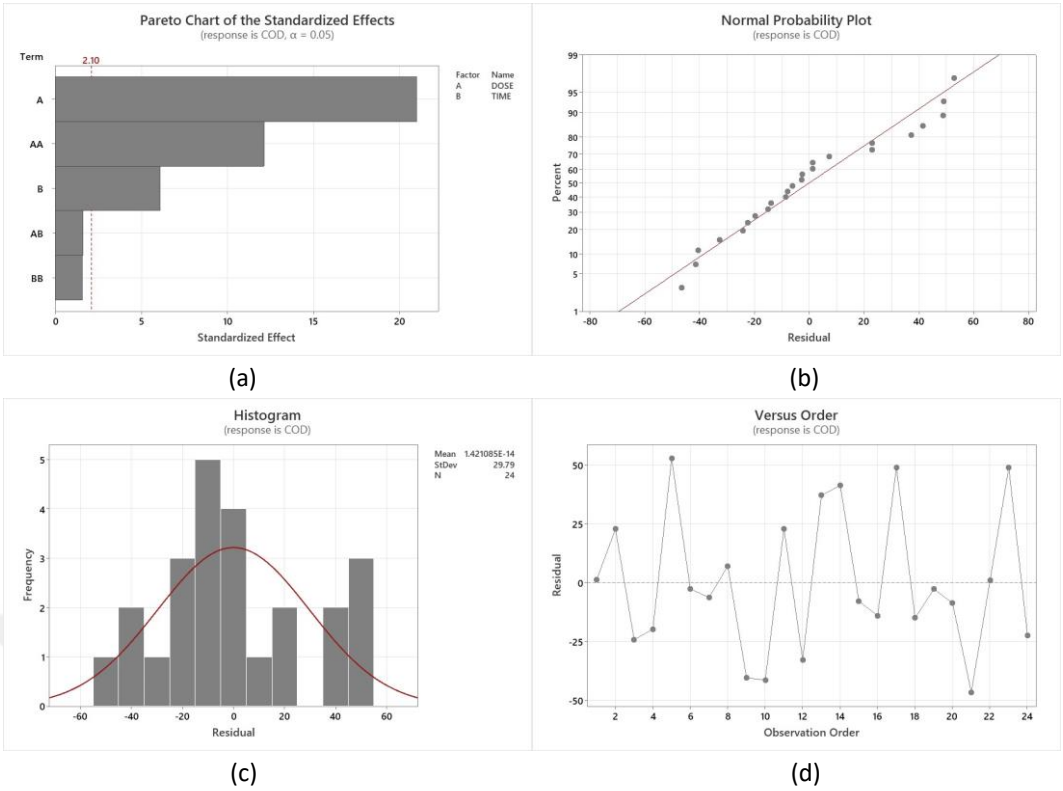

Figure 4. 35 Residual plots of dosage and time as variables and COD as response for ACF-NC-LDH.

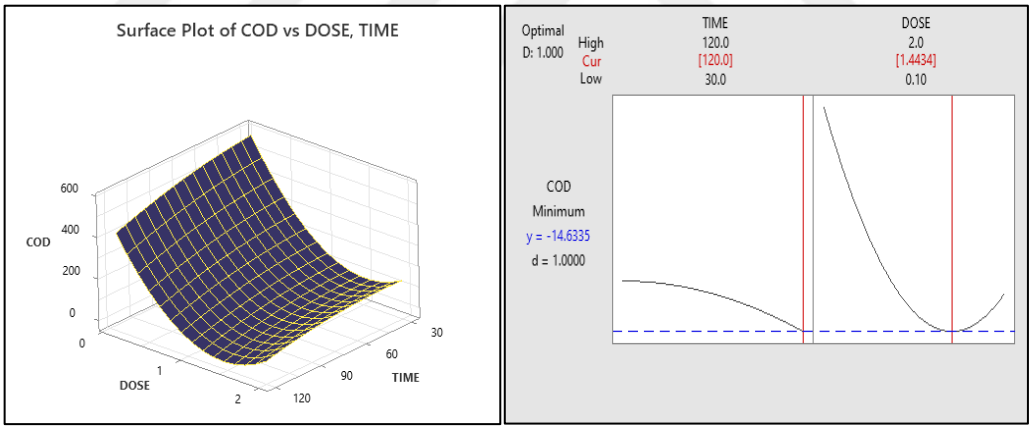

Figure 4. 36 The left: 3d surface plot for COD vs time and dosage, The right: the optimum values of time and dosage for lower COD for ACF-NC-LDH.

The P-value and F-value for the ANOVA analysis with temperature and time as variables and COD as the response are shown in Table 4.11. According to the F-value for the temperature, which was 957.92, the regression equation can explain the majority of the variance in response in Table 4.11. The statistical significance of the F distribution is determined by the P-value. The model is considered statistically significant when the P-value is less than 0.05. It should be noted that the P-values for the temperature and time were (0.000, and 0.000), indicating that

the variables do impact the process's results and that the model is statistically significant. One way to determine the normality of a distribution is to examine how closely the points on a normal probability plot resemble a straight line. Minitab typically provides the normal probability plot directly as seen in Figure 4.37. The Pareto chart (Figure 4.37 a) may be used to discover which factors have the most influence on the experiment, revealing that the vector of temperature is the most relevant variable. The vertical line can be observed at 2.06, which indicates that the distribution is statistically significant when the line intersects more vectors. When evaluated in Figure 4.37b, the model looks to have a normal distribution. Looking at the points, the distribution is seen to be more consistently distributed the closer the points are to the reference line. A pyramid-shaped histogram with a peak in Figure 4.37c depicts the model's normal distribution. The amount of dots on the versus order that have an irregular form with pulses affects the target's effectiveness, as shown in Figure 4.37d. The greater the number of such points, the more strongly the distribution is regarded to be normal. The response optimizer tool (Figure 4.38) demonstrates that a temperature of 84.34 ℃ for 120min produces the lowest COD, and presents a 3D surface plot of COD against temperature and time.

Table 4. 11 The ANOVA table of temperature and time as variables and COD as response for ACF-NC-LDH.

Source	**DF**	**Adj SS**	**Adj MS**	**F-Value**	**P-Value**
Model	5	768283	153657	310.47	0.000
Linear	2	704596	352298	711.84	0.000
TEMP	1	474088	474088	957.92	0.000
TIME	1	230508	230508	465.76	0.000
Square	2	63600	31800	64.25	0.000
TEMP*TEMP	1	53411	53411	107.92	0.000
TIME*TIME	1	10189	10189	20.59	0.000
2-Way Interaction	1	87	87	0.18	0.678
TEMP*TIME	1	87	87	0.18	0.678
Error	26	12868	495		
Total	31	781150			

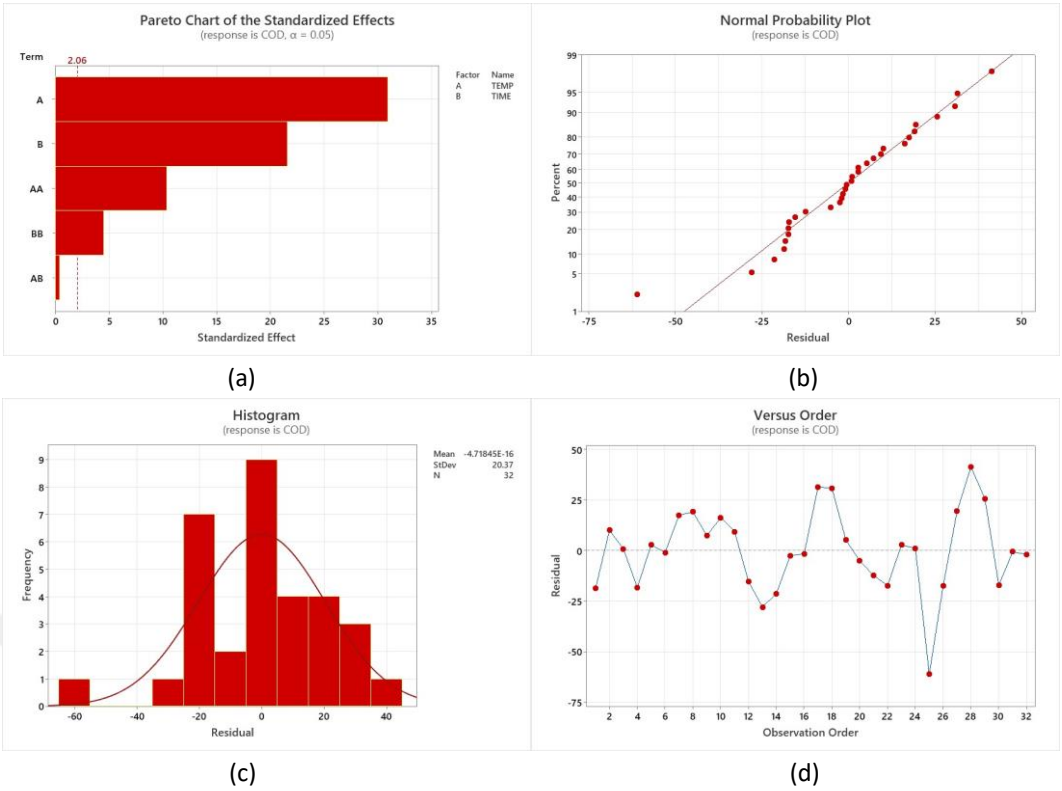

Figure 4. 37 Residual plots of temperature and time as variables and COD as response for ACF-NC-LDH.

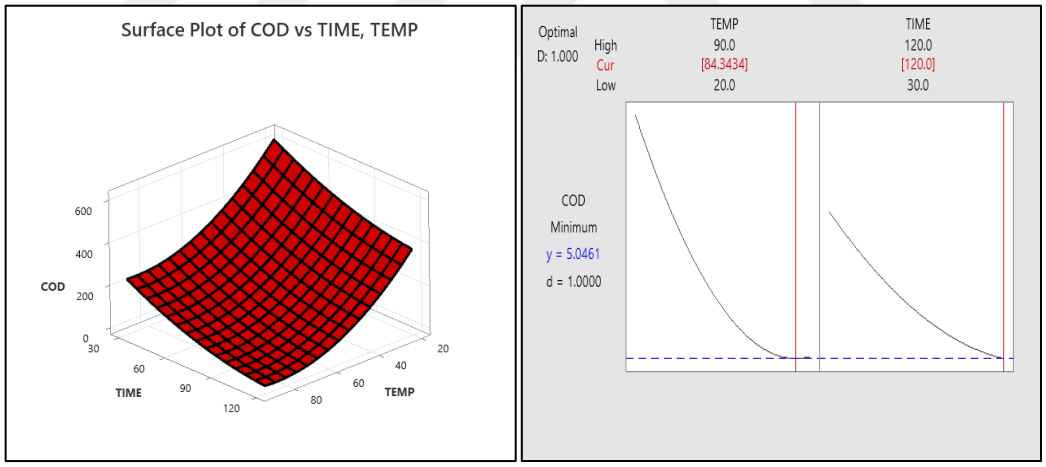

Figure 4. 38 The left: 3d surface plot for COD vs time and temperature, The right: the optimum values of time and temperature for lower COD for ACF-NC-LDH.

For PAC-NC-LDH, analysis of variance was performed on the COD results obtained from previous experiments. Regarding the effect of pH on the efficiency of reducing the amount of COD, the results of the ANOVA table showed that changing the pH does not greatly affect adsorption, or more precisely, we can say that adsorption does not depend primarily on changing the pH. As shown in Table 4.12, the P-value was about 0.935, which is a value much higher than the value of

the highest specified error rate, which is equal to 0.05. In addition, as shown in Figure 4.39a, the pH vector does not intersect the critical line at 2.101, meaning that the distribution does not depend on the pH vector. Figure 4.39b shows that most of the points are close to the reference line, and some are relatively far away. The closer the points are to the reference line, the more it indicates that the distribution is normal and that the variables have an impact on the process. Figure 4.39c shows an unorganized shape, as the shape should be a pyramid with a peak so that we can say that the distribution is similar to the normal distribution. There are also spaces in the columns that expose the deficiency of some sources or variables, and here it can be said that the distribution is not statistically significant. To confirm the notion that the residuals are independent from one another, use the residuals against the order plot (Figure 4.39d). When exhibited in temporal order, independent residuals do not exhibit any trends or patterns. The patterns in the data may suggest that residuals close to one another are likely connected and hence not independent. The residuals on the plot should ideally be distributed randomly about the center line. The right part of Figure 4.40 shows that the lowest COD obtained was at a pH of 6.74 and a time of 120 minutes. The left part shows a 3D surface plot for both pH and time versus COD.

Table 4. 12 The ANOVA table of PH and time as variables and COD as response for PAC-NC-LDH.

Source	**DF**	**Adj SS**	**Adj MS**	**F-Value**	**P-Value**
Model	5	490586	98117	14.53	0.000
Linear	2	158460	79230	11.74	0.001
PH	1	46	46	0.01	0.935
TIME	1	158413	158413	23.46	0.000
Square	2	328128	164064	24.30	0.000
PH*PH	1	319002	319002	47.25	0.000
TIME*TIME	1	9126	9126	1.35	0.260
2-Way Interaction	1	3999	3999	0.59	0.452
PH*TIME	1	3999	3999	0.59	0.452
Error	18	121526	6751		
Total	23	612112			

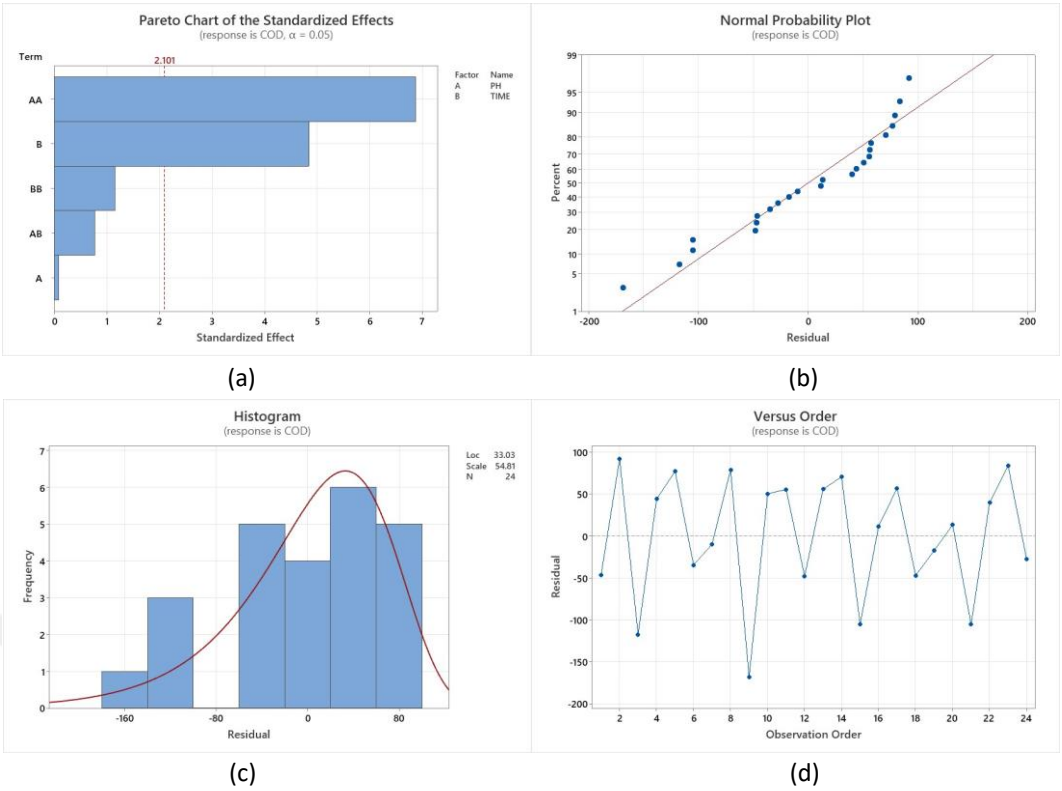

Figure 4. 39 Residual plots of PH and time as variables and COD as response for PAC-NC-LDH

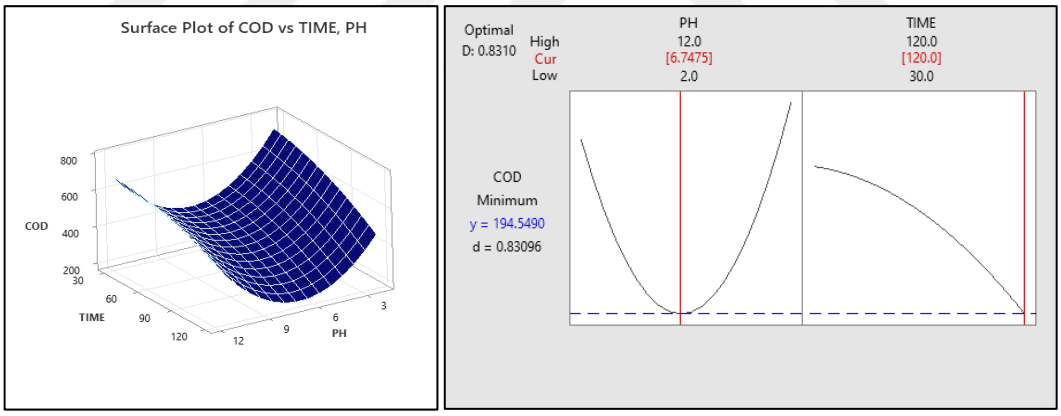

Figure 4. 40 The left: 3D surface plot for COD vs time and PH, The right: the optimum values of time and PH for lower COD for PAC-NC-LDH.

According to the results of the ANOVA table, altering the stirring speed greatly influences the adsorption, or more precisely, we can say that the adsorption mostly depends on altering the stirring speed when examining the impact of stirring speed on the effectiveness of lowering the quantity of COD. The P-value was 0, as shown in Table 4.13, which is significantly less than the value of the greatest specified error rate, which is 0.05. Additionally, as seen in Figure 4.41 a, the distribution is dependent on the stirring speed vector, which is the biggest and most

significant vector in the experiment and meets the critical line at 2.101. The majority of the spots are near the reference line, but a few are somewhat far away, as shown in Figure 4.41b. The more closely the points resemble the reference line, the more normal the distribution is and the more the variables affect the process. An unstructured form could be seen in Figure 4.41c. To state that the distribution resembles a normal distribution, the form must be a pyramid with a summit. The columns also include gaps, which indicate the absence of some sources or variables. Use the residual versus system diagram (Figure 4.41 d) to demonstrate the residuals' independence from one another. The independent residuals do not exhibit any patterns or trends when studied in chronological order. Data patterns may suggest that residues near one another are probably connected and hence not independent. The plot's leftovers are best dispersed at random along the middle line. The right part of Figure 4.42 shows that the lowest COD obtained was at a stirring speed of 514.14 rpm and a time of 120 min. The left part shows a 3D surface plot of both stirring speed and time versus COD.

Table 4. 13 The ANOVA table of stirring speed and time as variables and COD as response for PAC-NC-LDH.

Source	DF	Adj SS	Adj MS	F-Value	P-Value
Model	5	1060485	212097	263.77	0.000
Linear	2	910172	455086	565.96	0.000
Stirring speed	1	816372	816372	1015.27	0.000
TIME	1	93800	93800	116.65	0.000
Square	2	142445	71222	88.57	0.000
Stirring speed*Stirring speed	1	124240	124240	154.51	0.000
TIME*TIME	1	18205	18205	22.64	0.000
2-Way Interaction	1	7868	7868	9.79	0.006
Stirring speed*TIME	1	7868	7868	9.79	0.006
Error	18	14474	804		
Total	23	1074959			

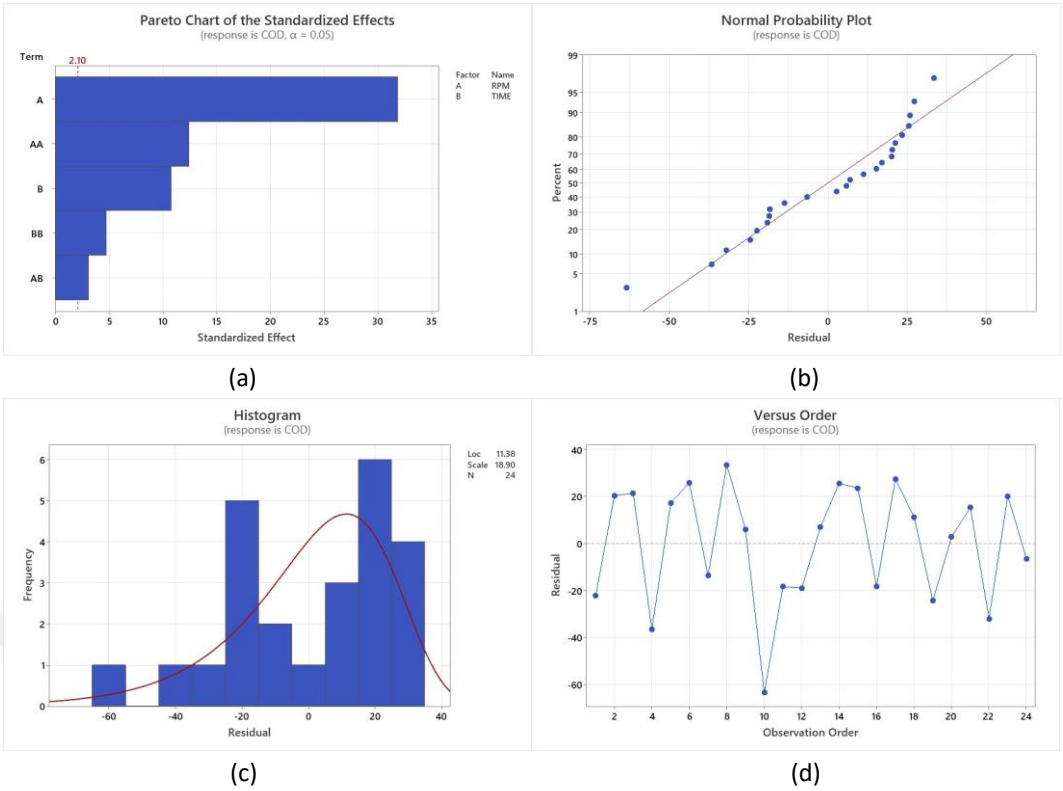

Figure 4. 41 Residual plots of stirring speed and time as variables and COD as response for PAC-NC-LDH

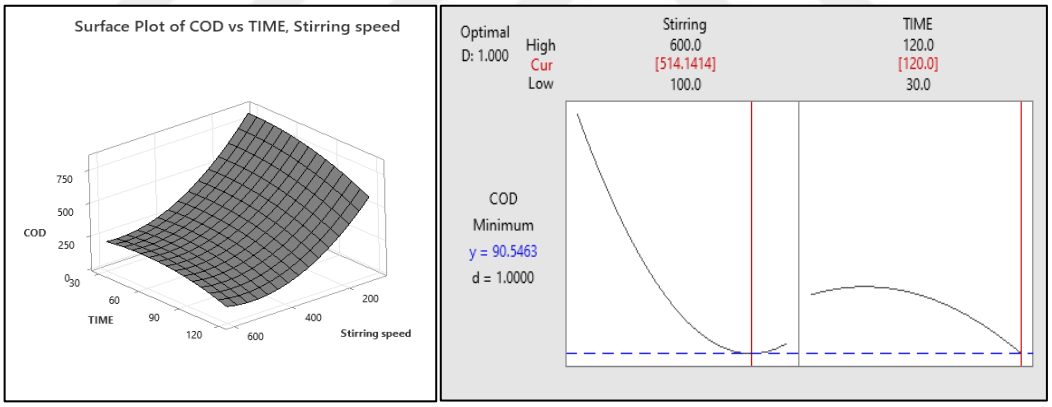

Figure 4. 42 The left: 3D surface plot for COD vs time and stirring speed, the right: the optimum values of time and stirring speed for lower COD for PAC-NC-LDH

In terms of the influence of carbon dosage on the effectiveness of lowering COD, the ANOVA table revealed that adsorption is mostly affected by modifying the stirring speed. The P-value was 0, as shown in Table 4.14 which is substantially lower than the value of the greatest specified error rate, which is 0.05. Furthermore, as shown in Figure 4.43a, the carbon dosage vector is the largest and most important vector in the experiment, intersecting the crucial line at 2.101, indicating that the distribution is influenced by the carbon dose vector. Figure 4.43b illustrates that the

majority of the points are near the reference line, while a few are somewhat far away. The closer the points are to the reference line, the more normal the distribution is, and the variables influence the process. Figure 4.43c depicts an unstructured shape. To say that the distribution is similar to a normal distribution, the shape must be a pyramid with a peak. There are also gaps in the columns, indicating the absence of some sources or variables. The residual versus system diagram (Figure 4.43d) can be used to confirm the idea that the residuals are independent of one another. The independent residuals show no trends or patterns when viewed in chronological order. Data patterns may indicate that residues near each other are likely related and thus not independent. The plot's remains are best distributed at random around the center line. The right part of Figure 4.44 shows that the lowest COD obtained was at a carbon dose of 1.4434 g/300ml and a time of 120 min. The left part shows a 3D surface plot of both carbon dose and time versus COD.

Table 4. 14 The ANOVA table of dosage and time as variables and COD as response for PAC-NC-LDH.

Source	**DF**	**Adj SS**	**Adj MS**	**F-Value**	**P-Value**
Model	5	831386	166277	123.73	0.000
Linear	2	581911	290956	216.50	0.000
Dosage	1	499892	499892	371.98	0.000
TIME	1	82019	82019	61.03	0.000
Square	2	180552	90276	67.18	0.000
Dosage*Dosage	1	167298	167298	124.49	0.000
TIME*TIME	1	13254	13254	9.86	0.006
2-Way Interaction	1	2942	2942	2.19	0.156
Dosage*TIME	1	2942	2942	2.19	0.156
Error	18	24190	1344		
Total	23	855576			

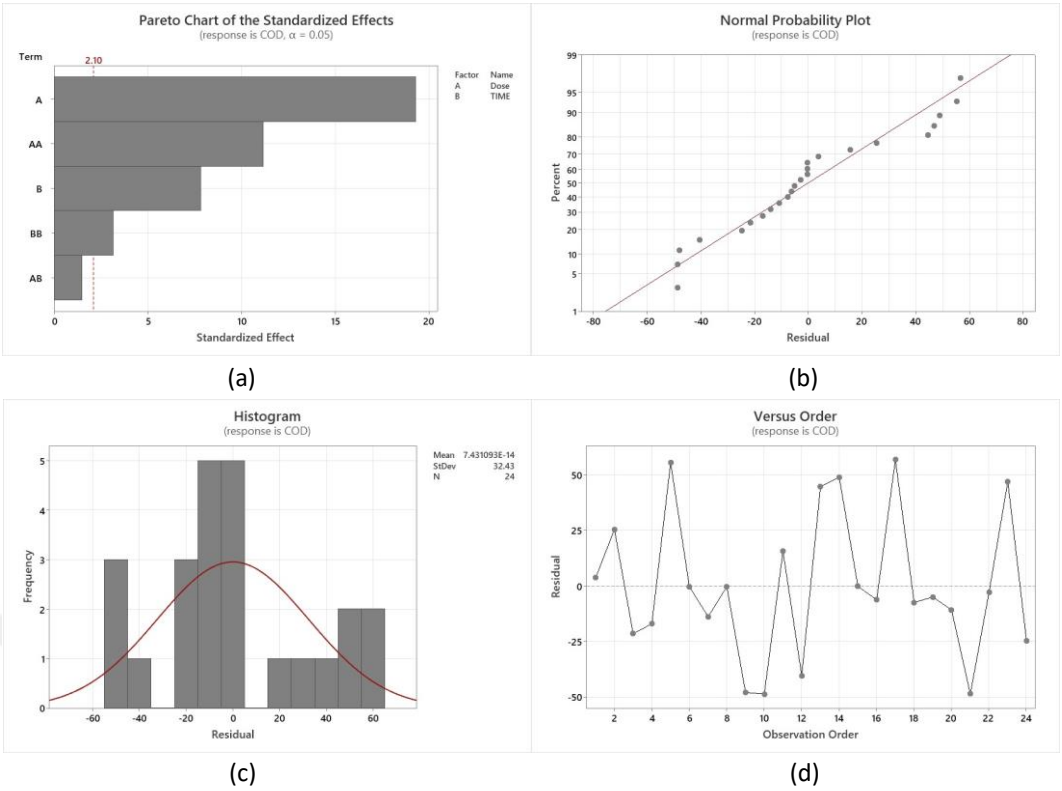

Figure 4. 43 Residual plots of dosage and time as variables and COD as response for PAC-NC-LDH.

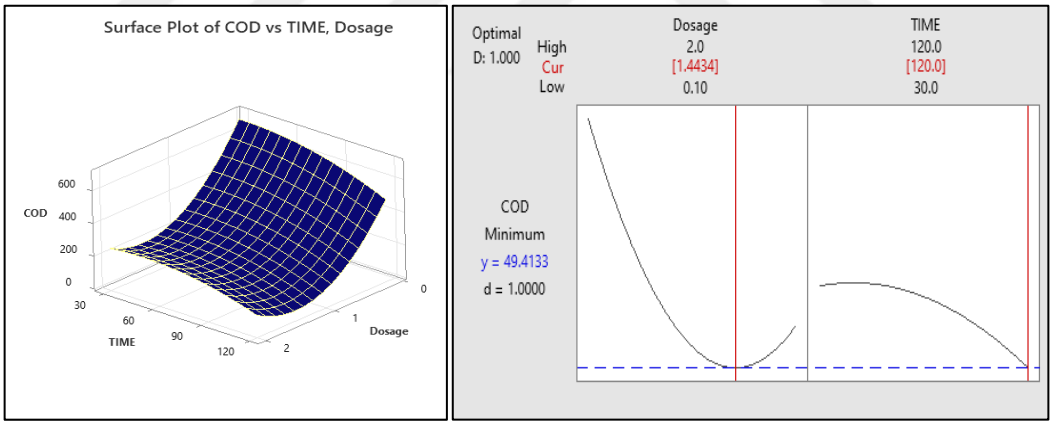

Figure 4. 44 The left: 3D surface plot for COD vs time and dosage, The right: the optimum values of time and dosage for lower COD for PAC-NC-LDH.

In terms of the effect of temperature on the efficiency of reducing the amount of COD, the ANOVA table results revealed that adsorption is primarily affected by temperature changes. The P-value was 0, as shown in Table 4.15, which is much lower than the value of the highest specified error rate, which is 0.05. Furthermore, as shown in Figure 4.45a, the temperature vector is the largest and most influential vector in the experiment, intersecting the critical line at 2.06, indicating that the distribution is affected by the temperature vector. All of the points in Figure 4.45b

are close to the reference line. The closer the points are to the reference line, the more normal the distribution is, and the variables affect the process. Figure 4.45c depicts an organized shape, which should be a pyramid with a top, and the distribution is similar to the normal distribution. There are no blank spaces in the columns, indicating that there is no deficiency in any of the sources or variables. The residual versus system diagram (Figure 4.45d) can be used to confirm the idea that the residuals are independent of one another. The independent residuals show no trends or patterns when viewed in chronological order. Data patterns may indicate that residues near each other are likely related and thus not independent. The plot's remains are best distributed at random around the center line. The right part of Figure 4.46 shows that the lowest COD obtained was at a temperature of 83.63 ℃ and a time of 120 min. The left part shows a 3D surface plot of both temperature and time versus COD.

Table 4. 15 The ANOVA table of temperature and time as variables and COD as response for PAC-NC-LDH.

Source	**DF**	**Adj SS**	**Adj MS**	**F-Value**	**P-Value**
Model	5	966763	193353	725.86	0.000
Linear	2	877819	438910	1647.69	0.000
TEMP	1	536863	536863	2015.41	0.000
TIME	1	340956	340956	1279.97	0.000
Square	2	88321	44161	165.78	0.000
TEMP*TEMP	1	72833	72833	273.42	0.000
TIME*TIME	1	15488	15488	58.14	0.000
2-Way Interaction	1	622	622	2.34	0.138
TEMP*TIME	1	622	622	2.34	0.138
Error	26	6926	266		
Total	31	973689			

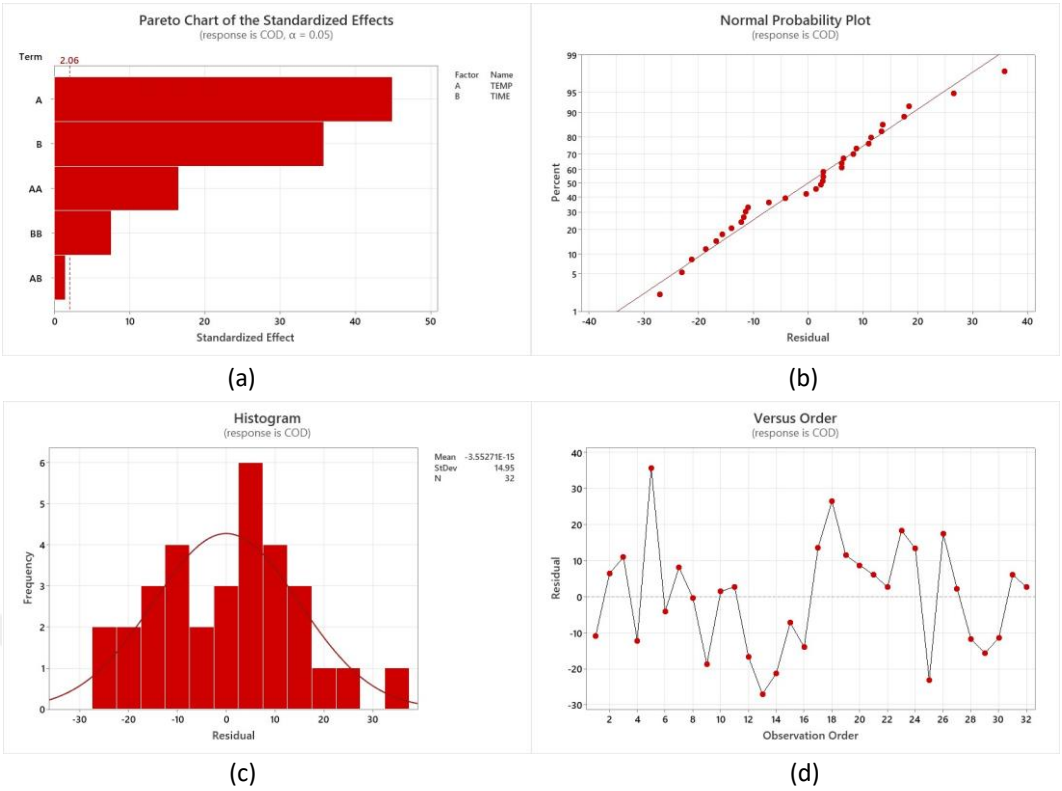

Figure 4. 45 Residual plots of Temperature and time as variables and COD as response for PAC-NC-LDH

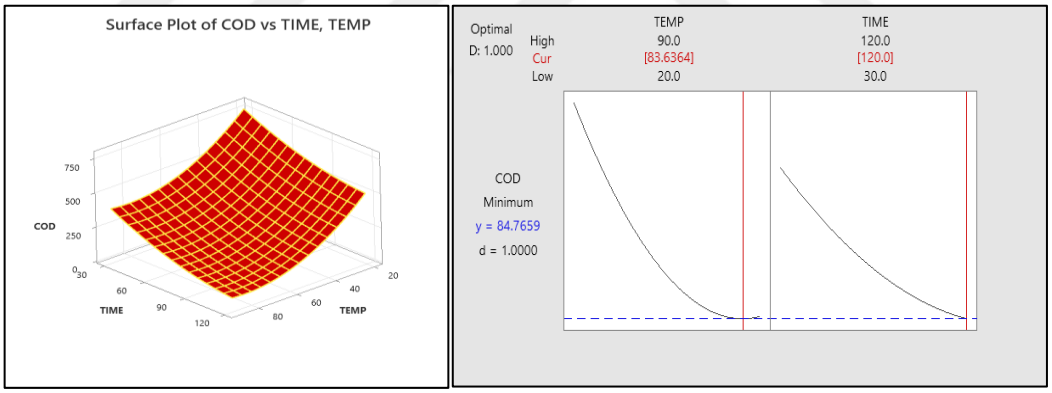

Figure 4. 46 The left: 3D surface plot for COD vs time and Temp., The right: the optimum values of time and Temperature for lower COD for PAC-NC-LDH

The outcomes derived from the experimental data were analyzed using Response Surface Methodology (RSM), which is a statistical technique. This analysis facilitated the development of mathematical models, as detailed in Table 4.16.

Table 4. 16 Mathematical models of the variables in RSM.

Variables	Mathematical Models for **(ACF-NC-LDH)**
PH	939 - 157.7 PH - 2.67 TIME + 10.62 PH*PH - 0.0039 TIME*TIME + 0.181 PH*TIME
Mix Speed	1042.6 - 3.393 RPM - 0.425 TIME + 0.00294 RPM*RPM - 0.01440 TIME*TIME+ 0.003409 RPM*TIME
Dosage	660.6 - 756.1 DOSE + 0.03 TIME + 241.8 DOSE*DOSE - 0.01213 TIME*TIME + 0.484 DOSE*TIME

Temp.	1027.1 - 15.28 TEMP - 5.622 TIME + 0.089TEMP*TEMP + 0.0198TIME*TIME + 0.00215 TEMP*TIME
Variables	Mathematical Models for **(PAC-NC-LDH)**
PH	1030 - 169.8 PH + 0.04 TIME + 11.55 PH*PH - 0.0217 TIME*TIME + 0.113 PH*TIME
Mix Speed	1094.5 - 3.336 RPM + 1.62 TIME + 0.002884 RPM*RPM - 0.03060 TIME*TIME + 0.00316 RPM *TIME
Dosage	735.0 - 756.7 DOSE + 1.62 TIME + 242.2 DOSE*DOSE - 0.02611 TIME*TIME + 0.483 DOSE*TIME
Temp.	1228.1-16.674 TEMP - 6.429 TIME + 0.104 TEMP*TEMP + 0.0244 TIME*TIME - 0.00574 TEMP*TIME

5. CONCLUSIONS AND DISCUSSION

In this study, the effect of variables (pH, stirring speed, carbon dose, temperature, and contact time) on the efficiency of adsorption of organic pollutants was studied using activated carbon fibers produced from date palm fibers. Chemical oxygen demand (COD) was determined as a value to determine the amount of organic pollutants and oil factory wastewater. Two samples were produced with different activation methods in addition to being chemically treated to improve their properties. (ACF-NC-LDH, PAC-NC-LDH) were obtained. The results were calculated and analyzed using kinetic, thermodynamic, and isothermal calculations, in addition to using the response surface method (RSM) to show the optimal way to reduce organic pollutants in water.

- The results showed that the two treatment processes used to improve the product properties had a great benefit in increasing the efficiency of the physical, mechanical, and chemical properties, as activated carbon fibers were produced coated with a layer of doped carbon in addition to the lamination network (ACF-NC-LDH), which gave more active sites that led to greater adsorption of pollutants.
- Chemical treatments were applied to the second sample, and activated carbon powder coated with a layer of doped carbon and a double layer of hydroxide (PAC-NC-LDH) was obtained.
- Concerning ACF-NC-LDH, the experimental findings demonstrated that 99.32% of the COD was removed at pH 6, 400 rpm stirring speed, 1 g/300 ml carbon dosage, and 70 ℃ temperature for 120 min.
- Regarding PAC-NC-LDH, the experimental results showed that the highest percentage of COD removal was at pH 6, stirring speed of 400 rpm, carbon dose of 1 g/300ml, and temperature of 70 ℃ for 120 min, where it reached 89.66%.
- The efficiency of removing oil from factory wastewater using ACF-NC-LDH was about 99.51%, and 89.44% using PAC-NC-LDH.
- The efficiency of removing heavy metals from factory wastewater using ACF-NC-LDH was about 99.13%, and 92.62% using PAC-NC-LDH.

- The efficiency of removing TDS from factory wastewater using ACF-NC-LDH was about 98.75%, and 87.38% using PAC-NC-LDH.
- The total removal rate of all organic pollutants was 99.26% and 90.38% using ACF-NC-LDH and PAC-NC-LDH, respectively.
- The predicted positive values of ΔH° in the thermodynamic findings demonstrate the endothermic nature of the activated carbon from the COD absorption system. Negative results of ΔG° validate the adsorption process's validity and spontaneous nature. The magnitude (ΔG°) rose as the temperature rose, suggesting that the system's level of spontaneity rose as well. The computed positive values (ΔS°) indicate enhanced randomness and disorder at the activated carbon/treated industrial waste interface in the adsorption process.
- The kinetic results indicate that the correlation coefficient values of pseudo-first-order kinetics (R^2 = 0.8983) and pseudo-second-order kinetics (R^2 = 0.9987) for (ACF-NC-LDH) and (PAC-NC-LDH), respectively, are lower. Compared with the pseudo-second-order mobility (R^2 = 0.9954), the pseudo-first-order mobility (R^2 = 0.8825) is lower. In the studied adsorption procedure for removing COD from industrial wastewater by preparing activated carbon fibers, the chemisorption reaction is the primary adsorption mechanism, as demonstrated by the correlation coefficient values of the results with a pseudo-second-order kinetic model that closely fits the obtained experimental data.
- The results of the response surface method, through which ANOVA tables and normal distribution forms were used, showed complete agreement with the typical objectives. The P-value for all variables was less than 0.05, which is the value that the method aims not to reach, as it represents the error value in the experiments.
- The standard graphs of the residual values are in good agreement. Examining the produced histograms reveals that the data is symmetric and closely resembles a normal distribution. The locations where the residues are 0 are where the data is denser, as seen by an examination of the typical probability plots. The histograms show that the highest frequency values are near zero or very close to zero. The versus order chart also shows that the

values are distributed positively and negatively in a waveform around zero areas. This arrangement shows that the analysis is highly acceptable and is like a typical histogram.

- The results of the response surface method showed that the optimal design through which the lowest COD can be obtained is achieved at a pH of 6.74, a stirring speed of 514.14 rpm, a carbon dose of 1.44 g/300ml, a temperature of 84.34 °C, and a duration of 120 min for ACF-NC-LDH. As for the optimal design through which the lowest COD can be obtained using PAC-NC-LDH, the analysis results showed that it is achieved at a pH of 6.409, a stirring speed of 509.09 rpm, a carbon dose of 1.44 g/300ml, and a temperature of 83.63 °C for 120 min.

6. REFERENCES

"Vancouver citation system was used in this thesis."

1. Sajida S, Hemlata B. Sorption studies of radionuclides from simulated low level waste using green biosorbent. Res J Chem Environ. 2021;25(1):68–73.

2. Al-Majed AA, Adebayo AR, Hossain ME. A sustainable approach to controlling oil spills. J Environ Manage. 2012;113:213–27.

3. Boehm PD, Gundlach ER, Page DS. The phases of an oil spill and scientific studies of spill effects. Oil Environ Legacies Lessons Exxon Vald Oil Spill. 2011;(January):37–53.

4. Burton NHK, Musgrove AJ, Rehfisch MM, Clark NA. Birds of the Severn Estuary and Bristol Channel: Their current status and key environmental issues. Mar Pollut Bull. 2010;61(1–3):115–23.

5. Etkin DS, Nedwed TJ. Effectiveness of mechanical recovery for large offshore oil spills. Mar Pollut Bull [Internet]. 2021;163(November 2020):111848. Available from: https://doi.org/10.1016/j.marpolbul.2020.111848

6. Saleem J, Adil Riaz M, Gordon M. Oil sorbents from plastic wastes and polymers: A review. J Hazard Mater [Internet]. 2018;341:424–37. Available from: http://dx.doi.org/10.1016/j.jhazmat.2017.07.072

7. Cumo F, Gugliermetti F, Guidi G. Best available techniques for oil spill containment and clean-up in the Mediterranean Sea. WIT Trans Ecol Environ. 2007;103:527–35.

8. Perkovic M. Oil Spill Modeling and Combat. 2016;(February).

9. Iriakuma CT, Obomanu T, Idogun AK, Rowland Ukotije-Ikwut P, Idogun AK. A Novel Method for Adsorption using Human Hair as a Natural Oil Spill Sorbent Want more papers like this? A Novel Method for Adsorption using Human Hair as a Natural Oil Spill Sorbent. 2016;7(8):1754–64. Available from: http://www.ijser.org

10. Sundaravadivelu D. Parametric Study to Determine the Effect of Operational Variables on Oil Solidifier Performance for Oil Spill Remediation .. Dr Diss Univ Cincinnati. 2015;

11. Guia J, Teixeira AP, Guedes Soares C. Probabilistic modelling of the hull girder target safety level of tankers. Mar Struct [Internet]. 2018;61(January):119–41. Available from: https://doi.org/10.1016/j.marstruc.2018.04.007

12. Kandanelli R, Meesala L, Kumar J, Raju CSK, Peddy VCR, Gandham S, et al. Cost effective and practically viable oil spillage mitigation: Comprehensive study with biochar. Mar Pollut Bull. 2018;128(January):32–40.

13. Ben Jmaa S, Kallel A. Chemically Treated Seagrass Fibers as Biosorbent for Crude Oil Removal. In New Prospects in Environmental Geosciences and Hydrogeosciences: Proceedings of the 2nd Springer Conference of the Arabian Journal of Geosciences (CAJG-2), Tunisia 2019 . Cham Springer Int Publ. 2022;325–8.

14. Praba Karana C, Rengasamy RS, Das D. Oil spill cleanup by structured fibre assembly. Indian J Fibre Text Res. 2011;36(2):190–200.

15. Alaa El-Din G, Amer AA, Malsh G, Hussein M. Study on the use of banana peels for oil spill removal. Alexandria Eng J [Internet]. 2018;57(3):2061–8. Available from: https://doi.org/10.1016/j.aej.2017.05.020

16. Abdullah MA, Rahmah AU, Man Z. Physicochemical and sorption characteristics of Malaysian Ceiba pentandra (L.) Gaertn. as a natural oil sorbent. J Hazard Mater. 2010;177(1–3):683–91.

17. AlAmeri K, Giwa A, Yousef L, Alraeesi A, Taher H. Sorption and removal of crude oil spills from seawater using peat-derived biochar: An optimization study. J Environ Manage [Internet]. 2019;250(August):109465. Available from: https://doi.org/10.1016/j.jenvman.2019.109465

18. Waisi BIH, Karim UF, Augustijn DC, Al-Furaiji MHO, Hulscher SJA. study on the quantities and potential use of produced water in southern Iraq. Water Sci Technol water supply. 2015;15(2):370–6.

19. Al-Furaiji M. Hyper-saline produced water treatment for beneficial use [Internet]. University of Twente. 2016. Available from: https://research.utwente.nl/files/6047734/thesis_M_Al-Furaiji.pdf%0Ahttp://purl.org/utwente/doi/10.3990/1.9789036541565

20. WU L, GE G, WAN J. Biodegradation of oil wastewater by free and immobilized Yarrowia lipolytica W29. J Environ Sci [Internet]. 2009;21(2):237–42. Available from: http://dx.doi.org/10.1016/S1001-0742(08)62257-3

21. Lazarević VB, Krstić IM, Lazić ML, Savić DS, Skala DU, Veljković VB. Povećanje razmere hemijskog prečišćavanja otpadne vodene emulzije mineralnog ulja iz fabrike za obradu obojenih metala. Hem Ind. 2013;67(1):59–68.

22. Kundu P, Mishra IM. Removal of emulsified oil from oily wastewater (oil-

in-water emulsion) using packed bed of polymeric resin beads. Sep Purif Technol. 2013;118:519–29.

23. Kim CS, Cho YK, Choi BJ, Jung KT, You SH. Improving a prediction system for oil spills in the Yellow Sea: Effect of tides on subtidal flow. Mar Pollut Bull. 2013;68(1–2):85–92.

24. Farajnezhad H, Gharbani P, Branch A. Coagulation Treatment of Wastewater in Petroleum Industry using Poly Aluminium Chloride and Ferric. Ijrras. 2012;13(October):306–10.

25. Wang D, Silbaugh T, Pfeffer R, Lin YS. Removal of emulsified oil from water by inverse fluidization of hydrophobic aerogels. Powder Technol. 2010;203(2):298–309.

26. Ahmad T, Guria C, Mandal A. A review of oily wastewater treatment using ultrafiltration membrane: A parametric study to enhance the membrane performance. J Water Process Eng [Internet]. 2020;36(June):101289. Available from: https://doi.org/10.1016/j.jwpe.2020.101289

27. Xiong X, Jianguo B, Hassan Omer S, Hui, G., Yu Z, Hong W. Study for adsorption behaviors of emulsion oil on a novel ZrO2/PVDF modified membrane.. Desalin Water Treat. 2016;57(25):11736–45.

28. Majeed, Saber N, Sabbar HA, Nawar OA Al-Musawi. "Preparation activated carbon from scrap tires by microwave assisted KOH activation for removal emulsified oil.". Iraqi J Chem Pet Eng. 2017;(18.1):57–69.

29. Vickers NJ. Animal Communication: When I'm Calling You, Will You Answer Too? Curr Biol [Internet]. 2017;27(14):R713–5. Available from: http://dx.doi.org/10.1016/j.cub.2017.05.064

30. Li X, Zhang C, Liu J. Adsorption of oil from waste water by coal: Characteristics and mechanism. Min Sci Technol [Internet]. 2010;20(5):778–81. Available from: http://dx.doi.org/10.1016/S1674-5264(09)60280-5

31. Costa C. Improving the Removal of Emulsified Oil from Wastewater with a Membrane Bioreactor using Powdered Activated Carbon. 2016;(April).

32. Okiel K, El-Sayed M, El-Kady MY. Treatment of oil–water emulsions by adsorption onto activated carbon, bentonite and deposited carbon. Egypt J Pet [Internet]. 2011;20(2):9–15. Available from: http://dx.doi.org/10.1016/j.ejpe.2011.06.002

33. Emam EA. Modified Activated Carbon and Bentonite Used to Adsorb Petroleum Hydrocarbons Emulsified in Aqueous Solution. Am J Environ Prot. 2013;2(6):161.

34. Mysore D, Viraraghavan T, Jin YC. Treatment of oily waters using vermiculite. Water Res. 2005;39(12):2643–53.

35. Foo KY, Hameed BH. An overview of landfill leachate treatment via activated carbon adsorption process. J Hazard Mater. 2009;171(1–3):54–60.

36. Lee T, Ooi CH, Othman R, Yeoh FY. Activated carbon fiber - The hybrid of carbon fiber and activated carbon. Rev Adv Mater Sci. 2014;36(2):118–36.

37. Gómez V, Larrechi MS, Callao MP. Kinetic and adsorption study of acid dye removal using activated carbon. Chemosphere. 2007;69(7):1151–8.

38. Malik R, Ramteke DS, Wate SR. Adsorption of malachite green on groundnut shell waste based powdered activated carbon. Waste Manag. 2007;27(9):1129–38.

39. Abbas M. Experimental investigation of activated carbon prepared from apricot stones material (ASM) adsorbent for removal of malachite green (MG) from aqueous solution. Adsorpt Sci Technol. 2020;38(1–2):24–45.

40. Sawalha H, Bader A, Sarsour J, Al-Jabari M, Rene ER. Removal of Dye (Methylene Blue) from Wastewater Using Bio-Char Derived from Agricultural Residues in Palestine: Performance and Isotherm Analysis. Processes. 2022;10(10).

41. Auta M. FIXED BED ADSORPTION STUDIES OF RHODAMINE B DYE USING Address for Correspondence. J Eng Res Stud. 2012;3(3):3–6.

42. Sudamalla P, Matheswaran M, Saravanan P. Optimization of operating parameters using response surface methodology for adsorption of crystal violet by activated carbon prepared from mango kernel. Sustain Environ Res. 2012;22(1):1–7.

43. Dakroury GA, El-Shazly EAA, Hassan HS. Sorption of lead (II) and strontium (II) ions from aqueous solutions onto non-living Chlorella Vulgaris Alga/ Date pit activated carbon composite. Carbon Lett [Internet]. 2022;32(2):495–512. Available from: https://doi.org/10.1007/s42823-021-00280-z

44. Buvaneswari K, Singanan M. WITHDRAWN: Review on scanning electron microscope analysis and adsorption properties of different activated carbon materials. Mater Today Proc [Internet]. 2020; Available from: https://doi.org/10.1016/j.matpr.2020.09.426

45. Manasa P, Lei ZJ, Ran F. Biomass Waste Derived Low Cost Activated Carbon from Carchorus Olitorius (Jute Fiber) as Sustainable and Novel Electrode Material. J Energy Storage [Internet]. 2020;30(April):101494. Available from: https://doi.org/10.1016/j.est.2020.101494

46. Vaddi DR, Gurugubelli TR, Koutavarapu R, Lee DY, Shim J. Bio-Stimulated Adsorption of Cr(VI) from Aqueous Solution by Groundnut Shell Activated Carbon@Al Embedded Material. Catalysts. 2022;12(3).

47. Sun Z, Qu K, Cheng Y, You Y, Huang Z, Umar A, et al. Corncob-derived Activated Carbon for Efficiently Adsorption Dye in Sewage. ES Food Agrofor. 2021;61–74.

48. Khuong DA, Nguyen HN, Tsubota T. Activated carbon produced from bamboo and solid residue by CO2 activation utilized as CO2 adsorbents. Biomass and Bioenergy [Internet]. 2021;148(March):106039. Available from: https://doi.org/10.1016/j.biombioe.2021.106039

49. Chikri R, Elhadiri N, Benchanaa M, El maguana Y. Efficiency of sawdust as low-cost adsorbent for dyes removal. J Chem. 2020;2020.

50. Marsin FM, Wan Ibrahim WA, Nodeh HR, Sanagi MM. New magnetic oil palm fiber activated carbon-reinforced polypyrrole solid phase extraction combined with gas chromatography-electron capture detection for determination of organochlorine pesticides in water samples. J Chromatogr A [Internet]. 2020;1612:460638. Available from: https://doi.org/10.1016/j.chroma.2019.460638

51. Hassan MF, Sabri MA, Fazal H, Hafeez A, Shezad N, Hussain M. Recent trends in activated carbon fibers production from various precursors and applications—A comparative review. J Anal Appl Pyrolysis [Internet]. 2020;145(October 2019):104715. Available from: https://doi.org/10.1016/j.jaap.2019.104715

52. Gao Y, Yue Q, Gao B, Li A. Insight into activated carbon from different kinds of chemical activating agents: A review. Sci Total Environ [Internet]. 2020;746:141094. Available from: https://doi.org/10.1016/j.scitotenv.2020.141094

53. Oprea M, Voicu SI. Recent advances in composites based on cellulose derivatives for biomedical applications. Carbohydr Polym [Internet]. 2020;247(April):116683. Available from: https://doi.org/10.1016/j.carbpol.2020.116683

54. Boruah BD, Wen B, Nagane S, Zhang X, Stranks SD. Photo-Rechargeable Zinc-Ion Capacitors using V 2 O 5 – Activated Carbon Electrodes Table of Content (TOC) Graphic Voltage (mV) Time (min). :1–26.

55. Vicentini R, Nunes WG, da Costa LH, Da Silva LM, Freitas B, Pascon AM, et al. Multi-walled carbon nanotubes and activated carbon composite material as electrodes for electrochemical capacitors. J Energy Storage [Internet]. 2021;33(February 2019):100738. Available from:

https://doi.org/10.1016/j.est.2019.04.012

56. Kim KH, Lee JS, Ahn HJ. Simultaneous effect of fluorine impregnation on highly mesoporous activated carbon used in high-performance electrical double layer capacitors. Appl Surf Sci [Internet]. 2021;550(February):149266. Available from: https://doi.org/10.1016/j.apsusc.2021.149266

57. Pal A, Uddin K, Rocky KA, Thu K, Saha BB. CO2 adsorption onto activated carbon–graphene composite for cooling applications. Int J Refrig [Internet]. 2019;106:558–69. Available from: https://doi.org/10.1016/j.ijrefrig.2019.04.022

58. Pal A, Uddin K, Thu K, Saha BB. Activated carbon and graphene nanoplatelets based novel composite for performance enhancement of adsorption cooling cycle. Energy Convers Manag [Internet]. 2019;180(October 2018):134–48. Available from: https://doi.org/10.1016/j.enconman.2018.10.092

59. Pérez E, Romero I, Albis A, Carmona M. Modeling and experiments on a finned cylindrical reactor with expanded graphite/activated carbon/lithium chloride-ammonia for chemisorption refrigeration systems. Appl Therm Eng. 2021;184(October 2020).

60. Yang J, Ren S, Zhang T, Su Z, Long H, Kong M, et al. Iron doped effects on active sites formation over activated carbon supported Mn-Ce oxide catalysts for low-temperature SCR of NO. Chem Eng J [Internet]. 2020;379(March 2019):122398. Available from: https://doi.org/10.1016/j.cej.2019.122398

61. Li Y, Yan X, Hu X, Feng R, Zhou M. Trace pyrolyzed ZIF-67 loaded activated carbon pellets for enhanced adsorption and catalytic degradation of Rhodamine B in water. Chem Eng J [Internet]. 2019;375(June):122003. Available from: https://doi.org/10.1016/j.cej.2019.122003

62. Wang H, Han J, Bo Z, Qin L, Wang Y, Yu F. Non-thermal plasma enhanced dry reforming of CH4 with CO2 over activated carbon supported Ni catalysts. Mol Catal. 2019;475(June).

63. Zhang S, Yu Y, Xie M, Du C, Chen J, Wan L, et al. Clean production of N, O-doped activated carbon by water vapor carbonization/activation of expired coffee for high-volumetric supercapacitor. Appl Surf Sci. 2022;589(November 2021).

64. Memetova A, Tyagi I, Karri RR, Kumar V, Tyagi K, Suhas, et al. Porous carbon-based material as a sustainable alternative for the storage of natural gas (methane) and biogas (biomethane): A review. Chem Eng J [Internet]. 2022;446(P4):137373. Available from:

https://doi.org/10.1016/j.cej.2022.137373

65. Januszewicz K, Cymann-Sachajdak A, Kazimierski P, Klein M, Łuczak J, Wilamowska-Zawłocka M. Chestnut-derived activated carbon as a prospective material for energy storage. Materials (Basel). 2020;13(20):1–17.

66. Trang Nguyen D, Nguyen HUD, Taguchi K. A biodegradable water-activated battery: Using an activated carbon-based anode and a CNT-based air-cathode. IOP Conf Ser Earth Environ Sci. 2022;994(1):0–5.

67. Byatarayappa G, G RM, R S, V T, Venkatesh K, N N, et al. A comparative study on electrochemical performance of KOH activated carbons derived from different biomass sources - Musa acuminata stem, Pongamia pinnata seed oil extract cake, cajanus cajan stem and Asclepias syriaca floss. Heliyon [Internet]. 2023;9(4):e15399. Available from: https://doi.org/10.1016/j.heliyon.2023.e15399

68. Wang J, Lin Z, He X, Song M, Westerhoff P, Doudrick K, et al. Critical Review of Thermal Decomposition of Per- and Polyfluoroalkyl Substances: Mechanisms and Implications for Thermal Treatment Processes. Environ Sci Technol. 2022;56(9):5355–70.

69. Chiang YC, Chen YJ, Wu CY. Effect of relative humidity on adsorption breakthrough of CO2 on activated carbon fibers. Materials (Basel). 2017;10(11).

70. Sun Z, Li S, Ding H, Zhu Y, Wang X, Liu H, et al. Electrochemical/Fe3+/peroxymonosulfate system for the degradation of Acid Orange 7 adsorbed on activated carbon fiber cathode. Chemosphere [Internet]. 2020;241:125125. Available from: https://doi.org/10.1016/j.chemosphere.2019.125125

71. El-Naas MH, Al-Zuhair S, Alhaija MA. Reduction of COD in refinery wastewater through adsorption on date-pit activated carbon. J Hazard Mater. 2010;173(1–3):750–7.

72. Raji M, Mirbagheri SA, Ye F, Dutta J. Nano zero-valent iron on activated carbon cloth support as Fenton-like catalyst for efficient color and COD removal from melanoidin wastewater. Chemosphere [Internet]. 2021;263:127945. Available from: https://doi.org/10.1016/j.chemosphere.2020.127945

73. Li K, Wang X. Adsorptive removal of Pb(II) by activated carbon prepared from Spartina alterniflora: Equilibrium, kinetics and thermodynamics. Bioresour Technol [Internet]. 2009;100(11):2810–5. Available from: http://dx.doi.org/10.1016/j.biortech.2008.12.032

74. Gayathiri M, Pulingam T, Lee KT, Sudesh K. Activated carbon from biomass waste precursors: Factors affecting production and adsorption mechanism. Chemosphere [Internet]. 2022;294(December 2021):133764. Available from: https://doi.org/10.1016/j.chemosphere.2022.133764

75. Mcmullen RL, Acqua GD. History of Natural Ingredients in Cosmetics. 2023;1–31.

76. Farahani M, Behbahaninia A. Using natural adsorbents to reduce polycyclic aromatic hydrocarbons contamination of oily wastewater. Online) [Internet]. 2014;5(6):274–81. Available from: http://www.innspub.net

77. Sessa F, Merlin G, Canu P. Pine bark valorization by activated carbons production to be used as VOCs adsorbents. Fuel [Internet]. 2022;318(October 2021):123346. Available from: https://doi.org/10.1016/j.fuel.2022.123346

78. Haykiri-Acma H, Yaman S, Kucukbayrak S. Does carbonization avoid segregation of biomass and lignite during co-firing? Thermal analysis study. Fuel Process Technol [Internet]. 2015;137:312–9. Available from: http://dx.doi.org/10.1016/j.fuproc.2015.03.017

79. Benedetti V, Patuzzi F, Baratieri M. Gasification Char as a Potential Substitute of Activated Carbon in Adsorption Applications. Energy Procedia [Internet]. 2017;105:712–7. Available from: http://dx.doi.org/10.1016/j.egypro.2017.03.380

80. Jalalabadi T, Glenn M, Tremain P, Moghtaderi B, Donne S, Allen J. Modification of Biochar Formation during Slow Pyrolysis in the Presence of Alkali Metal Carbonate Additives. Energy and Fuels. 2019;33(11):11235–45.

81. Rehrah D, Reddy MR, Novak JM, Bansode RR, Schimmel KA, Yu J, et al. Production and characterization of biochars from agricultural by-products for use in soil quality enhancement. J Anal Appl Pyrolysis. 2014;108(November 2017):301–9.

82. Sharma M, Singh J, Baskar C, Kumar A. A comprehensive review of renewable energy production from biomass-derived bio-oil. Biotechnologia. 2019;100(2):179–94.

83. Rodriguez-Reinoso. F. Preparation and Characterization of Activated Carbons. NATO ASI Ser Ser E Appl Sci. 1986;(105):601–42.

84. Sultana M, Rownok MH, Sabrin M, Rahaman MH, Alam SMN. A review on experimental chemically modified activated carbon to enhance dye and heavy metals adsorption. Clean Eng Technol [Internet]. 2022;6:100382.

Available from: https://doi.org/10.1016/j.clet.2021.100382

85. Kuśmierek K, Białek A, Świątkowski A. Effect of activated carbon surface chemistry on adsorption of phenoxy carboxylic acid herbicides from aqueous solutions. Desalin Water Treat. 2020;186(September 2019):450–9.

86. Jjagwe J, Olupot PW, Menya E, Kalibbala HM. Synthesis and Application of Granular Activated Carbon from Biomass Waste Materials for Water Treatment: A Review. J Bioresour Bioprod [Internet]. 2021;6(4):292–322. Available from: https://doi.org/10.1016/j.jobab.2021.03.003

87. Khalaf Erabee I, M. Ethaib S. Performane of Activated Carbon Adsorption in Removing of Organic Pollutants from River Water. Int J Eng Technol. 2018;7(4.20):356.

88. Nayl AEA, Elkhashab RA, El Malah T, Yakout SM, El-Khateeb MA, Ali MMS, et al. Adsorption studies on the removal of COD and BOD from treated sewage using activated carbon prepared from date palm waste. Environ Sci Pollut Res. 2017;24(28):22284–93.

89. Ferraz FM, Yuan Q. Performance of oat hulls activated carbon for COD and color removal from landfill leachate. J Water Process Eng [Internet]. 2020;33(November 2019):101040. Available from: https://doi.org/10.1016/j.jwpe.2019.101040

90. Nabavi E, Sabour M, Dezvareh GA. Ozone treatment and adsorption with granular activated carbon for the removal of organic compounds from agricultural soil leachates. J Clean Prod [Internet]. 2022;335(December 2021):130312. Available from: https://doi.org/10.1016/j.jclepro.2021.130312

91. Carrott PJM, Nabais JMV, Ribeiro Carrott MML, Pajares JA. Preparation of activated carbon fibres from acrylic textile fibres. Carbon N Y. 2001;39(10):1543–55.

92. Angelo M, Matsushima JT, Rezende MC, Gonçalves S, Marcuzzo JS, Baldan MR. Production and Characterization of Activated Carbon Fiber from Textile PAN Fiber. 2017;9:423–30.

93. Kumari M, Chaudhary GR, Chaudhary S, Umar A. Transformation of solid plastic waste to activated carbon fibres for wastewater treatment. Chemosphere [Internet]. 2022;294(November 2021):133692. Available from: https://doi.org/10.1016/j.chemosphere.2022.133692

94. Teng Y, Zhu J, Xiao S, Ma Z, Huang T, Liu Z. Exploring chitosan-loaded activated carbon fiber for the enhanced adsorption of Pb (II) -EDTA complex from electroplating wastewater in batch and continuous processes.

Sep Purif Technol [Internet]. 2022;299(July):121659. Available from: https://doi.org/10.1016/j.seppur.2022.121659

95. Matsuzawa F, Amano Y, Machida M. Phosphates Ion Adsorption Characteristics of Activated Carbon Fibers. 2023;34(1):7–10.

96. Muhammad R, Nah Y chae, Oh H. Spider silk-derived nanoporous activated carbon fiber for CO 2 capture and CH 4 and H 2 storage. J CO2 Util [Internet]. 2023;69(October 2022):102401. Available from: https://doi.org/10.1016/j.jcou.2023.102401

97. Wu W, Wu C, Zhang G, Liu J, Li Y, Li G. Synthesis and characterization of magnetic K 2 CO 3 -activated carbon produced from bamboo shoot for the adsorption of Rhodamine b and CO 2 capture. Fuel [Internet]. 2023;332(P1):126107. Available from: https://doi.org/10.1016/j.fuel.2022.126107

98. Li B, Dai F, Xiao Q, Yang L, Shen J, Zhang C, et al. Nitrogen-doped Activated Carbon for High Energy Hybrid Supercapacitor. Energy Environ Sci. 2023;

99. Park S jin, Kim B joo. Ammonia removal of activated carbon fibers produced by oxyfluorination. 2010;291(2005):597–9.

100. Lin J, Choowang R, Zhao G. Fabrication and Characterization of Activated Carbon Fibers from Oil Palm Trunk. 2020;

101. Chiu K lok, Ng DHL. Synthesis and characterization of cotton-made activated carbon fiber and its adsorption of methylene blue in water treatment. Biomass and Bioenergy [Internet]. 2012;46:102–10. Available from: http://dx.doi.org/10.1016/j.biombioe.2012.09.023

102. Ooi1 CH, Ang1 CL, Yeoh FY. The Properties of Activated Carbon Fiber Derived from Direct Activation from The Properties of Activated Carbon Fiber derived from Direct Activation from Oil Palm Empty Fruit Bunch Fiber. 2013;(April).

103. Tan WC, Othman R, Matsumoto A, Yeoh FY. The effect of carbonisation temperatures on nanoporous characteristics of activated carbon fibre (ACF) derived from oil palm empty fruit bunch (EFB) fibre. J Therm Anal Calorim. 2012;108(3):1025–31.

104. Ooi C heong, Cheah W keat, Sim Y leng, Pung S yong, Yeoh F yee. Conversion and characterization of activated carbon fi ber derived from palm empty fruit bunch waste and its kinetic study on urea adsorption. J Environ Manage [Internet]. 2017;197:199–205. Available from: http://dx.doi.org/10.1016/j.jenvman.2017.03.083

105. Gaur V, Sharma A, Verma N. Preparation and characterization of ACF for the adsorption of BTX and SO 2. 2006;45:1–13.

106. Wu Y, Yao R, Zhang X, Zhang B, Wang T. Journal of Environmental Chemical Engineering Preparation and characterization of ACF / carbon composite membranes for efficient oil / water separation. J Environ Chem Eng [Internet]. 2021;9(3):105164. Available from: https://doi.org/10.1016/j.jece.2021.105164

107. Zhang L, Tu L, Y. L, Y. C, Q. L, Z. S. L, et al. Coconut-based activated carbon fibers for efficient adsorption of various organic dyes. . RSC Adv. 2018;8(74):42280-42291.

108. Pophali A, Singh S, Verma N. A dual photoelectrode-based double-chambered microbial fuel cell applied for simultaneous COD and Cr (VI) reduction in wastewater. Int J Hydrogen Energy [Internet]. 2021;46(4):3160–70. Available from: https://doi.org/10.1016/j.ijhydene.2020.06.162

109. Samuchiwal S, Bhattacharya A, Malik A. Treatment of textile effluent using an anaerobic reactor integrated with activated carbon and ultrafiltration unit (AN-ACF-UF process) targeting salt recovery and its reusability potential in the pad-batch process. J Water Process Eng. 2021;40(October).

110. Sharma A, Lee BK. Growth of TiO2 nano-wall on activated carbon fibers for enhancing the photocatalytic oxidation of benzene in aqueous phase. Catal Today [Internet]. 2017;287:113–21. Available from: http://dx.doi.org/10.1016/j.cattod.2016.11.019

111. Berhe RN, Kassahun SK, Kang JW, Lee I, Verma M, Kim H. Performance evaluation of Fe3O4@ACF-supported bio-electro Fenton system for simultaneous sewage treatment and methyl orange degradation. Mater Today Commun [Internet]. 2023;35(April):106331. Available from: https://doi.org/10.1016/j.mtcomm.2023.106331

112. Dehghani Y, Honarvar B, Azdarpour A, Nabipour M. Treatment of wastewater by a combined technique of adsorption, electrocoagulation followed by membrane separation. Adv Environ Technol. 2021;7(3):171–83.

113. Al-kazwini MJ, Al-ani FH, Al-najar MA. Environmental Study for the Oil Pollutants Treatment of Wadi Al Naft Water / Kirkuk 27;2009 .ةصلاخلا(8).

114. Prasetya N, Gede Wenten I, Franzreb M, Wöll C. Metal-organic frameworks for the adsorptive removal of pharmaceutically active compounds (PhACs): Comparison to activated carbon. Coord Chem Rev [Internet]. 2023;475:214877. Available from:

https://doi.org/10.1016/j.ccr.2022.214877

115. Dou Z, Wang Y, Liu Y, Zhao Y, Huang R. Enhanced adsorption of gaseous mercury on activated carbon by a novel clean modification method. Sep Purif Technol [Internet]. 2023;308(September 2022):122885. Available from: https://doi.org/10.1016/j.seppur.2022.122885

116. Yao Y, Ge D, Yu Y, Zhang Y, Du C, Ye H, et al. Filling macro/mesoporosity of commercial activated carbon enables superior volumetric supercapacitor performances. Microporous Mesoporous Mater. 2023;350(January).

117. Malini K, Selvakumar D, Kumar NS. Activated carbon from biomass: Preparation, factors improving basicity and surface properties for enhanced CO2capture capacity - A review. J CO2 Util [Internet]. 2023;67(September 2022):102318. Available from: https://doi.org/10.1016/j.jcou.2022.102318

118. Hussain OA, Hathout AS, Abdel-Mobdy YE, Rashed MM, Abdel Rahim EA, Fouzy ASM. Preparation and characterization of activated carbon from agricultural wastes and their ability to remove chlorpyrifos from water. Toxicol Reports [Internet]. 2023;10(January):146–54. Available from: https://doi.org/10.1016/j.toxrep.2023.01.011

119. Karimi M, Shirzad M, Silva JAC, Rodrigues AE. Biomass/Biochar carbon materials for CO2 capture and sequestration by cyclic adsorption processes: A review and prospects for future directions. J CO2 Util. 2022;57(January).

120. Serafin J, Narkiewicz U, Morawski AW, Wróbel RJ, Michalkiewicz B. Highly microporous activated carbons from biomass for CO2 capture and effective micropores at different conditions. J CO2 Util. 2017;18:73–9.

121. Sellaoui L, Dhaouadi F, Bedia J, Rtimi S, Belver C. Adsorption of emerging pollutants on lignin-based activated carbon : Analysis of adsorption mechanism via characterization , kinetics and equilibrium studies. 2023;452(September 2022).

122. Dziejarski B. Microporous and Mesoporous Materials Application of isotherms models and error functions in activated carbon CO 2 sorption processes. 2023;354.

123. Yurtay A, Kılıç M. Diamond & Related Materials Biomass-based activated carbon by flash heating as a novel preparation route and its application in high efficiency adsorption of metronidazole. Diam Relat Mater [Internet]. 2023;131(November 2022):109603. Available from: https://doi.org/10.1016/j.diamond.2022.109603

124. Ogungbenro AE, Quang D V., Al-Ali KA, Vega LF, Abu-Zahra MRM. Physical synthesis and characterization of activated carbon from date seeds

for CO2 capture. J Environ Chem Eng [Internet]. 2018;6(4):4245–52. Available from: https://doi.org/10.1016/j.jece.2018.06.030

125. DESOTEC. https://www.desotec.com/en/knowledge-hub/activated-carbon-size. 2023. Activated carbon size.

126. Ge L, Zhao C, Zhou T, Chen S, Li Q, Wang X, et al. An analysis of the carbonization process of coal-based activated carbon at different heating rates. Energy [Internet]. 2023;267(July 2022):126557. Available from: https://doi.org/10.1016/j.energy.2022.126557

127. Li M, Xiao R. Preparation of a dual Pore Structure Activated Carbon from Rice Husk Char as an Adsorbent for CO2 Capture. Fuel Process Technol [Internet]. 2019;186(December 2018):35–9. Available from: https://doi.org/10.1016/j.fuproc.2018.12.015

128. Zhang Q, Zhang M, Li T, Du R, Yu G, Deng S. FeOCl-confined activated carbon for improving intraparticle Fenton-like oxidation regeneration. J Hazard Mater [Internet]. 2023;442(September 2022):130026. Available from: https://doi.org/10.1016/j.jhazmat.2022.130026

129. Serafin J, Cruz OF. Promising activated carbons derived from common oak leaves and their application in CO2storage. J Environ Chem Eng. 2022;10(3).

130. Pu Q, Zou J, Wang J, Lu S, Ning P, Huang L, et al. Systematic study of dynamic CO2 adsorption on activated carbons derived from different biomass. J Alloys Compd [Internet]. 2021;887:161406. Available from: https://doi.org/10.1016/j.jallcom.2021.161406

131. Das S, Mishra S, Sahu H. A review of activated carbon to counteract the effect of iron toxicity on the environment. Environ Chem Ecotoxicol [Internet]. 2023;5(January):86–97. Available from: https://doi.org/10.1016/j.enceco.2023.02.002

132. Ameen F, Karimi-maleh H, Darabi R, Akin M, Ayati A. Synthesis and characterization of activated carbon supported bimetallic Pd based nanoparticles and their sensor and antibacterial investigation. Environ Res [Internet]. 2023;221(January):115287. Available from: https://doi.org/10.1016/j.envres.2023.115287

133. Valério Filho A, Tholozan L V., Arim AL, de Almeida ARF, da Rosa GS. High-performance removal of anti-inflammatory using activated carbon from water treatment plant sludge: fixed-bed and batch studies. Int J Environ Sci Technol. 2023;20(4):3633–44.

134. Reza S, Hasan A, Afroze S, Abu Bakar M, Taweekun J, Azad A. Analysis

on Preparation, Application, and Recycling of Activated Carbon to Aid in COVID-19 Protection. 2020;

135. Gouda MS, Shehab M, Helmy S, Soliman M, Salama RS. Nickel and cobalt oxides supported on activated carbon derived from willow catkin for efficient supercapacitor electrode. J Energy Storage [Internet]. 2023;61(January):106806. Available from: https://doi.org/10.1016/j.est.2023.106806

136. Qi G, Pan Z, Zhang X, Chang S, Wang H, Wang M, et al. Microwave biochar produced with activated carbon catalyst : Characterization and adsorption of heavy metals. Environ Res [Internet]. 2023;216(P4):114732. Available from: https://doi.org/10.1016/j.envres.2022.114732

137. Abbas A, Sabbar W, Abdul Salam R, Faraj S, Abdulrazzak F. Adsorption of dyes by activated carbon surfaces were prepared from plant residues, A Review. 2007;11. 2007-2.

138. Xiang S, Wu Q, Ren W, Guo W, Ren N. Mechanism of powdered activated carbon enhancing caproate production. Chinese Chem Lett [Internet]. 2023;34(4):107714. Available from: https://doi.org/10.1016/j.cclet.2022.07.057

139. Manz KE, Kulaots I, Greenley CA, Landry PJ, Lakshmi K V., Woodcock MJ, et al. Low-temperature persulfate activation by powdered activated carbon for simultaneous destruction of perfluorinated carboxylic acids and 1,4-dioxane. J Hazard Mater [Internet]. 2023;442(September 2022):129966. Available from: https://doi.org/10.1016/j.jhazmat.2022.129966

140. Zhang J, Yu S, Wang J, Zhao ZP, Cai W. Advanced water treatment process by simultaneous coupling granular activated carbon (GAC) and powdered carbon with ultrafiltration: Role of GAC particle shape and powdered carbon type. Water Res [Internet]. 2023;231(November 2022):119606. Available from: https://doi.org/10.1016/j.watres.2023.119606

141. Kalantzis D, Daskaloudis I, Lacoere T, Stasinakis AS, Lekkas DF, De Vrieze J, et al. Granular activated carbon stimulates biogas production in pilot-scale anaerobic digester treating agro-industrial wastewater. Bioresour Technol [Internet]. 2023;376(March):128908. Available from: https://doi.org/10.1016/j.biortech.2023.128908

142. Gao M, Dang H, Zou X, Yu N, Guo H, Yao Y, et al. Deciphering the role of granular activated carbon (GAC) in anammox: Effects on microbial succession and communication. Water Res [Internet]. 2023;233(April 2022):119753. Available from: https://doi.org/10.1016/j.watres.2023.119753

143. Ramirez Arenas L, Le Coustumer P, Ramseier Gentile S, Zimmermann S, Stoll S. Removal efficiency and adsorption mechanisms of CeO2 nanoparticles onto granular activated carbon used in drinking water treatment plants. Sci Total Environ. 2023;856(September 2022).

144. Chen Q, Li G, Lu Z, Su Y, Wu B, Shi B. Efficient Mn(II) removal by biological granular activated carbon filtration. J Hazard Mater [Internet]. 2023;458(April):131877. Available from: https://doi.org/10.1016/j.jhazmat.2023.131877

145. Wu X, Xia A, Feng D, Huang Y, Zhu X, Zhu X, et al. Intensifying anaerobic digestion of 5-hydroxymethylfurfural via granular activated carbon supplementation. Int J Hydrogen Energy [Internet]. 2023;(xxxx). Available from: https://doi.org/10.1016/j.ijhydene.2023.07.034

146. Xing X, Tang J, Yao S, Chen H, Zheng T, Wu J. Electrochemical regeneration of granular activated carbon saturated by p-nitrophenol in BDD anode system. Process Saf Environ Prot [Internet]. 2023;170(November 2022):207–14. Available from: https://doi.org/10.1016/j.psep.2022.11.082

147. Guilherme EPX, Forte MBS. Recovery of mixture of hydroxyethylammonium carboxylate protic ionic liquids from sugarcane pretreatment liquor using activated carbon in a fixed bed column. Sep Purif Technol [Internet]. 2023;319(April):124000. Available from: https://doi.org/10.1016/j.seppur.2023.124000

148. Tang X, Ma S, Xu S, Pei C, Dong T, Yang Q, et al. Boosted persulfate activation by hierarchically porous carbonaceous materials: Pivotal role of pore structure and electron-accepting capacity. Chem Eng J [Internet]. 2023;471(July):144765. Available from: https://doi.org/10.1016/j.cej.2023.144765

149. Niedziński T, Łabętowicz J, Stępień W, Pęczek T. Analysis of the Use of Biochar from Organic Waste Pyrolysis in Agriculture and Environmental Protection. J Ecol Eng. 2023;24(4):85–98.

150. Pj J, Shaji S. PRODUCTION AND CHARACTERIZATION OF ACTIVATED CHARCOAL FROM COCOA POD By DEPARTMENT OF PROCESSING AND FOOD ENGINEERING KELAPPAJI COLLEGE OF AGRICULTURAL ENGINEERING AND TECHNOLOGY PRODUCTION AND CHARACTERIZATION OF ACTIVATED CHARCOAL FROM COCOA POD. 2023;

151. Kumar N, Pandey A, Rosy, Sharma YC. A review on sustainable mesoporous activated carbon as adsorbent for efficient removal of hazardous dyes from industrial wastewater. J Water Process Eng [Internet]. 2023;54(July):104054. Available from:

https://doi.org/10.1016/j.jwpe.2023.104054

152. Hosseinzadegan A, Mahdiyar H, Raoof A, Nikooee E, Qajar J. The pore-network modeling of gas-condensate flow: Elucidating the effect of pore morphology, wettability, interfacial tension, and flow rate. Geoenergy Sci Eng [Internet]. 2023;229(May):211937. Available from: https://doi.org/10.1016/j.geoen.2023.211937

153. Chen F, Liang W, Qin X, Jiang L, Zhang Y, Fang S, et al. Preparation and recycled simultaneous adsorption of methylene blue and Cu2+ co-pollutants over carbon layer encapsulated Fe3O4 /graphene oxide nanocomposites rich in amino and thiol groups. Colloids Surfaces A Physicochem Eng Asp [Internet]. 2021;625(March):126913. Available from: https://doi.org/10.1016/j.colsurfa.2021.126913

154. Zhou Y, Sherpa S, McBride MB. Pb and Cd chemisorption by acid mineral soils with variable Mn and organic matter contents. Geoderma [Internet]. 2020;368(July 2019):114274. Available from: https://doi.org/10.1016/j.geoderma.2020.114274

155. Çetingürbüz E, Turkyilmaz A. Industrial Crops & Products Production of activated carbon by lithium activation and determination of hydrogen storage capacity. Ind Crop Prod [Internet]. 2023;203(July):117171. Available from: https://doi.org/10.1016/j.indcrop.2023.117171

156. Tiberg C, Sjöstedt C, Gustafsson JP. Metal sorption to Spodosol Bs horizons: Organic matter complexes predominate. Chemosphere. 2018;196:556–65.

157. Lan J, Wang B, Bo C, Gong B, Ou J. Progress on fabrication and application of activated carbon sphere in recent decade. J Ind Eng Chem [Internet]. 2023;120:47–72. Available from: https://doi.org/10.1016/j.jiec.2022.12.045

158. Farjadian F, Ghasemi S, Heidari R, Mohammadi-Samani S. In vitro and in vivo assessment of EDTA-modified silica nano-spheres with supreme capacity of iron capture as a novel antidote agent. Nanomedicine Nanotechnology, Biol Med [Internet]. 2017;13(2):745–53. Available from: http://dx.doi.org/10.1016/j.nano.2016.10.012

159. Zhang C, Yang S, Chen H, He H, Sun C. Adsorption behavior and mechanism of reactive brilliant red X-3B in aqueous solution over three kinds of hydrotalcite-like LDHs. Appl Surf Sci [Internet]. 2014;301:329–37. Available from: http://dx.doi.org/10.1016/j.apsusc.2014.02.073

160. Zhou H, Su Y, Zhang J, Li H, Zhou L, Huang H. A novel embedded all-solid-state composite structural supercapacitor based on activated carbon fiber electrode and carbon fiber reinforced polymer matrix. Chem Eng J [Internet]. 2023;454(P2):140222. Available from:

https://doi.org/10.1016/j.cej.2022.140222

161. Kang SH, Lee HM, Kim KW, Kim BJ. Preparation and characterization of polyethylene-based activated carbon fibers stabilized at low temperatures. J Ind Eng Chem [Internet]. 2023;121:401–8. Available from: https://doi.org/10.1016/j.jiec.2023.01.042

162. Song Y, Wang A, Ren S, Zhang Y, Zhang Z. Flow-through heterogeneous electro-Fenton system using a bifunctional FeOCl/carbon cloth/activated carbon fiber cathode for efficient degradation of trimethoprim at neutral pH. Environ Res [Internet]. 2023;222(December 2022):115303. Available from: https://doi.org/10.1016/j.envres.2023.115303

163. Ren J, Yao Z, Wei Q, Wang R, Liu Y, Wang L, et al. Degradation of ferulic acid and caffeic acid by dielectric barrier discharge plasma combined with Mn/CoOOH/activated carbon fiber. Sep Purif Technol [Internet]. 2023;306(PB):122691. Available from: https://doi.org/10.1016/j.seppur.2022.122691

164. Xing L an, Yang F, Zhong X, Liu Y, Lu H, Guo Z, et al. Ultra-microporous cotton fiber-derived activated carbon by a facile one-step chemical activation strategy for efficient CO 2 adsorption. Sep Purif Technol [Internet]. 2023;324(July):124470. Available from: https://doi.org/10.1016/j.seppur.2023.124470

165. Activated carbon. In Wikipedia. https://en.wikipedia.org/wiki/Activated_carbon.

166. Nobre C, Santos L, Paz J, Felipe M, Pego F, Nunes L, et al. Heliyon Potential of agro-industrial residues from the Amazon region to produce activated carbon. 2023;9(March).

167. Yi K, Yang W, Logan BE. Defect free rolling phase inversion activated carbon air cathodes for scale-up electrochemical applications. Chem Eng J [Internet]. 2023;454(P3):140411. Available from: https://doi.org/10.1016/j.cej.2022.140411

168. Xing L an, Yang F, Zhong X, Liu Y, Lu H, Guo Z, et al. Ultra-microporous cotton fiber-derived activated carbon by a facile one-step chemical activation strategy for efficient CO 2 adsorption. Sep Purif Technol [Internet]. 2023;324(June):124470. Available from: https://doi.org/10.1016/j.seppur.2023.124470

169. Kim S, Kim S, Lee S. Activated carbon modified with polyethyleneimine and MgO: Better adsorption of aldehyde and production of regenerative VOC adsorbent using a photocatalyst. Appl Surf Sci [Internet]. 2023;631(March):157565. Available from:

https://doi.org/10.1016/j.apsusc.2023.157565

170. Schurer R, de Ridder DJ, Schippers JC, Hijnen WAM, Vredenbregt L, van der Wal A. Advanced drinking water production by 1 kDa hollow fiber nanofiltration – Biological activated carbon filtration (HFNF – BACF) enhances biological stability and reduces micropollutant levels compared with conventional surface water treatment. Chemosphere. 2023;321(November 2022).

171. Sahu A, Kumar A, Dashairya L, Saha P, Bhuyan SK, Sen S, et al. Performance of wasteland biomass Calotropis gigantea derived activated carbon as Lithium-ion battery anode. Diam Relat Mater [Internet]. 2023;136(March):110053. Available from: https://doi.org/10.1016/j.diamond.2023.110053

172. Bozacı G, Acaralı N. Chemical production of activated carbon from green coffee with adsorption isotherm support by Taguchi model. J Indian Chem Soc. 2023;100(1).

173. Wiśniewska M, Pawlak N, Sternik D, Pietrzak R, Nowicki P. Production of Activated Carbons from Food/Storage Waste. Materials (Basel). 2023;16(4).

174. Amin M, Chung E, Shah HH. Effect of different activation agents for activated carbon preparation through characterization and life cycle assessment. Int J Environ Sci Technol [Internet]. 2023;20(7):7645–56. Available from: https://doi.org/10.1007/s13762-022-04472-6

175. Junaid M, Siddiqui JA, Liu S, Lan R, Abbas Z, Chen G, et al. Adverse multigeneration combined impacts of micro(nano)plastics and emerging pollutants in the aquatic environment. Sci Total Environ [Internet]. 2023;882(March):163679. Available from: https://doi.org/10.1016/j.scitotenv.2023.163679

176. Jimoh JO, Rahmah S, Mazelan S, Jalilah M, Olasunkanmi JB, Lim LS, et al. Impact of face mask microplastics pollution on the aquatic environment and aquaculture organisms. Environ Pollut [Internet]. 2023;317(October 2022):120769. Available from: https://doi.org/10.1016/j.envpol.2022.120769

177. Kumar M, Xiong X, He M, Tsang DCW, Gupta J, Khan E, et al. Microplastics as pollutants in agricultural soils. Environ Pollut. 2020;265.

178. Ullah A, Khan D, Khan I, Zheng S. Does agricultural ecosystem cause environmental pollution in Pakistan? Promise and menace. Environ Sci Pollut Res. 2018;25(14):13938–55.

179. Oyegoke T, Emo O, Sardauna M, Bamigbala O, Owolabi O. Utilization of

Rice Husk for the Bioethanol Production: “A Waste to Wealth Innovation Study”. 2020;(10.13140/RG.2.2.15491.22561.).

180. Graça CAL. Research on Micropollutants in Urban Water. Water (Switzerland). 2023;15(4):2–5.

181. Antonkiewicz J, Kowalewska A, Mikołajczak S, Kołodziej B, Bryk M, Spychaj-Fabisiak E, et al. Phytoextraction of heavy metals after application of bottom ash and municipal sewage sludge considering the risk of environmental pollution. J Environ Manage. 2022;306(January).

182. Rangabhashiyam S, Lins PV do. S, Oliveira LMT d. M, Sepulveda P, Ighalo JO, Rajapaksha AU, et al. Sewage sludge-derived biochar for the adsorptive removal of wastewater pollutants: A critical review. Environ Pollut. 2022;293(December 2021).

183. Wasi S, Tabrez S, Ahmad M. Toxicological effects of major environmental pollutants: An overview. Environ Monit Assess. 2013;185(3):2585–93.

184. Zhang QS. Environment Pollution Analysis on Smart Cities Using Wireless Sensor Networks. Strateg Plan Energy Environ. 2023;42(1):239–62.

185. united state environmental protection agency. EPA EcoBox Tools by Exposure Pathways - Air [Internet]. Available from: https://www.epa.gov/ecobox/epa-ecobox-tools-exposure-pathways-air

186. Verma VK, Mishra AK. Kinetic and isotherm modeling of adsorption of dyes onto rice husk carbon. Glob Nest J. 2010;12(2):190–6.

187. Foo KY, Hameed BH. Insights into the modeling of adsorption isotherm systems. Chem Eng J. 2010;156(1):2–10.

188. Sampranpiboon P, Charnkeitkong P, Feng X. Equilibrium isotherm models for adsorption of zinc (II) ion from aqueous solution on pulp waste. WSEAS Trans Environ Dev. 2014;10(Ii):35–47.

189. Ouaissa YA, Chabani M, Amrane A, Bensmaili A. Removal of tetracycline by electrocoagulation: Kinetic and isotherm modeling through adsorption. J Environ Chem Eng. 2014;2(1):177–84.

190. Malek A, Farooq S. Comparison of Isotherm Models for Hydrocarbon Adsorption on Activated Carbon. AIChE J. 1996;42(11):3191–201.

191. Al-Ghouti MA, Da’ana DA. Guidelines for the use and interpretation of adsorption isotherm models: A review. J Hazard Mater [Internet]. 2020;393(January):122383. Available from: https://doi.org/10.1016/j.jhazmat.2020.122383

192. Chen X. Modeling of experimental adsorption isotherm data. Inf.

2015;6(1):14–22.

193. Zana Hassan Rada. Adsorption of gases (CO2, CH4) using novel porous materials (MOFs). 2016;

194. Králik M. Adsorption, chemisorption, and catalysis. Chem Pap. 2014;(68. 10.2478/s11696-014-0624-9.).

195. Lima ÉC, Adebayo MA, Machado FM. Kinetic and equilibrium models of adsorption. Vol. 0, Carbon Nanostructures. 2015. 33–69 p.

196. Hamdaoui O, Naffrechoux E. Modeling of adsorption isotherms of phenol and chlorophenols onto granular activated carbon. Part II. Models with more than two parameters. J Hazard Mater. 2007;147(1–2):401–11.

197. Deng S, Ting YP. Characterization of PEI-modified biomass and biosorption of Cu(II), Pb(II) and Ni(II). Water Res. 2005;39(10):2167–77.

198. Vijayaraghavan K, Yun YS. Bacterial biosorbents and biosorption. Biotechnol Adv. 2008;26(3):266–91.

199. Naseeruteen F, Hamid NSA, Suah FBM, Ngah WSW, Mehamod FS. Adsorption of malachite green from aqueous solution by using novel chitosan ionic liquid beads. Int J Biol Macromol [Internet]. 2018;107(PartA):1270–7. Available from: http://dx.doi.org/10.1016/j.ijbiomac.2017.09.111

200. Arshadi M, Soleymanzadeh M, Salvacion JWL, SalimiVahid F. Nanoscale Zero-Valent Iron (NZVI) supported on sineguelas waste for Pb(II) removal from aqueous solution: Kinetics, thermodynamic and mechanism. J Colloid Interface Sci [Internet]. 2014;426:241–51. Available from: http://dx.doi.org/10.1016/j.jcis.2014.04.014

201. Sheth Y, Dharaskar S, Khalid M, Sonawane S. An environment friendly approach for heavy metal removal from industrial wastewater using chitosan based biosorbent: A review. Sustain Energy Technol Assessments [Internet]. 2021;43(December 2020):100951. Available from: https://doi.org/10.1016/j.seta.2020.100951

202. Dubey R, Bajpai J, Bajpai AK. Chitosan-alginate nanoparticles (CANPs) as potential nanosorbent for removal of Hg (II) ions. Environ Nanotechnology, Monit Manag [Internet]. 2016;6:32–44. Available from: http://dx.doi.org/10.1016/j.enmm.2016.06.008

203. He X, Zhang T, Xue Q, Zhou Y, Wang H, Bolan NS, et al. Enhanced adsorption of Cu(II) and Zn(II) from aqueous solution by polyethyleneimine modified straw hydrochar. Sci Total Environ [Internet]. 2021;778:146116. Available from: https://doi.org/10.1016/j.scitotenv.2021.146116

204. Lu C, Chiu H. Adsorption of zinc(II) from water with purified carbon nanotubes. Chem Eng Sci. 2006;61(4):1138–45.

205. Sadeghi MH, Tofighy MA, Mohammadi T. One-dimensional graphene for efficient aqueous heavy metal adsorption: Rapid removal of arsenic and mercury ions by graphene oxide nanoribbons (GONRs). Chemosphere. 2020;253.

206. Ibrahim NA, Abdellatif FHH, Hasanin MS, Abdellatif MM. Fabrication, characterization, and potential application of modified sawdust sorbents for efficient removal of heavy metal ions and anionic dye from aqueous solutions. J Clean Prod [Internet]. 2022;332(November 2021):130021. Available from: https://doi.org/10.1016/j.jclepro.2021.130021

207. Liu YP, Lv YT, Guan JF, Khoso FM, Jiang XY, Chen J, et al. Rational design of three-dimensional graphene/graphene oxide-based architectures for the efficient adsorption of contaminants from aqueous solutions. J Mol Liq [Internet]. 2021;343:117709. Available from: https://doi.org/10.1016/j.molliq.2021.117709

208. He S, Chen Q, Chen G, Shi G, Ruan C, Feng M, et al. N-doped activated carbon for high-efficiency ofloxacin adsorption. Microporous Mesoporous Mater [Internet]. 2022;335(December 2021):111848. Available from: https://doi.org/10.1016/j.micromeso.2022.111848

209. Zhao Z, Sun W, Ray MB. Adsorption isotherms and kinetics for the removal of algal organic matter by granular activated carbon. Sci Total Environ [Internet]. 2022;806:150885. Available from: https://doi.org/10.1016/j.scitotenv.2021.150885

210. Kareem SL, Mohammed AA. Removal of Tetracycline from Wastewater Using Circulating Fluidized Bed. Iraqi J Chem Pet Eng. 2020;21(3):29–37.

211. Mahdi E, Ochoa D, Vaziri A, Eltai E. Energy absorption capability of date palm leaf fiber reinforced epoxy composites rectangular tubes. Compos Struct. 2019;224(May).

212. Althoey F, IY H, MA H, S Q, HF I, H H, et al. Behavior of Concrete Reinforced with Date Palm Fibers. Materials (Basel). 2022;(15(22):7923.).

213. Wang L, Chang Y, Li A. Hydrothermal carbonization for energy-efficient processing of sewage sludge: A review. Renew Sustain Energy Rev. 2019;108(June 2018):423–40.

214. Czerwińska K, Śliz M, Wilk M. Hydrothermal carbonization process: Fundamentals, main parameter characteristics and possible applications including an effective method of SARS-CoV-2 mitigation in sewage sludge.

A review. Renew Sustain Energy Rev. 2022;154(October 2021).

215. Lee T, Zubir ZA, Jamil FM, Matsumoto A, Yeoh FY. Combustion and pyrolysis of activated carbon fibre from oil palm empty fruit bunch fibre assisted through chemical activation with acid treatment. J Anal Appl Pyrolysis [Internet]. 2014;110(1):408–18. Available from: http://dx.doi.org/10.1016/j.jaap.2014.10.010

216. Moon SY, Kim MS, Hahm HS, Lim YS. Preparation of Activated Carbon Fibers by Chemical Activation Method with Hydroxides. Mater Sci Forum. 2006;510–511:750–3.

217. Ulla Gro Nielsen. Chapter Two - Solid state NMR studies of layered double hydroxides,. Annu Reports NMR Spectrosc. 2021;104:75–140.

218. SD. L. Water and wastewater calculations manual. 2003;

219. Hong SH, Chung K, Bang G, Kim KM, Lee CH. Adsorption equilibria and kinetics of CO2, CH4, CO, N2, and H2 on KOH-treated activated carbon pellets up to 1000 kPa. Chem Eng J [Internet]. 2022;431(P4):133396. Available from: https://doi.org/10.1016/j.cej.2021.133396

220. Raji Y, Nadi A, Mechnou I, Saadouni M, Cherkaoui O, Zyade S. High adsorption capacities of crystal violet dye by low-cost activated carbon prepared from Moroccan Moringa oleifera wastes: Characterization, adsorption and mechanism study. Diam Relat Mater [Internet]. 2023;135(March):109834. Available from: https://doi.org/10.1016/j.diamond.2023.109834

221. Serafin J, Dziejarski B. Application of isotherms models and error functions in activated carbon CO2 sorption processes. Microporous Mesoporous Mater. 2023;354.

222. By-nc-sa CC. M IDDLE S CHOOL M ATHEMATICS C LASSROOMS P RACTICE B ASED ON 5E I NSTRUCTIONAL M ODEL The Texas Tech community has made this publication openly available . Please share how this access benefits you . Your story matters to us . Citation Citable Link. 2021;9(1):22–39.

223. El-Habacha M, Dabagh A, Lagdali S, Miyah Y, Mahmoudy G, Sinan F, et al. An efficient and adsorption of methylene blue dye on a natural clay surface: modeling and equilibrium studies. Environ Sci Pollut Res [Internet]. 2023;(May). Available from: https://doi.org/10.1007/s11356-023-27413-3

224. Guerra DJL, Mello I, Resende R, Silva R. Application as absorbents of natural and functionalized Brazilian bentonite in Pb2+ adsorption: Equilibrium, kinetic, pH, and thermodynamic effects. Water Resour Ind

[Internet]. 2013;4:32–50. Available from: http://dx.doi.org/10.1016/j.wri.2013.11.001

225. Shahat A, Kubra KT, El-marghany A. Equilibrium, thermodynamic and kinetic modeling of triclosan adsorption on mesoporous carbon nanosphere: Optimization using Box-Behnken design. J Mol Liq [Internet]. 2023;383(March):122166. Available from: https://doi.org/10.1016/j.molliq.2023.122166

226. Spinelli VA, Laranjeira MCM, Fávere VT. Preparation and characterization of quaternary chitosan salt: Adsorption equilibrium of chromium(VI) ion. React Funct Polym. 2004;61(3):347–52.

227. Hu Q, Lan R, He L, Liu H, Pei X. A critical review of adsorption isotherm models for aqueous contaminants: Curve characteristics, site energy distribution and common controversies. J Environ Manage [Internet]. 2023;329(December 2022):117104. Available from: https://doi.org/10.1016/j.jenvman.2022.117104

228. Sari A, Tuzen M. Kinetic and equilibrium studies of biosorption of Pb(II) and Cd(II) from aqueous solution by macrofungus (Amanita rubescens) biomass. J Hazard Mater. 2009;164(2–3):1004–11.

229. Kumar KV, Gadipelli S, Wood B, Ramisetty KA, Stewart AA, Howard CA, et al. Characterization of the adsorption site energies and heterogeneous surfaces of porous materials. J Mater Chem A. 2019;7(17):10104–37.

230. Chowdhury S, Mishra R, Saha P, Kushwaha P. Adsorption thermodynamics, kinetics and isosteric heat of adsorption of malachite green onto chemically modified rice husk. Desalination [Internet]. 2011;265(1–3):159–68. Available from: http://dx.doi.org/10.1016/j.desal.2010.07.047

231. Mohammed AA, Al-Musawi TJ, Kareem SL, Zarrabi M, Al-Ma'abreh AM. Simultaneous adsorption of tetracycline, amoxicillin, and ciprofloxacin by pistachio shell powder coated with zinc oxide nanoparticles. Arab J Chem [Internet]. 2020;13(3):4629–43. Available from: https://doi.org/10.1016/j.arabjc.2019.10.010

232. Nnadozie EC, Ajibade PA. Data for experimental and calculated values of the adsorption of Pb(II) and Cr(VI) on APTES functionalized magnetite biochar using Langmuir, Freundlich and Temkin equations. Data Br [Internet]. 2020;32:106292. Available from: https://doi.org/10.1016/j.dib.2020.106292

233. Wang J, Muhammad Y, Gao Z, Jalil Shah S, Nie S, Kuang L, et al. Implanting polyethylene glycol into MIL-101(Cr) as hydrophobic barrier for enhancing toluene adsorption under highly humid environment. Chem Eng

J. 2021;404(August 2020).

234. Ezzati R. Derivation of Pseudo-First-Order, Pseudo-Second-Order and Modified Pseudo-First-Order rate equations from Langmuir and Freundlich isotherms for adsorption. Chem Eng J [Internet]. 2020;392(December 2019):123705. Available from: https://doi.org/10.1016/j.cej.2019.123705

235. Budhiary KNS, Sumantri I. Langmuir and Freundlich isotherm adsorption using activated charcoal from banana peel to reduce total suspended solid (TSS) levels in tofu industry liquid waste. IOP Conf Ser Mater Sci Eng. 2021;1053(1):012113.

236. Rozanov LN. Kinetic equations of non-localized physical adsorption in vacuum for Freundlich adsorption isotherm. Vacuum [Internet]. 2021;189(April):110267. Available from: https://doi.org/10.1016/j.vacuum.2021.110267

237. Erdogan FO. Freundlich, langmuir, temkin and harkins-jura isotherms studies of h2 adsorption on porous adsorbents. Chem Chem Technol. 2019;13(2):129–35.

238. Fouad M. Effect of temperature and soil type on the adsorption and desorption isotherms of thiamethoxam using the Freundlich equation. Egypt J Chem. 2022;0(0):0–0.

239. Ragadhita R, Nandiyanto ABD. Curcumin Adsorption on Zinc Imidazole Framework-8 Particles: Isotherm Adsorption Using Langmuir, Freundlich, Temkin, and Dubinin-Radushkevich Models. J Eng Sci Technol. 2022;17(2):1078–89.

240. Harrache Z, Abbas M, Aksil T, Trari M. Thermodynamic and kinetics studies on adsorption of Indigo Carmine from aqueous solution by activated carbon. Microchem J [Internet]. 2019;144(July 2018):180–9. Available from: https://doi.org/10.1016/j.microc.2018.09.004

241. Hasanzadeh M, Simchi A, Shahriyari Far H. Nanoporous composites of activated carbon-metal organic frameworks for organic dye adsorption: Synthesis, adsorption mechanism and kinetics studies. J Ind Eng Chem [Internet]. 2020;81:405–14. Available from: https://doi.org/10.1016/j.jiec.2019.09.031

242. Somsesta N, Sricharoenchaikul V, Aht-Ong D. Adsorption removal of methylene blue onto activated carbon/cellulose biocomposite films: Equilibrium and kinetic studies. Mater Chem Phys [Internet]. 2020;240(September 2019):122221. Available from: https://doi.org/10.1016/j.matchemphys.2019.122221

243. Ahmad A, Khan N, Giri BS, Chowdhary P, Chaturvedi P. Removal of methylene blue dye using rice husk, cow dung and sludge biochar: Characterization, application, and kinetic studies. Bioresour Technol [Internet]. 2020;306(March):123202. Available from: https://doi.org/10.1016/j.biortech.2020.123202

244. Qu W, Yuan T, Yin G, Xu S, Zhang Q, Su H. Effect of properties of activated carbon on malachite green adsorption. Fuel [Internet]. 2019;249(February):45–53. Available from: https://doi.org/10.1016/j.fuel.2019.03.058

245. Lütke SF, Igansi A V., Pegoraro L, Dotto GL, Pinto LAA, Cadaval TRS. Preparation of activated carbon from black wattle bark waste and its application for phenol adsorption. J Environ Chem Eng [Internet]. 2019;7(5):103396. Available from: https://doi.org/10.1016/j.jece.2019.103396

246. Alasadi AM, Khaili FI, Awwad AM. ADSORPTION OF Ni (II), Zn (II) AND Cu (II) IONS ONTO NANO KAOLINITE Adsorption of Cu (II), Ni (II) and Zn (II) ions by nano kaolinite : Thermodynamics and kinetics studies. 2020;(June):258–68.

247. Silva LMS, Muñoz-Peña MJ, Domínguez-Vargas JR, González T, Cuerda-Correa EM. Kinetic and equilibrium adsorption parameters estimation based on a heterogeneous intraparticle diffusion model. Surfaces and Interfaces. 2021;22.

248. Danish M, Ansari KB, Danish M, Khatoon A, Ali Khan Rao R, Zaidi S, et al. A comprehensive investigation of external mass transfer and intraparticle diffusion for batch and continuous adsorption of heavy metals using pore volume and surface diffusion model. Sep Purif Technol [Internet]. 2022;292(April):120996. Available from: https://doi.org/10.1016/j.seppur.2022.120996

249. Gelis K, Ozbek K, Huwaish M. Entropy generation minimization for different types of heat exchangers using nanofluids. Energy Sources, Part A Recover Util Environ Eff [Internet]. 2024;46(1):1403–18. Available from: https://doi.org/10.1080/15567036.2023.2299698

250. Zdravkov BD, Čermák JJ, Šefara M, Janků J. Pore classification in the characterization of porous materials: A perspective. Cent Eur J Chem. 2007;5(2):385–95.

251. Hu Z, Srinivasan MP. Mesoporous high-surface-area activated carbon. Microporous Mesoporous Mater. 2001;43(3):267–75.

252. Wang J, Duan H, Wang M, Shentu Q, Xu C, Yang Y, et al. Construction of

durable superhydrophilic activated carbon fibers based material for highly-efficient oil/water separation and aqueous contaminants degradation. Environ Res [Internet]. 2022;207(July 2021):112212. Available from: https://doi.org/10.1016/j.envres.2021.112212

253. Hashem A, Aniagor CO, Nasr MF, Abou-Okeil A. Efficacy of treated sodium alginate and activated carbon fibre for Pb(II) adsorption. Int J Biol Macromol. 2021;176(February):201–16.

254. Xinga L an, Yanga F, Zhonga X, Liua Y, Lua H, Guoc Z, et al. Ultra-microporous cotton fiber-derived activated carbon by a facile one-step chemical activation strategy for efficient CO2 adsorption. Sep Purif Technol. 2023;324.

255. Hall KR, Eagleton LC, Acrivos A, Vermeulen T. Vermeulen, Pore-and solid-diffusion kinetics in fixed-bed adsorption under constant-pattern conditions,. Ind Eng Chem Fundam. 1966;212–223.